TECHNISCHE UNIVERSITÄT MÜNCHEN
Fakultät für Maschinenwesen
Institut für Luft- und Raumfahrt
Lehrstuhl für Leichtbau

Optimization of Steered-Fibers Composite Stiffened Panels including Postbuckling Constraints handled via Equivalent Static Loads

Tanut Ungwattanapanit

Vollständiger Abdruck der von der Fakultät für Maschinenwesen der Technischen Universität München zur Erlangung des akademischen Grades eines

Doktor-Ingenieurs (Dr.-Ing.)

genehmigten Dissertation.

Vorsitzender:	Prof. Dr.-Ing. Manfred Hajek
Prüfer der Dissertation:	
	1. Prof. Dr.-Ing. Horst Baier (i.R.)
	2. Prof. Dr.-Ing. Kai-Uwe Bletzinger

Die Dissertation wurde am 03.04.2017 bei der Technische Universität München eingereicht und durch die Fakultät für Maschinenwesen am 21.10.2017 angenommen.

♦ Dedication ♦

This thesis is dedicated to my parents, family, and friends.
All I have achieved and will accomplish are only possible due to their love, sacrifices and endless support.

With highest respect to the Buddha, Dharma, and Sangha,
Tanut Ungwattanapanit

Acknowledgement

First, I would like to express my gratitude to my supervisor Prof. Dr.-Ing. Horst Baier i.R. for his continuing support and guidance during our time at the Institute of Lightweight Structures and even after his retirement. I am in deed grateful for the opportunity he has given to me, who was just a young Asian student back there in 2011, when I started this doctoral dissertation. It continued with his openness to allow myself to freely conduct this research work as well as an important opportunity to be involved in Airbus Sagitta UAV project.

My appreciation definitely extends to every colleague at the Institute of Lightweight Structures, Technische Universität München. Special thanks go to Rainer Wehrle, Jan Both, Luiz da Rocha-Schmidt, Erich Wehrle, Markus Schatz, Bernhard Sauerer, Martin Mahl, Andreas Hermanutz, Felix Stroscher, Qian Xu, Yang Zhang, and last but not least our beloved secretary Amely Schwoerer.

I would also like to thank the Thai community in Munich, especially my current and former roommates: Su, Koo, Yui, and P'Toy, Sor for transferring their apartment to myself.

Finally, I would like to give my sincere gratitude to my parents, family and friends in Thailand. Without their endless support, understanding, and encouragement, I would not have been able to succeed the presented work.

Garching, 10th December 2016
Tanut Ungwattanapanit

Abstract

Continuous fiber angle variation at the ply level producing steered-fiber laminates can be optimized to improve various structural performances e.g. strength, stiffness, stability, or natural frequency. As geometrical stability is one of the most critical design requirements in aerospace structures, an innovative optimization method which is able to efficiently account for structural responses in nonlinear postbuckling regime is sought after. In order to facilitate a conventional gradient-based optimization, postbuckling responses are handled via Equivalent Static Loads Method (ESLM). As a result, a weight-optimized design can be achieved in an effective manner. Significant mass saving benefited from steered-fiber laminates as well as from postbuckling allowance is demonstrated through fuselage stiffened panels. Influence of loading condition and ESLM parameters towards optimal solutions are studied in details. Comparison of the proposed method to other applicable optimization techniques is moreover conducted. Importance of strength, pre- and postbuckling constraints including global panel buckling and stiffener crippling is described. Finally, important considerations and limitations of the introduced method is underlined in the form of optimizers' guidelines.

Kurzfassung

Eine kontinuierliche Faserwinkeländerung an der Lage, der gebogene Faserlaminat erzeugt, kann optimiert werden, um verschidene strukturelle Leistungen, z.B. Festigkeit, Steifigkeit, Stabilität oder Eigenfrequenz zu verbessern. Eine der kritischsten Konstruktionsanforderungen im Bereich der Lufts- und Raumfahrtskonstruktion ist die geometrische Stabilität. Eine innovative Optimierungsmethode, durch die mann wirksam nichtlineares Nachbeulenverhalten einschließen kann, wird in der folgenden Arbeit gesucht. Um eine herkömmliche gradientenbasierte Optimierung zu ermöglichen, werden Nachbeulverhalten über Equivalent Static Load Method (ESLM) bearbeitet. In Folge dessen kann eine gewichtsoptimierte Konstruktion effektiv erreicht werden. Durch die Laminate mit kurvenförmigen Fasern, sowie die Erlaubnis des Nachbeulens ermöglicht eine signifikanter Gewicht-Einsparungseffekt. Die wird durch verstärkte Rumpfschale demonstriert. Der Einfluss die Belastungsbedingungen und die ESLM-Parameter auf optimale Lösungen werden im Detail dieser Arbeit untersucht. Darüber hinaus wird ein Vergleich des vorgeschlagenen Verfahrens mit andern anwenbaren Optimierungstechniken durchgeführt. Die Wichtigkeit die Anforderungen des Spannungs und Vor-und Nachbeulen einschließlich den globalen Panel-Zusammenbruch und die Beschädigung der Versteifung werden in der Dissertation erläutert. Zum Schluss werden die wichtige Berücksichtigung und die Einschränkungen der angewendeten Methode in Form von Optimierungsrichtlinien zusammen gefasst.

Contents

List of Figures

List of Tables

Nomenclature

D_{xy}	Torsional rigidity in xy direction, Nmm^2
D_x	Flexural rigidity in x direction, Nmm^2
D_y	Flexural rigidity in y direction, Nmm^2
$\bar{u}$	Normalized shortening wrt. reference design, -
$\bar{A}$	Cross-sectional area of stiffened panel segment bounded by p, mm^2
$\bar{E}_i$	Section's effective bending stiffness modulus, MPa
$\bar{I}_c$	Moment of inertia, per unit width, of the combined stringer foot and skin, mm^4/mm
β	Panel aspect ratio a/c, -
δ	Relative change of optimized values in two successive cycles, -
ϵ_{GXX}	Green strain in XX direction, -
ϵ_{XX}	Engineering strain in XX direction, -
η	Neutral axis of stringer, -
η_o	Neutral axis of stringer and skin combined, -
λ	Lagrange multiplier, -
λ_1	The first critical buckling eigenvalue, -
μ	Iterative nonlinear analysis convergence threshold, -
ν_{12}	Lamina Poisson's ratio, -
φ	Failure index correction factor, -
ρ	Stiffener radius of gyration, mm
$\sigma_{cripp,i}$	Section's crippling stress, MPa
$\sigma_{cripp,str}$	Stringer's crippling stress, MPa
θ	Omega stringer's web angle, rad
$\theta(z)$	fiber orientation at z, $^\circ$
ε	ESLM convergence threshold, -

a Panel length, mm

A_{11} Laminate in-plane stiffness coefficient in 11 direction, N/mm

A_{str} Cross-sectional area of a stringer, mm^2

b Section length, mm

b plate width in z-axis, mm

b_i Omega stringer section width, mm

c Panel arc length, mm

d Omega stringer's web half length, mm

D_{11} Laminate bending stiffness coefficient in 11 direction, Nmm

E_{11} Lamina Young's modulus along fibers, MPa

E_{22} Lamina Young's modulus normal to fibers, MPa

$E_{sk,xx}$ Skin young's modulus in longitudinal direction, MPa

F Force matrix, N

$f'(x)$ unfitness function, kg

$f(x)$ objective function, kg

F^{REF} Reference shortening force, N

f_1 Omega stringer's feet length, mm

f_2 Omega stringer's flange length, mm

$F_{c\|}$ Sectional crippling strength, MPa

F_{cc} Sectional compressive strength, MPa

F_{eq} Equivalent static force, N

FI_{11C} Failure index in compression along the fiber direction, -

FI_{11T} Failure index in tension along the fiber direction, -

FI_{22C} Failure index in compression perpendicular to the fiber direction, -

FI_{22T} Failure index in tension perpendicular to the fiber direction, -

FI_{max} Maximum failure index, -

$g(x)$ constraint function, -

G_{12} Lamina shear modulus, MPa

h Distance between the middle skin surface and the stringer top flange, mm

h nonlinear analysis iteration, -

h_c Omega stringer height, mm

h_o Distance between the middle skin surface and the centroid of the stiffened panel, mm

i Time step index, -

I_c^* Moment of inertia of stringer of length l taken with respect to η, mm^4

I_{sk} Moment of inertia of the skin, mm^4

I_{sk} Skin moment of inertia per unit width with respect to η_o axis, mm^4/mm

j Constraint index, -

K Stiffness matrix, N/mm

k ESLM iteration, -

K_L Linear stiffness matrix, N/mm

$k_{x,global}$ Global panel collapse load coefficient, -

L Lagrange function, -

l Design variable index, -

l Length of half stringer profile, mm

L' Effective stiffener length, mm

m Number of buckle half-waves in longitudinal direction, -

n Number of buckle half-waves in circumferential direction, -

$N_{x,cripp}$ Total panel crippling force, N

$N_{x,cripp}$ Total panel crippling force, N

$N_{x,global}$ Global panel collapse load, N

o Number of selected designs based on ranking, -

P Buckling load, N

p One-half of reinforcing omega pitch, mm

p penalty power, -

q Number of chosen time steps, -

R Radius of omega stringer corners, mm

r Design response, -

r penalty multiplier, -

$R_{cripp,FEM}$ Crippling force correction factor based on FEM results, -

$s_{11,c}$ Lamina compressive failure strain in fiber direction, -

t Section thickness, mm

T_0 Control fiber orientation at z=0, °

T_1 Control fiber orientation at z=b/2, °

u Shortening displacement, mm

u position in XX direction, mm

v position in YY direction, mm

w Transverse displacement, mm

X Set of feasible design variables x, -

X initial position in XX direction, mm

y Number of sampling points in DOE, -

z Displacement matrix, mm

z distance along z axis from the panel center, mm

Acronyms

1D . . . . . one-dimensional

2D . . . . . two-dimensional

3D . . . . . three-dimensional

AFP . . . . . Automated Fiber Placement

ATL . . . . . Automated Tape laying

CFRP . . . . . Carbon Fiber Reinforced Plastic

CS . . . . . Certification Specifications

CTS . . . . . Continuous Tow Shearing

DMAP . . . . . Direct Matrix Abstraction Program
DOE . . . . . Design Of Experiments
DQM . . . . . Differential Quadrature Method

ESLM . . . . . Equivalent Static Load optimization Method

FAR . . . . . Federal Aviation Regulations
FE . . . . . Finite Element
FEM . . . . . Finite Element Method
FI . . . . . Failure Index
FPP . . . . . Fiber Patch Preforming

GA . . . . . Genetic Algorithm
GRSM . . . . . Global Response Surface Method

KKT . . . . . Karush Kuhn Tucker

MSCADS . . . . MSC version of Automated Design Synthesis

QI . . . . . Quasi Isotropic

TFP . . . . . Tailored Fiber Placement

UAV . . . . . Unmanned Aerial Vehicle
UD . . . . . Unidirectional

VAT . . . . . Variable Angle Tow

1 Introduction

In this chapter, the motivation for the conducted research is provided and followed by literature review relevant to the research topic. At the end of the chapter, the objectives of this dissertation is described. However, fundamentals of optimization theories and mechanics of composite materials are assumed to be known by the readers, thus they are only briefly discussed.

1.1. Motivation

Since Carbon Fiber Reinforced Plastic (CFRP) offer very attractive lightweight potential thanks to their weight-specific properties, they have become the choice of material in various primary and secondary aerospace structures. Thanks to cutting-edge manufacturing technique such as Automated Fiber Placement (AFP) machine, in-plane, curvilinear fiber laminates have been able to be realized. This has opened up a great opportunity for engineers to further optimize laminates' structural performance albeit additional manufacturing concerns. Among other improvements, significant buckling stability obtained by steered-fiber laminates has, in recent years, widely attracted interests from aerospace structure community and industrial players whose ultimate goal is radical structural weight reduction. As buckling stability is undoubtedly one of the most important aspects in thin-walled structural designs, considerable mass reduction is expected should buckling performance is largely improved.

After the advent of initial skin buckling of a stiffened panel, the panel shortening stiffness is likely to reduce but higher shortening load can still be withstood thanks to unbuckled longitudinal stiffeners. The panel shortening curve generally goes along the secondary stiffness path in the postbuckling regime. Shown in figure 1.1, for example, the design load is restricted by the first buckling load in the buckling-free design. Assuming the first-ply failure load as the ultimate design load, this ultimate design load must be greater than 150% design load level, given a safety factor of 1.5. In a buckling-free stiffened panel, such ultimate load is however considerably greater than the 150% design load threshold. A more exploited design which allows the design load well beyond the first buckling occurrence and narrows down unnecessary margin between the ultimate load requirement and the actual ultimate load would lead to significant increase in load capability. In other words, considerable weight saving can be expected when load level is kept constant. Beyond the first-ply failure load, higher load could still be absorbed until the final laminate failure, which is caused by either global panel collapse or stringers crippling depending on panel geometry and load redistribution between skin and stiffeners. The ultimate load in this research is however conservatively restricted by traditional first-ply failure and not the final panel failure caused

by global collapse or crippling load.

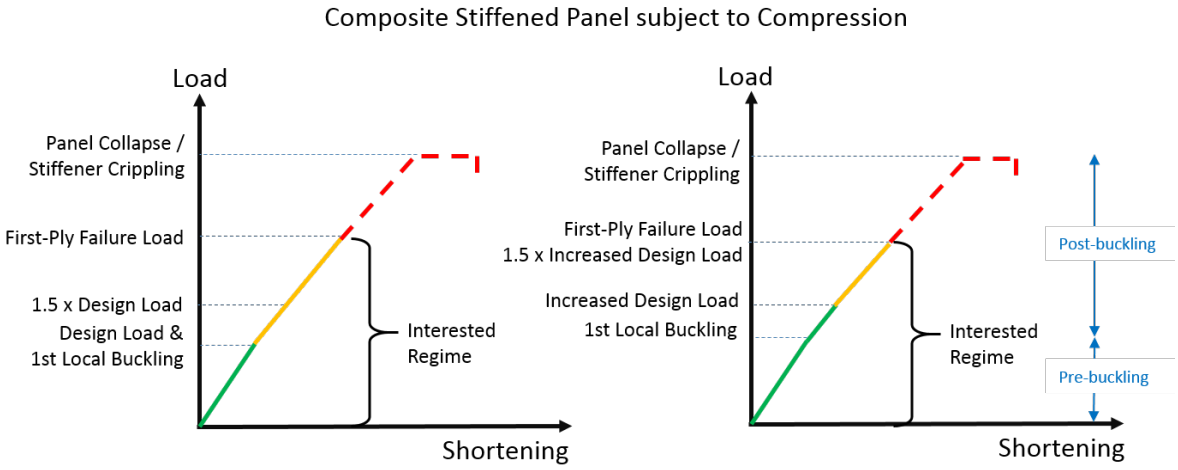

Figure 1.1.: Design scenarios of a stiffened panel under shortening load: buckling-free design (left), proposed design (right)

Achieving the weight-optimal, steered-fiber stiffened panel, in which postbuckling is allowed, is however far from straight-forward, albeit with the help of automated design optimization process. Firstly a design with variable fiber orientations mean larger number of design variables have to be considered. The fact that these design variables introduce highly multi-modal design space makes the design optimization problem even more complex. Secondly a need of nonlinear postbuckling responses would prohibit an efficient linear static analysis-based optimization procedure. Lastly manufacturing considerations specific to steered-fiber laminates, like fiber buckling, fiber bending, tow gaps, tow overlaps would also have to be considered. Apparently there exists no suitable nor efficient design methodology applicable to thin-walled aerospace structures made by steered-fiber laminates. Therefore new design methodology is sought after in order to reach the ultimate goal: radical weight reduction in a relatively short timeframe.

1.2. Background and literature review

1.2.1. Steered-Fiber Laminates

One of the earliest efforts in optimizing steered-fiber laminates was done in 1989. Hyer and Charette[17] showed that 89% tensile failure load increase, with respect to Quasi Isotropic (QI) plate with a central circular hole, can be obtained because of curvilinear fibers ability to favorably re-distribute load path. Further investigation done by Hyer and Lee[18] identified optimal fiber course for compressive buckling resistance, and found up to 85% improvement compared to a quasi-isotropic plate with a central circular hole. Single-loadcase scenarios however do not reflect typical real-world applications. Besides, these promising figures did not account for any manufacturing requirements. It is also worth noting that the aforementioned outcomes were not achieved by an automated design optimization procedure but rather from a fiber angle sensitivity analysis. Interest in steered-fiber laminates has stepped

up over time. A linear variation of the fiber orientation over a single axis was introduced by Gürdal and Olmedo[12]. This way only two design angles per ply are required for the optimization. Less chance of fiber format complexity is also an advantage at the price of less design flexibility.

As advanced, automated tow placement machine has been made available, variable-stiffness laminates have been designed, optimized, manufactured, and tested[49;57]. Since either tow gaps or overlaps are unavoidable by such process, several researchers therefore shifted their attention towards effects of these impurities or even developed new manufacturing techniques where gaps and overlaps were diminished e.g. Continuous Tow Shearing (CTS)[24]. The effects of defect layers caused by gaps and overlaps were studied by Fayazbakhsh et al.[9]. It was found that a gap area of 12% would result in 12% reduction in buckling resistance whereas an overlap area of 10% would result in 30% increase in buckling load. In terms of stiffness, 15% reduction and 10% increase were shown in case of gap and overlap design, respectively. Nevertheless both types of defects are detrimental to laminate strength as compared to pristine conditions. Gaps and overlaps therefore definitely alter laminate performance. However their influence in terms of buckling resistance is considered not so significant that it must always be considered. For instance, a proper gap-overlap hybrid design would likely result into an insignificant drop in buckling performance (albeit a higher reduction in terms of strength). These effects are hence neglected in this buckling-related dissertation to provide a clear demonstration of the thesis focal point: optimization technique via equivalent static loads when postbuckling constraints are included.

Lamina's planar mechanical properties are known to be varied by trigonometric functions when fiber orientation changes. Optimizing laminate fiber orientations would very likely fall into a local optimum due to highly-multimodal design space caused by superimposing of several trigonometric functions unless inefficient non-gradient based strategies are chosen instead. The more number of variable fiber angles, the higher degree of multi-modality is. To tackle a fiber angles optimization problem, there have been mainly two approaches followed by the research community: direct fiber angle optimization and lamination parameters optimization. Direct fiber angle optimization is relatively straight-forward as fiber orientations are optimized until an optimal design objective is achieved. However, providing gradient-based optimization is utilized, there is no guarantee whether the optimum design retrieved is a local or global one. This approach is suitable when a limited number of angles or laminate layers are interested. Fiber paths in this case can be constructed by a certain number of control points per layer. Fiber orientations between control points are interpolated by spline curves. Two points would form a linear variation format, while more than two points would give nonlinear fiber formats and subsequent improvement over the linearly-varied fiber format[59].

Lamination parameters on the other hand assure convex design space[11] ,but with a price to pay. Although only eight lamination parameters are enough to construct any arbitrary symmetric laminate, its optimization process is much more complex than the direct angle optimization. First, the feasible design region has to be identified; meaning interpretation of all design constraints in terms of lamination parameters is required prior to the optimization process[58]. Second, an optimal set of lamination parameters needs to be converted back to realistic fiber angles[54]. A single set of lamination parameters may as well lead to more than

one laminate stacking sequences. Lamination parameters however deem effective for a very large design problem with a large number of design angles. Ijsselmuiden et al.[19] found 189% buckling load improvement compared to a quasi-isotropic counterpart albeit lack of realistic fiber angle realization.

In this dissertation, the more straight-forward approach is followed, but with the help of thin-ply laminates which greatly mitigate multi-modality caused by stacking shuffling. Thin-ply laminates are to be discussed in details in sub-chapter 2.3.

1.2.2. Postbuckling Response Optimization via Equivalent Static Load Method

Most of the previous researches involving structural stability of stiffened, steered-fiber panels have focused on bifurcation buckling load maximization problems[55;59]. Highly efficient analytical buckling load formulation e.g. Rayleigh-Ritz energy method were developed and employed[7;20]. Less efficient but more accurate infinite strip method which discretize panels by one-dimensional strips was successfully implemented by Liu and Butler[29]. These efficient buckling load estimation methods were also expanded to postbuckling responses. Rahman et al.[43] used finite element-based perturbation method to calculate postbuckling coefficients, subsequent postbuckling stiffness, and reduced-order model beneficial for a quick optimization process. Wu et al.[60] developed a semi-analytical model based on variational principle and the Rayleigh-Ritz method to predict Variable Angle Tow (VAT) plate stiffness and stress in the postbuckling regime. Raju et al.[44] instead derived stress and transverse displacement functions based on coupled geometrically nonlinear governing differential equations. These differential equations were solved by Differential Quadrature Method (DQM). The method showed accurate results but with superior efficiency than the finite element method. White et al.[56] successfully demonstrated the application of DQM to curved panels. Raju et al.[45] investigated the effect of in-plane extension-shear coupling via the aforementioned DQM. Apparently attention by researchers on postbuckling optimization of composite panels has been limited, let alone steered-fiber stiffened panels.

The main reasons of such limitation could well be expensive postbuckling finite element analysis as well as design response sensitivities needed for gradient-based optimization techniques. Although semi-analytical methods mentioned above are very economical, they are specific to certain types of structural behavior and are limited to only initial postbuckling estimation and are no longer sufficiently accurate in the deep-postbuckling regime. Despite being less efficient, finite element method on the other hand offers more generic approach applicable to wide variety of different type of structures, loadcases, and boundary conditions.

Equivalent Static Load optimization Method (ESLM) for nonlinear analysis responses was initiated by Park and Kang[41] to efficiently transform nonlinear analysis responses into series of linear static response via equivalent static loads before conventional gradient-based optimization can be directly employed. Initial application target was to represent nonlinear dynamic responses from crash analysis, metal forming analysis, aerodynamic transient analysis, etc, by equivalent static loads and to apply the method to conventional

gradient-based size, shape, or topology optimization[25]. A few applications to nonlinear static analysis with geometrical nonlinearity and/or material nonlinearity were later successfully conducted[47]. These demonstrations nevertheless have been limited to non-buckled metallic structures. As the proposed ESLM significantly reduces the number of nonlinear analyses, which consumes a large portion of overall optimization duration, the method is very attractive especially during the preliminary design phase where high computational efficiency with acceptable accuracy is more desirable. Furthermore, gradient-based optimization procedures for linear static loadcases are already well established. Seamless inclusion of an optimization problem with nonlinear analysis responses into conventional gradient-based linear static optimization also has the edge over other techniques in terms of familiarity, usability, and reliability in the eyes of optimizers who have experienced the conventional methods for a long time.

1.3. Objectives

As only few researchers have paid attention to weight optimization of stiffened panels made by steered-fiber laminates with a consideration of postbuckling constraints, this dissertation intends to explore weight reduction potential when postbuckling constraints are taken into consideration. Demonstration of the proposed method applied against real-life aerospace structures i.e. aircraft fuselage panels subject to the most relevant loadcases are illustrated. Weight saving comparison between optimized straight-fiber and optimized steered-fiber designs is also conducted to gage viability of steered-fiber structures.

Detailed study of equivalent static load method parameters influence is also focused. Subject to a similar optimization task, comparison of ESLM behavior to that of other applicable optimization techniques is presented and discussed. Efficiency and optimality verification along with influence of different optimization convergence criteria, influence of number of equivalent static loads, and verification of nonlinear responses represented by equivalent static loads are studied and presented.

Finally practical optimizers' guidelines are written for those who are new to ESLM for postbuckling responses. The proposed methodology should pave a way towards postbuckling optimization of large-scale structures with real number of loadcases.

2

Steered-Fiber Laminates

This chapter introduces steered-fiber laminates to the readers. Spatially, linearly-varied fiber format utilized throughout the research work is described and illustrated. Thin-ply laminate is introduced before a demonstration of their benefits towards design space multi-modality is described. Several automated manufacturing technologies suitable for steered-fiber, thin-walled panels are also briefly outlined.

2.1. Introduction

Steered-fiber path or curvilinear fiber format causing in-plane, variable stiffness properties has attracted aerospace research community since 1990s thanks to its ability to exploit anisotropic nature of fiber reinforced plastic materials. In particular, strength, stiffness, and geometrical stability can be considerably improved by the utilization of optimized steered-fiber laminates. Vice versa, these improvements can be converted into structural mass saving providing the same external loads are exerted. When maturity of automated fiber placement machine enabled the realization of such innovative type of structures, interests towards them has continued to grow. However, curvilinear-fiber laminates will only outperform straight-fiber counterparts when few loadcases are highly dominant from the rest. If there were a number of loadcases reside in the same order of magnitude without the prevailing ones, then the benefit would become marginal. Having said that, certain aerospace structures, e.g. fuselage keel and crown panels, where few, if not a single, loadcases dominate seem to be good candidates for steered-fiber laminates. Apparently, pressure from aviation regulations and environmental concerns are driving the weight reduction demand. Steered-fiber laminates could well soon start replacing the traditional counterparts and taking off into the sky.

2.2. Linearly-Varied Fiber Path

Linearly-varied fiber path provides an in-plane curvilinear fiber path which is governed by two control points or two fiber angles. Firstly introduced by Gürdal and Olmedo[12], the simple, pre-defined fiber path has become the first choice of researchers who want to conduct a new investigation in this particular steered-fiber laminates field. Although being simple, its ability to distribute in-plane buckling loads towards stiffened edges where stringers are located led to 35-67% compressive buckling load improvement with respect to straight-fiber laminates[55]. Since cylindrical fuselage shells were chosen as investigation specimens in this research, the constitutive equation of linearly-varied fiber path along the circumferential direction (z) of a cylindrical panel is the following:

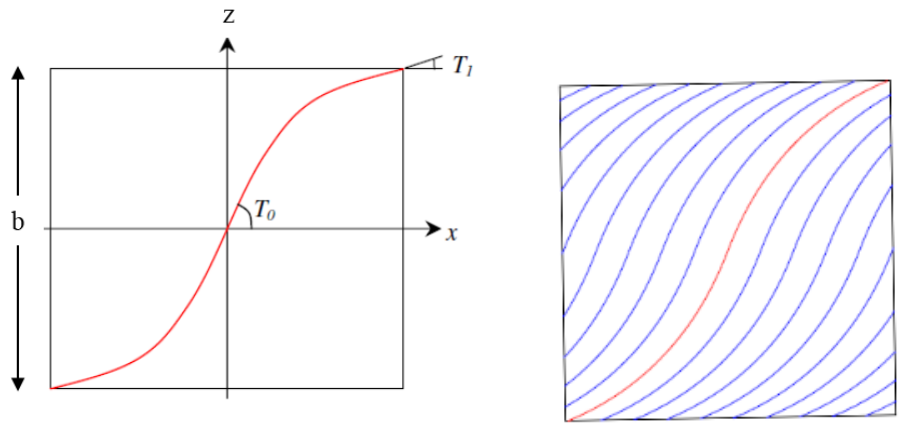

(a) Parameters (b) pattern $\langle 60|15 \rangle$ along z-axis

Figure 2.1.: Linearly varied fiber pattern

$$\theta(z) = T_0 + 2\frac{|z|}{b}(T_1 - T_0) \tag{2.1}$$

Corresponding linearly varied fiber path can be illustrated in figure 2.1. In order to model spatially linear variation of fiber orientation in a finite element model, the panel was spatially discretized into a number of finite element strips along the circumference of a stiffened fuselage cylindrical shell. As shown in figure 2.2 and 2.3, corresponding stiffened cylindrical panel consists of skin and longitudinal stringers. Each skin bay between two stringers is divided into nine longitudinal strips to allow linear ply angle variation from angle α_1 at the bay center (blue) to angle α_2 at the bay boundaries (yellow), where a stringer is located at. This pattern repeats till panel edges. Fiber orientation in every finite element belonging to the same strip was made identical. Discretization with smaller intervals would give simulated fiber paths closer to the real trajectory which would then result into more accurate, i.e. higher, structural improvement but at the cost of higher modeling complexity.

Optimal steered-fiber laminates, in which fibers vary along the fuselage circumference, were sought after in order to demonstrate structural performance gained by variable-stiffness panel. Ply angles α_i, β_i, γ_i as well as ply thicknesses were design variables. Relevant manufacturing aspects, e.g. gaps, overlaps, fiber path curvature, were neglected as they were not a focal point of interest as mentioned earlier.

2.3. Thin-ply Laminates

Baseline [+45/-45/0/90]2s skin laminates were reconfigured into thin-ply symmetric laminates with five-time repetition (5s), producing 60-ply smeared laminates [+45/-45/0_2/90_2]5s. There are several advantages from this kind of laminate. The most important reason being stacking sequence effects become almost nullified as the laminate is through-the-thickness homogenized; multi-modality in optimization design space thus subsequently becomes subtle.

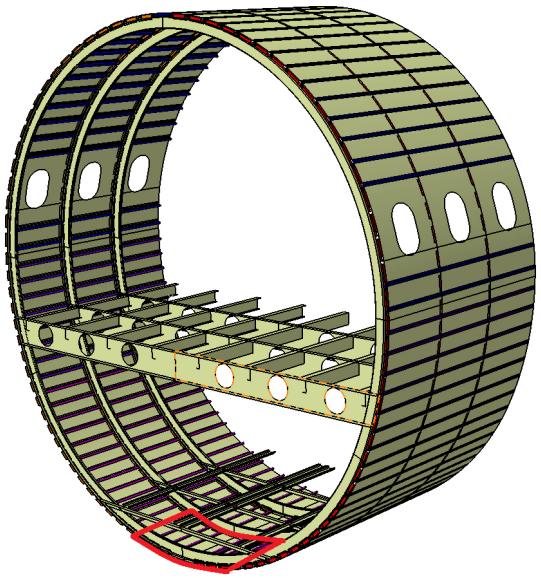

Figure 2.2.: Cylindrical fuselage: Stiffened keel panel

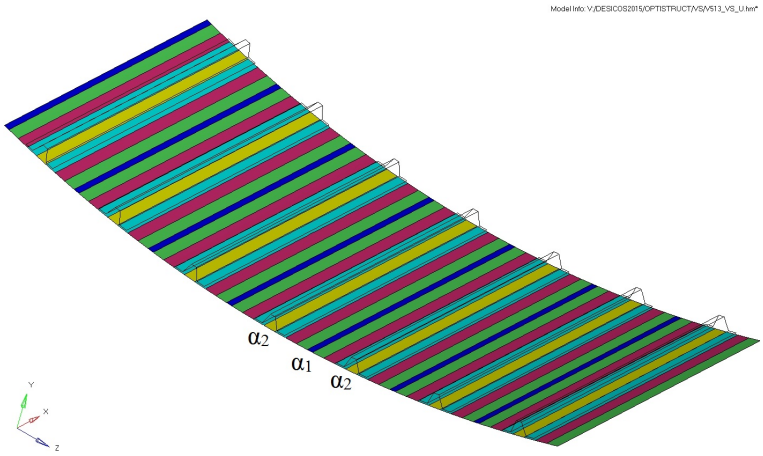

Figure 2.3.: Finite element model grouping for linearly varied fibre path and control angles

This was done to reduce the risk of being trapped in a local optimum. Furthermore, bending-twisting stiffness coefficients, D_{16} and D_{26}, would become marginal. Secondary bending (D_{22}) and twisting (D_{66}) coefficients are subsequently improved despite a compromise of the primary bending stiffness (D_{11}). Several other structural characteristic improvements, e.g. impact damage tolerance, secondary-axis and shear stiffness, shear buckling resistance, have also been proven and reported. Albeit having several advantages, smearing effect contracts design space by limiting bending stiffness tailoring (D_{11}), making obtainable optimum slightly inferior to that of optimized non-smeared laminate. Minimum ply thickness is also a practical limitation against the realization of thin-ply laminates. One of the most thinnest ply commercially available is TeXtreme spread tow Unidirectional (UD) tape. Its 0.02mm-tape thickness is reportedly available[39]. Computational efficiency gain has however been found to be on a superior side in the computational efficiency-design optimality trade-off[46].

To illustrate the effect of aforementioned homogenization towards laminate ABD matrix, results from Sasikumar's master thesis[46] is borrowed and revealed as the following. An optimized straight-fiber laminate for uni-axial buckling was found to be [±47/±90/±90]s. ABD matrix change when the laminate was homogenized to [±47/±90/±90]5s while retaining laminate thickness at 2mm is shown in table 2.1. It can be seen that the bending stiffness D_{11} is now reduced, affecting the optimized buckling resistance in this direction. However, Bending stiffness in transverse direction D_{22} and twisting stiffness D_{66} are improved to compensate the loss of D_{11}. Moreover, coupling bending stiffness D_{16} and D_{26} are almost eliminated, benefiting buckling performance by limiting energy loss due to coupled motions. Still, the thin-ply laminate was less resistant to buckling load in 11 direction thanks to Steiner's theorem. In the optimization process, the optimal fiber orientations retrieved from these two types of laminates will be different as the best fiber angles for conventional laminate will not be optimal for the thin-ply laminate configuration. The optimization routine will instead find the best fiber orientations that suit the given thin-ply laminate. Resulting optimality decrease by the use of thin-ply laminates thus becomes marginal, i.e. less than 4%[46].

2.4. Manufacturing Techniques

There are currently several manufacturing technologies deem applicable for producing steered-fiber laminates. Each of the manufacturing techniques requires specific attention to possible undesirable effects when fabricating such steered-fiber laminated components. Depending upon the extent of local fiber bending, in order to avoid fiber wrinkles, minimum, in-plane radius of fiber path curvature permitted by each technique is different. Obviously, the smaller radius allowed is, the better laminate property exploitation will be. Gaps and overlaps have also been concerned when producing this type of laminate via fiber tow placement machine. The effects of gaps and overlaps however are considered not compelling in terms of buckling and stiffness as discussed in subsection 1.2.1.

Consequently, manufacturing requirements, e.g. min. in-plane radius of fiber curvature, gaps/overlaps effects, were not included in this nonlinear buckling optimization work. Structural improvements gained by ideal variable-stiffness panels was instead of interest. In-plane radius verification of optimized fiber path obtained were anyway conducted and

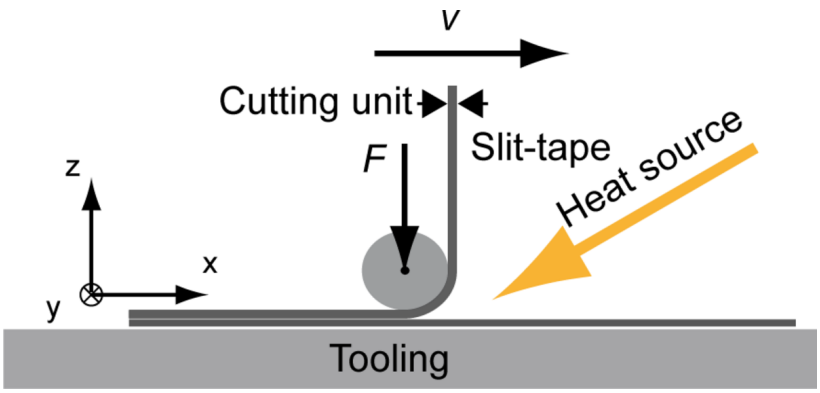

(a) AFP Process

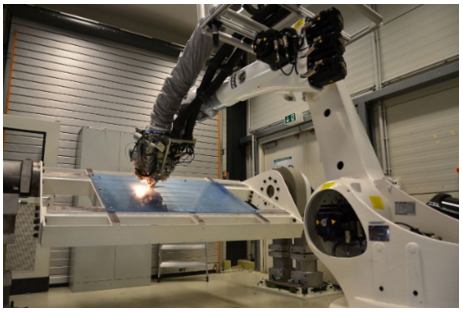

(b) AFP Machine

Figure 2.4.: Automated Fiber Placement Process and Machine[27]

discussed. Ultimately, the dissertation would rather shift the consideration of manufacturing constraints towards the need of manufacturing technology advancement. For example, an observation were to be made on how far the fiber tow curvature needs to be allowed in order to match a suggested optimized solution. Curvilinear-fiber laminates can be fabricated by several state-of-the-art automated manufacturing techniques described in the following subsections.

2.4.1. Automated Tape Laying (ATL) and Automated Fiber Placement (AFP)

The most established technique is currently the AFP machine in which pre-impregnated fiber tows are steered and placed on a mold surface by heat and pressure. The maximum curvature of steered tows is however somewhat limited by the machine as well as material characteristics. Overly curved fiber tow would lead to local fiber buckling. These limitations hinder a full exploitation of steered-fiber laminates. The minimum allowable radius of 635mm was reported[37]. Obviously, a radical improvement in materials and manufacturing process is desirable. Another disadvantage of variable angle tow manufactured by AFP machine is inherited gaps and overlaps caused by shifted finite tow width[13]. Automated Tape laying (ATL) machine uses the same concept as AFP, only that fiber tapes, instead of fiber tows, are laid onto a mold surface.The AFP technology is able to handle more complex layup geometries than the ATL robot. However the AFP is slower than ATL in terms of deposition rate. Figure 2.4 illustrates the machine process schematic.

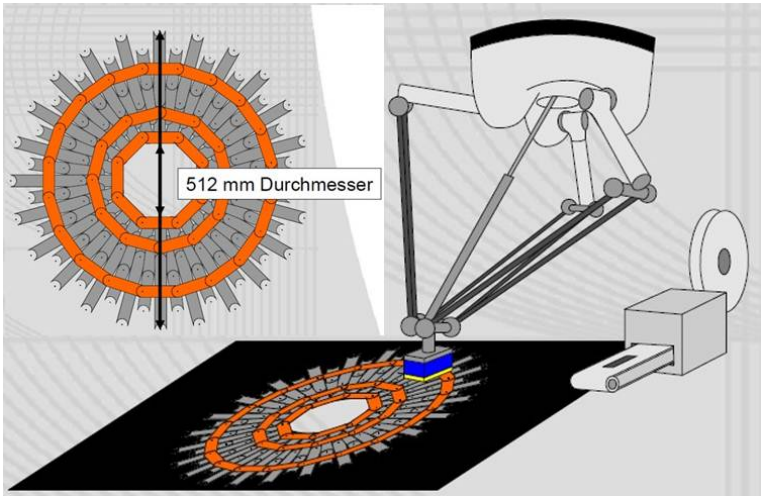

Figure 2.5.: Fiber Patch Preforming Schematic

2.4.2. Tailored Fiber Placement (TFP)

Invented by Leibniz Institute of Polymer Research, Dresden, Germany in 1992, Tailored Fiber Placement (TFP) is a steered-fiber composite manufacturing method utilizing textile process. Dry carbon fiber rovings may be stitched on a base material (substrate) in any desired orientation and any fiber quantity can be chosen. This method offers a very economical, automated, and repeatable manufacturing process for an optimized roving orientation and distribution. It has been applied to fabricate optimized complex structures derived from 3D topology optimization. In aerospace, the method has seen however quite a limited successful cases, partly due to limitation in size and speed. The biggest problem however is the stitching thread which creates micro-holes, which consequently create resin pockets when the preform is impregnated.

2.4.3. Fiber Patch Preforming (FPP)

The automated Fiber Patch Preforming (FPP) technique invented by Meyer[34] is conceived to provide more orientation freedom to steered-fiber laminate designers than the AFP. The process forms layers of repeatable fiber patches coated with adhesive along component surfaces. Patch geometry and orientation can be precisely specified thanks to automated robotic placement process. Figure 2.5 illustrates the fiber patch placement process schematic. Poor properties due to discontinuous fibers from one patch to another have to be compensated by effective patch overlapping pattern. 86% strength properties can be achieved while elastic moduli are practically the same compared to continuous fiber-reinforced laminates. Damage tolerance as well as strength after impact was found satisfying. However, significant increase in process speed would have to be found if FPP was poised to manufacture large commercial airframes as its current deposition rate is at 72 cm^2/minute. The FPP is especially attractive when high radius of fiber path curvature is required e.g. around cutouts.

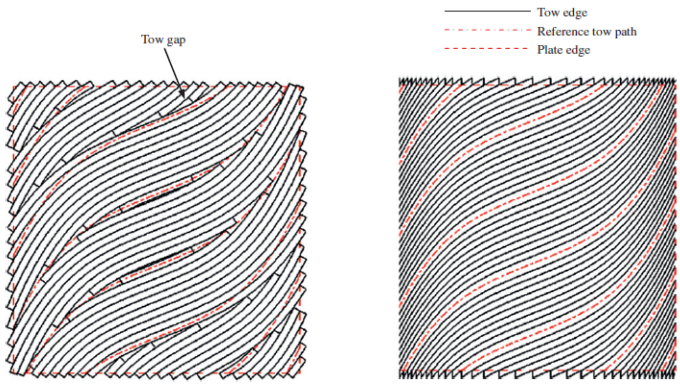

(a) AFP (tow drop) (b) CTS

Figure 2.6.: Tow arrangement of varaible angle tow plate madeby AFP and CTS techniques[24]

2.4.4. Continuous Tow Shearing (CTS)

Continuous Tow Shearing was invented and developed by Kim et al.[24] with a purpose of eliminating defects inherent from AFP process e.g. gaps and overlaps. Instead of bending fiber tow to create a curvilinear format, CTS steers the tow by continuous in-plane shear deformation. This way, local fiber wrinkling and straightening, normally occurred by conventional tow shearing, as well as process-induced defects i.e. gap and overlap can be prevented in return of tow thickness variation due to lateral compaction caused by poisson effect. The thickness build-up directly depends on shear angle. The newly introduced CTS offers much greater steering flexibility. While AFP limits minimum radius of curvature to be around 500 mm, that of the CTS technique is more than 10 times smaller depending on the tow laying speed. Tow arrangement comparison showing improvement of laminate quality by CTS over AFP is shown in figure 2.6.

Table 2.1.: Effect of thin-ply laminate

Matrix	[±47/±90/±90]s	[±47/±90/±90]5s
$[A]$	$\begin{bmatrix} 35130 & 23330 & 0 \\ 23330 & 216800 & 0 \\ 0 & 0 & 28590 \end{bmatrix}$	$\begin{bmatrix} 35130 & 23330 & 0 \\ 23330 & 216800 & 0 \\ 0 & 0 & 28590 \end{bmatrix}$
$[B]$	$\begin{bmatrix} 0 & 0 & 0 \\ 0 & 0 & 0 \\ 0 & 0 & 0 \end{bmatrix}$	$\begin{bmatrix} 0 & 0 & 0 \\ 0 & 0 & 0 \\ 0 & 0 & 0 \end{bmatrix}$
$[D]$	$\begin{bmatrix} 18530 & 16070 & 2823 \\ 16070 & 48850 & 3258 \\ 2823 & 1303 & 1782 \end{bmatrix}$	$\begin{bmatrix} 12960 & 9304 & 384 \\ 9304 & 67960 & 443 \\ 384 & 443 & 11050 \end{bmatrix}$

3

Structural Considerations of Composite Aerospace Structures subject to Buckling Loads

In this chapter, load definitions and operational design loads relevant to a fuselage keel/crown panel and a fuselage side panel are described. The selected fuselage panels serve as specimen for the proposed postbuckling responses optimization via equivalent static load method. Both panels would have to experience considerable buckling loads in flight operations, making them suitable candidates for a clear demonstration. Furthermore, all other non-dominant but relevant loadcases would also have to be considered. The major structural requirements such as strength, stability, stiffness, fatigue and damage tolerance have to be taken into account when designing an airframe structure as outlined in aviation regulations e.g. Federal Aviation Regulations (FAR) Part 25, EASA Certification Specifications (CS)-25. More details of each of the requirement are elaborated below.

In this dissertation, important requirements i.e. strength and stability were only taken into consideration as the main thesis purpose is to demonstrate their effects towards the proposed methodology in regards of weight reduction and optimization process efficiency, and not to complete a detailed design of fully compliant fuselage panels. Possible consequences of other structural constraints are however qualitatively discussed herein.

3.1. Load Definitions and Design Loads

Load definitions outlining design limit load and design ultimate load specify operational limit load and limit loads multiplied by a prescribed safety factor respectively. Design loadcases necessary for a subsequent design optimization process are also described.

3.1.1. Load Definitions

Design Limit Loads

Design limit loads are maximum loads expected in operational service of an interested structure. The structure must be able to withstand limit loads without permanent deformation or detrimental damages. At any loads up to limit loads, the elastic deformation may not interfere with safe operation.

Desgin Ultimate Loads

Design ultimate loads are limit loads multiplied by the prescribed factor of safety. This factor is generally 1.5 according to CS-25[2]. The structure shall have the strength to withstand all ultimate loads. Although permanent deformation is allowed, structural integrity must still persist.

$$Ultimate\ Load = 1.5 \times Limit\ Load \tag{3.1}$$

3.1.2. Design Loadcases

The following loadcases deem the most critical for the fuselage panels optimized in this research work. The fact that buckling loads i.e. compression, shear, and combined compression-shear are all the dominant ones in these fuselage airframes, the use of steered-fiber laminates as an improvement from conventional straight-fiber counterparts seems to be promising. Although there are numerous loadcases occurring during the aircraft's operation, the most three relevant loading scenarios for fuselage cylindrical panels were considered herein:

1. Positive longitudinal bending moment

2. Lateral bending moment and Torsion

3. Internal pressure difference

These were derived from a single-aisle airliner fuselage loading scenarios reported by Hofheinz[15]. Loadcases derived from these three operational loadings are shown below. Load magnitudes revealed are all design limit loads. Safety factor of 1.5 applies to all cases except for internal pressure loads where safety factor of 2.0 is prescribed.

Fuselage Crown/Keel Panels

1. Pure Axial Compression = 642 N/mm (376747 N compression)
   Longitudinal fuselage bending moment during the take-off and landing produces compressive forces at keel and crown sections respectively. In reality, the keel panels typically experience higher load magnitude then the crown counterparts, but the more severe keel load is assumed here. The compression was applied to the structure in the form of shortening displacement.

2. Pure Shear = 55 N/mm (128150-Nm torsion)
   Lateral fuselage bending moment and torsion caused by rudder deflection when yawing and rolling the aircraft produces resulting shear flow to the keel and crown panels. Equivalent torsional moment inducing the same shear flow was applied instead in our case. In fact there exists a small longitudinal bending in this loadcase, but its axial compressive load (approx. 15% of the first loadcase) is neglected.

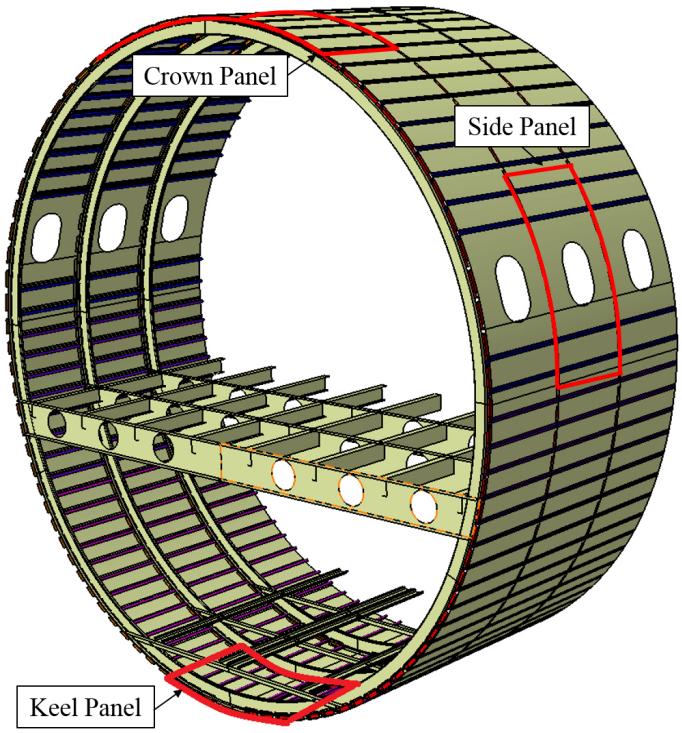

Figure 3.1.: Typical fuselage panels where buckling loads are critical: Crown, Keel, and Side panels

3. Internal Pressure = 0.06481 MPa
   Matching the same passenger comfort level to that of Airbus A350 or Boeing 787, cabin pressure is designed to be at 1,829 m (6,000 ft) at the aircraft's maximum cruise altitude of 13,137 m (43,100 ft). The resulting pressure difference marks approximately 14% higher than that of existing Airbus A320 or Boeing 737.

Fuselage Side Panels

1. Pure Shear = 100 N/mm (260000-Nm torsion)
   Longitudinal fuselage bending moment during the take-off and landing induces high vertical shear forces to the side panels. Equivalent torsional moment inducing the same shear flow was applied instead in our case.

2. Combined Compression-Shear = 294 N/mm (190877 N compression) & 40 N/mm (100360-Nm torsion)
   Lateral fuselage bending moment and torsion during yaw and roll generates compressive loads and shear flow, respectively, at fuselage side panels. Resulting shear flow derived from vertical shear force as well as torsional moment was taken into account. The compression was applied to the structure in the form of shortening displacement. Equivalent torsional moment inducing the same shear flow was applied instead in our case.

3. Internal Pressure = 0.06481 MPa
   The passenger cabin pressure is designed to be at 1,829 m (6,000 ft) at the aircraft's maximum cruise altitude of 13,137 m (43,100 ft).

3.2. Strength Requirement

As progressive failure mechanism determining the final failure of a composite material apparently requires a complex analysis and expensive experiments. Conservative, but straight-forward, first-ply failure criteria have been therefore employed instead, especially in a preliminary design phase. In many cases, the distance between the first-ply laminate failure and the final laminate failure is anyway not far apart, advocating the use of first-ply failure criteria. Maximum Strain first-ply failure criteria were chosen in this research. Direct relationship between spatial displacement gradient and engineering strain tensor supports the choice of selection since displacement-based equivalent static loads were later employed in the proposed optimization scheme. Other types of first-ply failure criterion could also have been used as well. No major differences in optimization results are expected due to different choice of laminate's first-ply failure criterion. A brief proof of the aforementioned spatial displacement gradient and engineering strain tensor relation is shown below:
Recalling two-dimensional (2D) normal Green strain for an infinitesimal material element:

$$\epsilon_{GXX} = \frac{\partial u}{\partial X} + \frac{1}{2}\Big[\Big(\frac{\partial u}{\partial X}\Big)^2 + \Big(\frac{\partial v}{\partial X}\Big)^2\Big] \tag{3.2}$$

Assuming geometrical nonlinearity but linear elastic material (valid assumption if first-ply failure index is less than unity), small strain - large displacement assumption can be made. The quadratic terms of displacement gradient can be neglected. Engineering strain equation is then achieved.

$$\epsilon_{XX} = \frac{\partial u}{\partial X} \tag{3.3}$$

The chosen maximum strain first-ply failure criteria are shown in equation 3.4. Although large deformation due to postbuckled skin was permitted, less or equal than unity Failure Index (FI) must be complied up to ultimate load level. This design strategy is still considered conservative as only structural integrity is demanded at ultimate loads i.e. damages are allowed as long as the structural components are still intact. It however offers a relatively straight-forward failure model consisting only a handful of simple equations. Exceeding beyond an advent of first-ply failure required highly expensive progressive damage simulation which is beyond our scope of study. Besides material linearity is also ensured as long as the first-ply failure criterion is obeyed.

$$\begin{gathered} FI_{11T} = \frac{\epsilon_{11T,max}}{\epsilon_{11T,allow}},\ FI_{11C} = \frac{\epsilon_{11C,max}}{\epsilon_{11C,allow}}, \\ FI_{22T} = \frac{\epsilon_{22T,max}}{\epsilon_{22T,allow}},\ FI_{22C} = \frac{\epsilon_{22C,max}}{\epsilon_{22C,allow}}, \\ FI_{12} = \frac{\gamma_{12,max}}{\gamma_{12,allow}}, \\ FI_{max} \leq 1.0 \end{gathered} \tag{3.4}$$

3.3. Stability Requirement

Thin-walled structures are often susceptible to buckling loads, i.e. compression, shear, and combined shear-compression loads, than other loading types as geometrical instability becomes an issue before their maximum stress reaches the material strength. As lighter structural weight is demanded due to economical and environmental reasons, thinner airframes are unavoidable. This makes stability requirement a very important consideration in aerostructures design process. Improper aerospace structures which overlook the critical buckling loads could result in a catastrophic scenario casted by a number of fatalities. A buckle-free design would offer the designer high confidence in safety, but this is opposite to weight saving demand. Thanks to stiffened panel's ability to absorb buckling load after the first local skin buckling, weight reduction potential for buckling-sensitive airframes therefore arises. The following subsections outline the initial buckling and postbuckling considerations in this dissertation.

3.3.1. Initial buckling

Referred to figure 1.1, the design limit load is typically restricted by the first local buckling load. In order to save more weight, the first buckling load can be allowed to be smaller than the limit load e.g. at 50% limit load, providing that the first-ply failure load occurs at or after the design ultimate load. Subject to limit load, linear bifurcation buckling requirement with respect to load factor can be formulated as follows.
Conventional Buckling-Free Design:

$$\lambda_1 \geq 1.0 \tag{3.5}$$

Proposed Postbuckled Design (50% limit load):

$$\lambda_1 \geq 0.5 \tag{3.6}$$

3.3.2. Postbuckling

After the first buckling, the applied shortening load follows a secondary stiffness path. As long as the first-ply failure load falls beyond 150% limit load level and the structure remains integral e.g. no stiffeners-skin separation until the ultimate load, the structure is considered safe.

3.3.3. Panel Collapse or Stiffener Crippling

As shortening load increases through deep postbuckling regime, either gradual stiffener crippling or sudden global panel collapse will occur, indicating the maximum load carrying capability has been reached. After this point, lower load might still be able to be withstood due to panel's residual load carrying. The destruction process quickly continues until a complete failure of the panel. In terms of design requirement, the design ultimate load must be lower than the peak load the panel can absorb; in other words, before the aforementioned

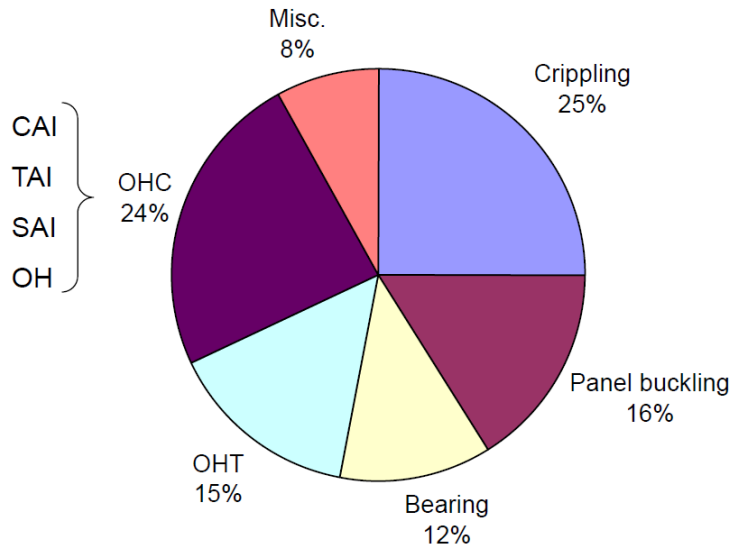

Figure 3.2.: Typical fuselage failure modes distribution[23]

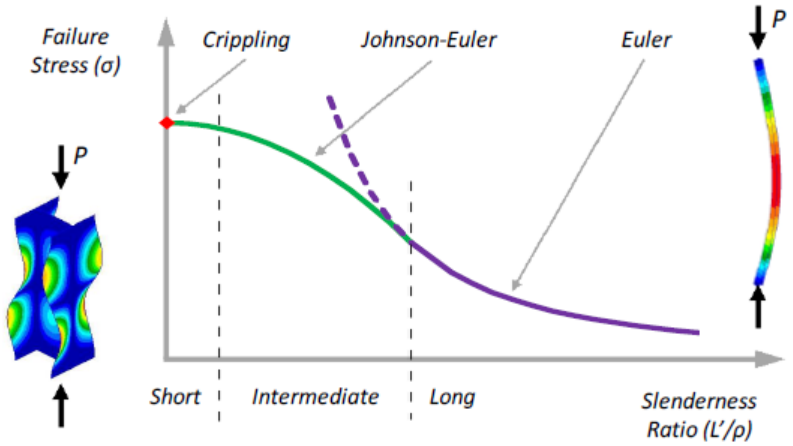

Figure 3.3.: Column stiffener failure behavior as a function of slenderness ratio[33]

failure event takes place. There are basically two modes of stiffened panel failure under shortening: global panel collapse and stiffener crippling. Shown in figure 3.2, crippling and global panel buckling are the most common failure modes found in typical fuselage structures.

Panel Collapse

Illustrated in figure 3.3, the buckling behavior of a thin-walled stringer is a function of slenderness ratio, which is defined by effective length (L') over radius of gyration (ρ). A long column will buckle in long waves with its cross-sections translating but the cross sectional shapes are maintained. The described buckling motion is so called global buckling or Euler buckling, which is named after the classical Euler formula. Since such a long column does

not exhibit considerable post-buckling capability, a long stiffened panel will collapse in a sudden manner when this kind of stiffener is buckled.

Stiffener Crippling

For a short column, the initial column buckling mode involves local short waves at the stiffener flanges, with the corners of the cross-section remaining straight. This type of buckling is called local stiffener crippling. Depending on their geometry, such columns has higher failure stress than the longer columns and tend to exhibit significant post-buckling capability, avoiding a sudden panel collapse. Accurate crippling simulation is presently still cumbersome and semi-empirical approach is usually followed. For the intermediate column slenderness, the semi-empirical Johnson-Euler curve is often used. Both global buckling and stiffener crippling modes can be expected to exhibit simultaneously in this intermediate regime.

Final panel failure must be ensured to commence after the design ultimate load is reached. As mentioned before, accurate prediction of collapse and crippling loads are somewhat complicate and expensive, a certain failure load margin was therefore prescribed in addition to aforementioned safety factor of 1.5. In this research work, 20% load margin between the design ultimate load and the advent of final failure was chosen. Any other margin value can be chosen as the current research focuses on relative improvement between straight- and steered-fiber laminates rather than a comprehensive fuselage structure design. The design requirements with respect to panel failure modes can be formulated as follows.

$$\begin{aligned} \lambda_{collapse} &\geq 1.2 \times S.F. \\ \lambda_{collapse} &\geq 1.2 \times 1.5 \\ \lambda_{collapse} &\geq 1.8 \end{aligned} \tag{3.7}$$

and

$$\begin{aligned} \lambda_{crippling} &\geq 1.2 \times S.F. \\ \lambda_{crippling} &\geq 1.2 \times 1.5 \\ \lambda_{crippling} &\geq 1.8 \end{aligned} \tag{3.8}$$

3.4. Stiffness Requirement

Stiffness requirements in the form of maximum allowable deformation, or natural frequency can be demanded. Elasticity and flexural rigidity determine how much structure is deformed when subject to in-plane loading and out-of-plane bending respectively. Too high displacement and/or rotation might cause collision between two or more components. Regarding the frequency restriction, the first few natural frequencies may be set to be greater than a certain value in order to prevent undesirable or unstable oscillation e.g. wing flutter which could lead to structure destruction. Material moduli play a vital role in structural stiffness characteristics. Based on Steiner's theorem, laminate stacking sequence tailoring offers flexural rigidity improvement without weight increase - an advantage of composites over metallic materials. Structural geometry and stiffening configuration also largely contribute to overall stiffness. In the presented work, there was no absolute stiffness constraint related to design

limit and ultimate load magnitudes, but equal or better stiffness than the baseline design can be asked for.

3.5. Fatigue and Damage Tolerance Requirements

Fatigue in structural mechanics is a degradation in material strength when the material undergoes repeating cyclic loading. Material fatigue has long been a critical design constraint in metallic structures. It was one of the main reasons justifying the employment of composite materials in aerospace structures as fiber reinforced composites exhibit much better fatigue behavior than the metals, significantly saving maintenance and repair cost.

Damage tolerance is the ability of a structure to tolerate a reasonable level of damage or defects that might be encountered during manufacturing or while in service, which do not result in catastrophic failure[38]. When thin-walled composites are introduced, fatigue is less a concern than damage tolerance behavior. Its delamination sensitivity to impact loading leading to considerable reduction in strength especially compression after impact (CAI) demands designer's close attention. Practical design guidelines have been followed to improve laminate damage tolerance. These include minimizing the grouping of too many plies, hybridizing CFRP with Kevlar or fiberglass, using fabric plies at the outer surface of the laminate.

Regarding the damage tolerance of buckling-optimized composite stiffened panel, Butler et al.[5] reported that damage tolerance constraint derived from compression after impact strength is less relevant than buckling constraint in thinner panels than thicker panels. However, damage tolerance constraint becomes relevant in steered-fiber panels with closely-spaced stiffening, while buckling constraint was found active in straight-fiber designs with the same stiffening topology. As critical damage tolerant strain is hardly influenced by skin thickness, it has been nevertheless observed that buckling constraint would be solely triggered once the panel skin became very thin e.g. less than 2 mm, regardless of stiffening spacing or fiber path curvature. As lightweight fuselage panels subject to buckling loads are generally very thin, though densely stiffened, omitting the damage tolerance constraint in such a shell design is thus not considered too optimistic. It was also interesting to see higher critical damage tolerance strain of steered-fiber panels than that of straight-fiber counterparts as buckling-optimized steered-fiber panels were more compliant than its straight-fiber counterparts. Moreover, the steered-fiber panels were less damage tolerant at mid-bay area than they were at stiffener locations.

Traditionally, a conservative design allowable ultimate strain is limited to around 0.4%. This is barely 35% of the prepreg ultimate strain used in this report. In order to fulfill more stringent weight saving demand, the allowable strain accounting for the damage tolerance requirements must obviously be adapted. This could be possible by new materials development and/or efficient design methodologies instead of applying the conservative allowable.

3.6. Environmental and Other Requirements

Apart from requirements depending on external loading condition described above, environment also affects material properties. Particularly, material properties in the well-known "hot-wet" conditions are reduced. For instance, fiber reinforced plastics' strength and stiffness decrease when absorbing moisture and being operated under elevated temperatures. A Hot-Wet knock-down factor has been therefore applied by structural engineers in order to be on a conservative side. Besides, notch sensitivity further undermine usable laminate strength. Although absolute, usable design allowables should be derived before designing a real structure, the consideration of these knock-down factors may not be necessary in a comparative study between straight- and steered-fiber laminated structures like in our case. As the environmental effects towards laminate properties are not at all influenced by fiber orientations, hence the proposed steered-fiber laminates are not at all more sensitive than the straight-fiber counterparts to these severe environmental conditions. Ultimately, a comparison of proposed steered-fiber panels to the best straight-fiber fellows is of interest rather than obtaining accurate optimized fuselage panel weight.

4

Challenges in Steered-Fiber Composite Aerostructures Optimization

In this chapter, challenges to be efficiently overcome when optimizing steered-fiber laminates taking postbuckling responses into account are elaborated. Two major problems exist: nonconvex design space and difficulty in postbuckling responses inclusion.

4.1. Nonconvex Design Space

Since traditional laminates normally consist of only $\pm 45°$, $0°$, $90°$ layers, decision on stacking sequence has to be made providing ply thicknesses are to be determined afterwards. Bending and twisting stiffness are greatly affected by laminate stacking sequence due to Steiner's effect (square of ply distance from laminate mid-plane). Tailoring such stiffness matrix by shuffling laminate stacking sequence optimization can be categorized as a combinatorial optimization problem. If conventional ply angles are allowed to vary, continuous-variable optimization algorithms can be applied. Parameterizing ply fiber angles have shown relatively considerable variation in laminate strength, stiffness, buckling resistance, among others, without an increase in mass. This has attracted composite structural designers coming with a view of further weight saving potential. It is however well-known that optimizing fiber orientation is associated with a non-convex design space consisting of many local minimums. For instance, figure 4.1 shows up to 15% buckling load variation when rotate ply orientation in a single segment. Non-convexity in buckling response is also observed.

As traditional sensitivities-based optimization algorithms could be trapped in a locally optimal design, previous research works in this particular field have deployed evolutionary or surrogate-based strategies despite their computational inefficiency. When solving a real-life optimization problem, computational efficiency is however often regarded as one of the highest priorities. A gradient-based optimization method was therefore employed in this research work to overcome the efficiency inferiority, but a supplemental scheme to reduce the chance of local optima trap was also proposed and implemented.

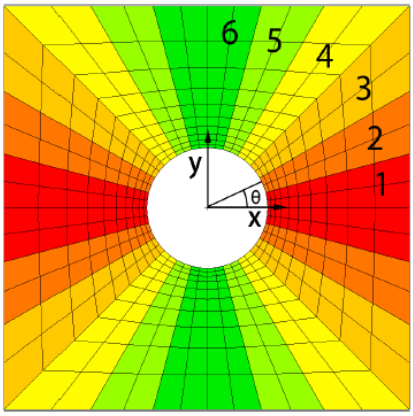

(a) Square plate with a circular hole

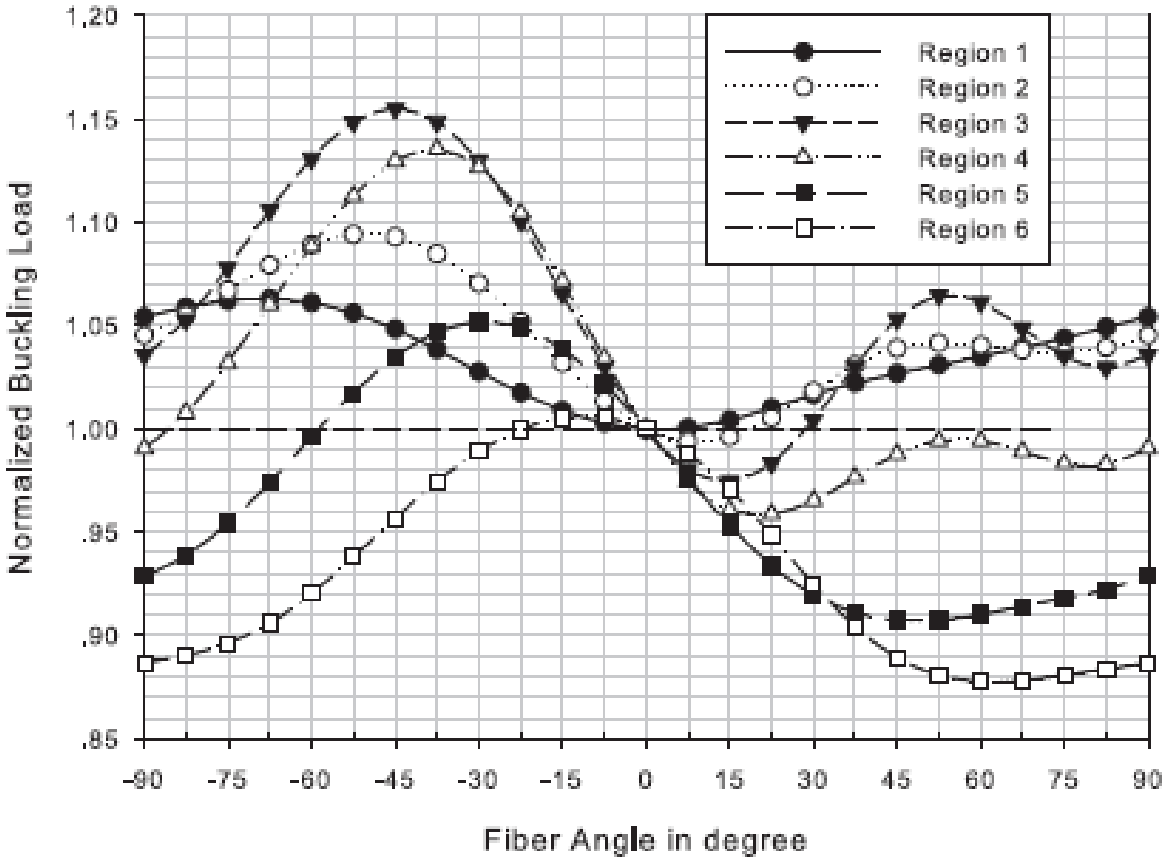

(b) Normalized buckling load vs Fiber angle variation

Figure 4.1.: Nonconvex variation in buckling loads when fiber angles are parameterized[31]

4.2. Inclusion of Pre- and Post-buckling Responses

4.2.1. Linear Bifurcation Buckling Responses

Compared to linear static analysis, solving an eigenvalue problem is time consuming per se even with an efficient power method like Lanczos algorithm. Solving a design optimization problem having buckling eigenvalues as design responses is more laborious since gradient analysis requires multiplications of finite element bifurcation buckling analysis, depending on design space dimension. Therefore, expensive finite element buckling analysis is often replaced with economical, closed-form approximate formulation, or analytical buckling sensitivities if available. There are several reports[10;50] citing that optimization process converges much faster and is less sensitive to number of buckling modes included when analytical buckling analysis is implemented. In the presented work, conventional but more accurate bifurcation buckling analysis was employed as efficient handling of postbuckling responses is to be demonstrated instead of linear buckling response handling.

4.2.2. Nonlinear Postbuckling Responses

More troublesome nonlinear postbuckling responses have been considered by only a few composite optimizers so far, albeit weight saving potential. The main reason being postbuckling analysis involving geometrical and/or material nonlinearity is computationally tedious, let alone more expensive optimization process. Especially when force loads are applied instead of displacement load, iterative nonlinear implicit finite element solvers e.g. Newton-Raphson tend to face divergence issue in Finite Element Method (FEM). The divergence problem comes from the stiffness matrix inversion process in force-displacement constitutive equation. Non-repeatable postbuckling design response is another concern. Iterative Newton-Raphson method is likely to struggle to give accurate design sensitivities as compared to non-iterative linear static analysis. In spite of these, input force loads are normally independent design parameters while displacements are dependent parameters or design responses. Subsequently, postbuckling gradients are either too expensive or difficult to obtain. More importantly, only a single unsuccessful nonlinear analysis would lead to premature termination of the whole optimization process. Maintaining convergent nonlinear buckling analysis is considered a very essential element in a gradient-based nonlinear analysis responses optimization. These deficiencies apparently advocate the selection of equivalent static loads method where number of nonlinear response analyses are greatly lessened, and direct nonlinear response sensitivities are omitted.

5

Optimization Techniques for Steered-Fiber Laminates

This chapter outlines the proposed gradient-based ESLM procedures. The procedures can be divided into two major stages: Design of experiments of thin-ply laminates and Equivalent static load method for postbuckling responses optimization. To comparatively study, an advanced response-surface based optimization technique i.e. Global Response Surface Method was additionally applied to fuselage side panels. Computational efficiency comparison of the two methods were compared afterwards.

5.1. Optimization assisted by Design Of Experiments of Thin-Ply Laminates

Because a gradient-based optimization is starting-point dependent, a global search procedure is proposed to provide few (3-5) good starting designs that would be then undergone the optimization scheme afterwards. In our case, Design Of Experiments (DOE) of thin-ply laminates introduced in sub-chapter 2.3 was carried out as the preparatory step. Global design space search via Latin-Hypercube DOE combined with homogenizing effect through thin-ply laminates helped alleviate the non-convexity caused by fiber orientation parameterization. It has been demonstrated by Sasikumar[46] that eliminating ply stacking sequence effect through laminate smearing significantly reduces the degree of design space multi-modality. As a result, less number of DOE sample points are needed to obtain the global optimum, despite slightly drop in performance compared to conventional optimized non-smeared laminates. For example, maximizing fuselage keel panel's bifurcation buckling load using a 60-ply laminate required 48% less number of initial sample points than a 12-ply laminate despite 3% decrease in optimized buckling load. Parametric study results obtained from other test cases are illustrated in table 5.1. Lesser degree of multi-modality was also reported in the case of constrained mass optimization problems.

For constrained mass optimization problems, constraints must also be taken into account in addition to design objective in oder to determine design ranking after the DOE process. In this dissertation, a penalized unfitness function commonly used in evolutionary algorithms was chosen as formulated in equation 5.1. As can be seen, the unfitness function ($f'(x)$) is only interested in violated or active constraints; non-active constraints do not contribute here. However, nonlinear analysis responses were too expensive to be included in this preparatory step; only linear analysis responses were therefore calculated. Usually set to be

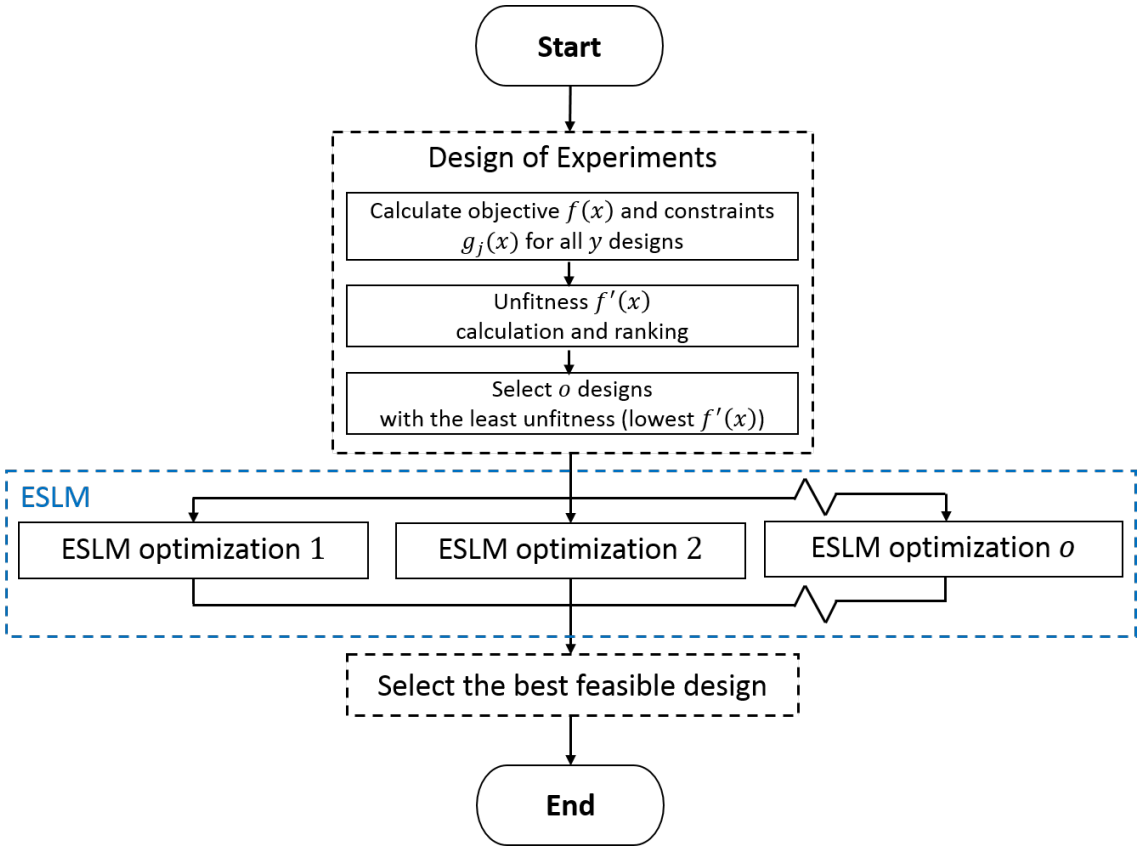

Figure 5.1.: Flowchart of Global Search Optimization Procedure

unity, larger-than-unity penalty power (p) can be given to constraints having higher priority than others. Greater-than-unity penalty multiplier (r) greatly differentiates infeasible design points apart from feasible designs; but too large value could result into sub-optimal solutions. After sorting the sample points with the prescribed unfitness function, the best few designs with smallest unfitness would be then fed to the gradient-based optimization scheme with ESLM as different starting designs. Decision on how many designs should be included is up to optimizer's discretion and problem non-convexity. On the one hand, more starting vectors would reduce the chance of local optimum trap. On the other hand, more initial points means more optimization runs, leading to cost and time expansion. Comparing all optimums, the best optimized design i.e. feasible lightest design suggested by the optimzation process with ESLM would be chosen. The proposed overall optimization scheme involving DOE of thin-ply laminates and ESLM is illustrated in figure 5.1. Although deem efficient compared to non-gradient methods, more effective design sampling such as an adaptive scheme generating infill points should further reduce the number of DOE.

$$f'(x) = f(x) + r \sum_{j=1}^{n} max[(g_j(x))^p, 0] \tag{5.1}$$

5.2. Optimization using Equivalent Static Loads to represent Postbuckling Responses

Shown in figure 5.2, the equivalent static load method specifically implemented for an optimization of composite stiffened panels comprises four main steps respectively: Geometrical nonlinear analysis, Equivalent static loads generation, Failure index correction, and Linear static gradient-based optimization process. The entire process reiterates until the predefined convergence threshold is met. In this case, design objective convergence dictates the ESLM process termination. The geometrical nonlinear static analysis was computed by MSC Nastran solution 106. Equivalent static loads were generated by a customized MSC Nastran Direct Matrix Abstraction Program (DMAP). MSC Nastran solution 200 was employed for the optimization task. The whole process was automated by an implementation of Altair HyperMath procedure. The details of each step are given below.

As can be observed, the outstanding advantage of this technique is the superior computational efficiency achieved by two key sources. First, the gradient-based scheme enables a quick optimized design search within a handful number of iterations, despite posing suboptimal solution risk. Second, sensitivities of the original nonlinear analysis responses do not need to be calculated, thus reducing computational burden drastically. Nonetheless, different nonlinear responses, e.g. displacement and stress, from an identical nonlinear loadcase may require different sets of corresponding static loads. Fortunately, only a single set of displacement-based static loads was required to represent both displacements, stress, strains, failure indexes in our case. Amidst postbuckling regime, infinitesimal strain assumption (equation 3.3) was still justified as material linearity was automatically persisted by the first-ply-failure constraint.

An argument of being unable to guarantee the global optimal solution can still be raised. The counterargument points to practicality in real-life design optimization process. The absolute global optimum is not interested as long as the process duration is unacceptable. A more efficient optimization procedure leading to a satisfactory design improvement is rather preferred due to the ever restricting time constraint in a real-world product development.

5.2.1. Geometrical Nonlinear Analysis

The first step of the introduced equivalent static load method for postbuckling responses optimization is solving geometrical nonlinear analysis and retrieve resulting nodal displacements. In our case, a uniform displacement load was applied instead of a uniform shortening force due to solver's significantly better convergence rate. Displacement-loaded panels (equation 5.2) do not require a time-consuming stiffness matrix inversion (K^{-1}), whereas force-loaded panels do require it (equation 5.3). However the applied displacement load must have been repeatedly adapted until it gave the specified ultimate shortening force (section 3.1.2). The iterative scheme for this displacement load is based on a linear interpolation (figure 5.3). The linear interpolation typically required three analyses per outer-loop optimization iteration (k) but the process could terminate anytime if the resulting reaction shortening force differed

Table 5.1.: Parametric Study: DOE of Thin-Ply Fuselage Panels $[\pm(T_{01}|T_{11})/\pm(T_{02}|T_{12})/\pm(T_{03}|T_{13})]_{nS}$ [46]

Parameter	n=1	n=3	n=5	n=∞
No. of Latin-Hypercube DOE	46	34	24	14
% Computational Cost	**100**	**78.3**	**52.2**	**30.5**
Optimized Buckling Factor	2.49	2.43	2.41	2.40
% Normalized Buckling Factor	**100**	**97.55**	**96.91**	**96.35**

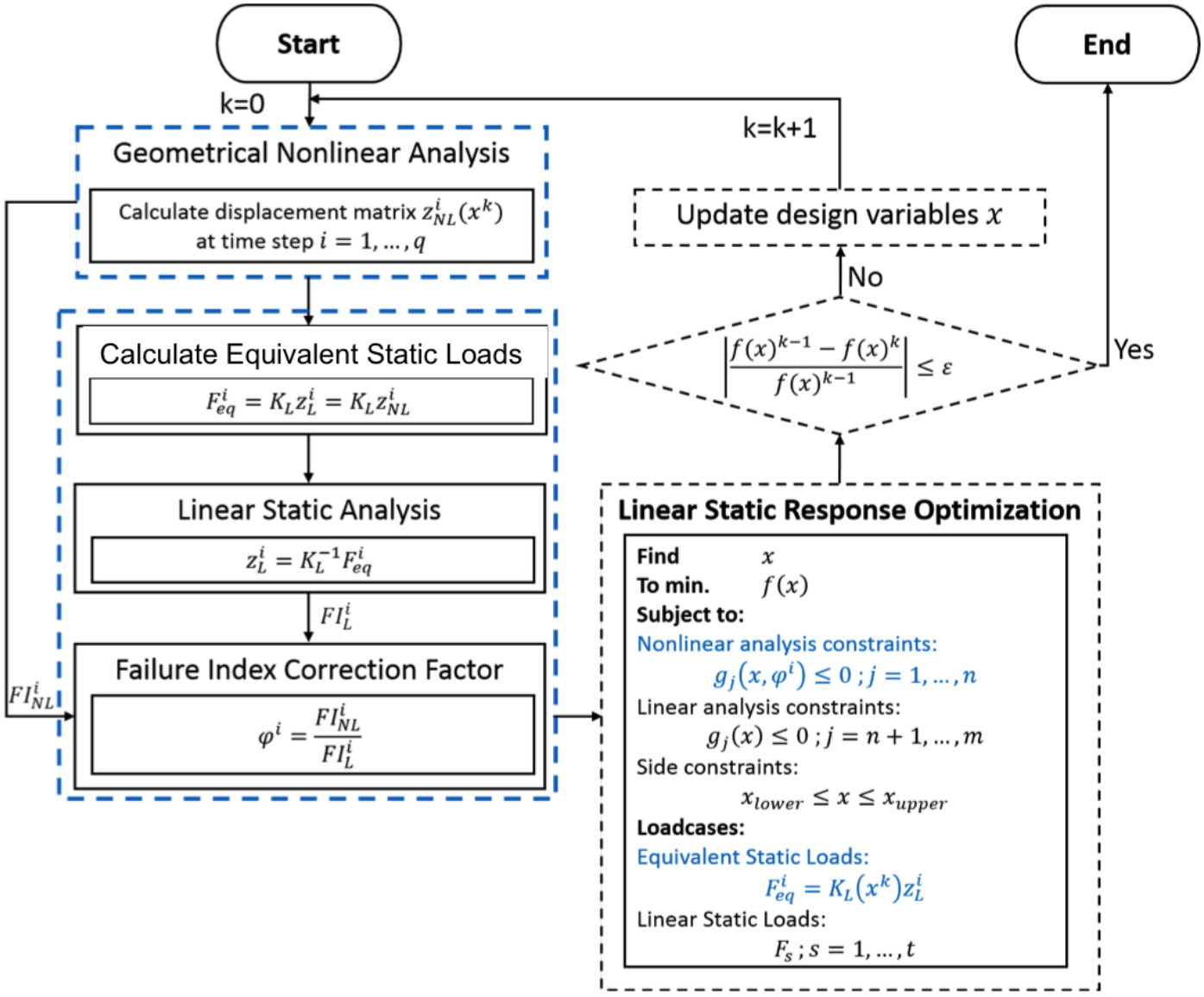

Figure 5.2.: Flowchart of Equivalent Static Loads Method for nonlinear analysis displacement and laminate failure index responses as part of the full optimization process

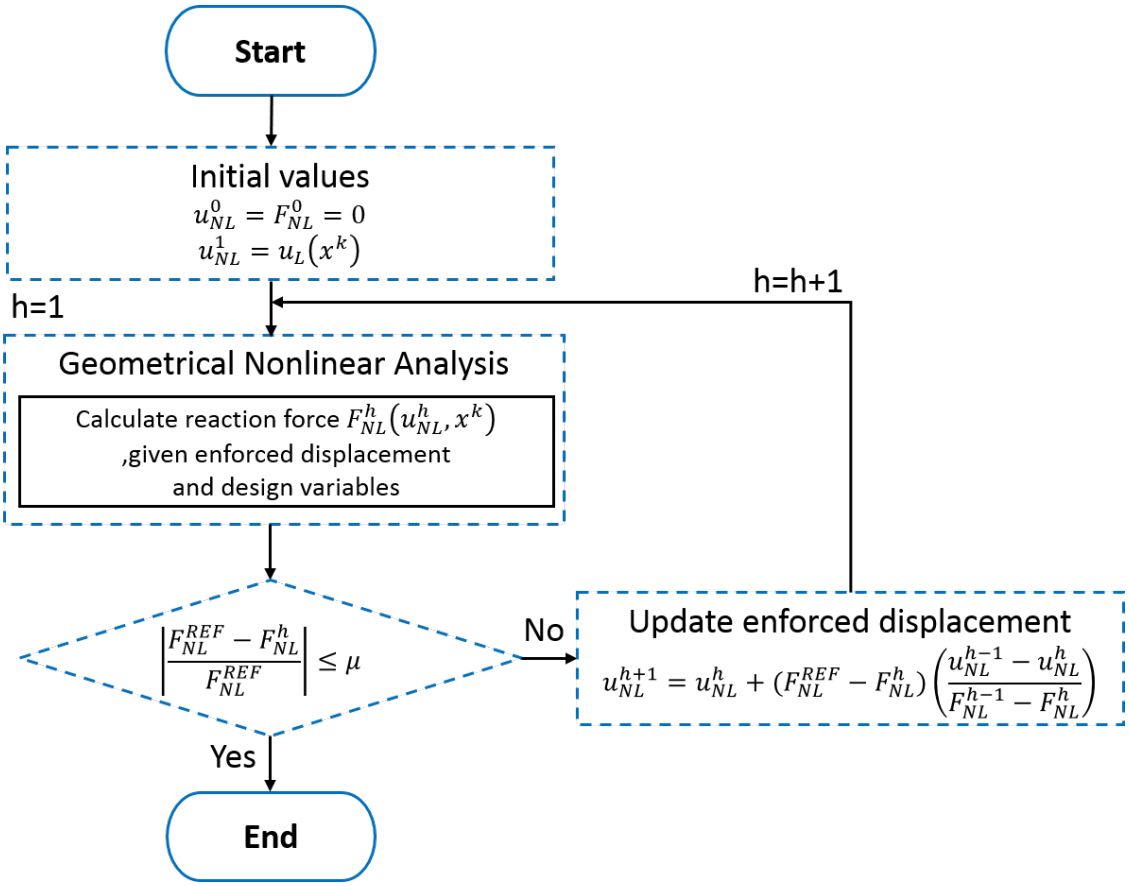

Figure 5.3.: Flowchart of iterative nonlinear analysis based on enforced displacement

less than μ from the specified input force load. μ was set to 1% in this research work. These re-analyses may offset the proposed method's computational superiority but it is still far economical than conventional gradient-based counterparts, where nonlinear analysis responses' sensitivities are obligatory. The presented scheme was also applied to an enforced rotation in the torsion loadcase.

$$F = Kz \tag{5.2}$$

$$z = K^{-1}F \tag{5.3}$$

5.2.2. Equivalent Static Loads Generation

A set of equivalent static loads representing interested nonlinear analysis responses e.g. postbuckling displacement, postbuckling stress/strain, were generated by a customized MSC Nastran DMAP using the displacement field obtained from the geometrical nonlinear analysis (section 5.2.1). The implemented DMAP codes are shown in appendix A.3. Shown in figure 5.4, a nonlinear analysis response type is represented by a series of linear static loads (f_{eq}^0 to f_{eq}^q) according to different time steps (t_0 to t_q). Equivalent static load (F_{eq}^i) generation from nonlinear nodal displacement field at time step (t_i) can be formulated as shown in equation 5.4. The displacement field at each time step can be converted into engineering strain per

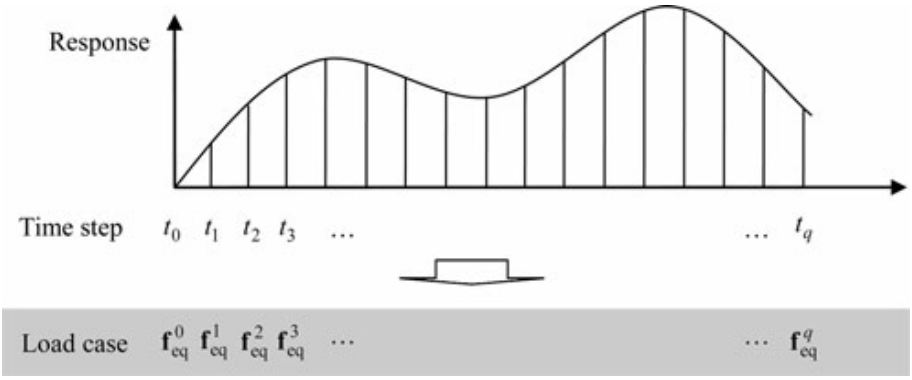

Figure 5.4.: Equivalent static loads generation[42]

equation 3.3 using the generated displacement-based equivalent static load. Number of equivalent static loads required depends on how nonlinear the response is; the most critical postbuckling reponse generally occurs at the last time step where load peak is reached.

$$F_{eq}^i = K_L z_{NL}^i; i = 1, 2, 3, ..., q \tag{5.4}$$

5.2.3. Corrected Failure Index Response

Resulting strains represented by equivalent static loads can be transformed into elemental ply failure indexes according to equation 3.4. Considering geometrical nonlinearity without material nonlinearity, equivalent displacement field provided by linear static loads should in theory arrive the same stress, strain and corresponding failure index results as in the original nonlinear analysis. However, small computational error may incur during the failure index derivation process. Besides, lack of rotating Lagrangian coordinate system amplified the error even further. As stiffener sections were only of interest and remained relatively straight up to the ultimate load level, the rotation effect was limited in this study. In order to account for this failure index discrepancy, failure index correction factors were necessary to ensure identical failure indexes between linear and nonlinear analyses. For the sake of simplification, only a single correction factor per ESLM iteration was computed and applied to all interested finite elements. Shown in equation 5.5 The failure index correction factor (φ) was calculated based on the ratio of nonlinear analysis and linear analysis maximum failure index. As a result, displacement-based equivalent static loads, in every initial linear-loop optimization iteration, generated the same displacement and maximum failure index responses as seen in the original geometrical nonlinear analysis. The failure index modification step was included in the ESLM process as shown in figure 5.2.

$$\varphi = \frac{FI_{NL,max}}{FI_{L,max}} \tag{5.5}$$

5.2.4. Conventional Gradient-based Optimization Techniques

All generated equivalent static loads are fed into a conventional gradient-based optimization procedure as input, prescribed static loadcases. Constraints specified for the nonlinear load are applied against all of its equivalent linear loads.The MSC version of Automated Design Synthesis (MSCADS) available in MSC Nastran solution 200[36] was deployed in this case. Design sensitivities of interested response (r) at a particular design point (x^k) were determined using forward finite differencing scheme as shown in equation 5.6. Design optimization parameters (DOPTPRM) including stopping criteria setup in MSC Nastran solution 200 are tabulated in table 5.2. The rest of parameters were set by a default setting. The first iteration of the nonlinear analysis response optimization completes when the inner, conventional optimization loop converges.

$$\frac{\partial r(x^k)}{\partial x_l} = \frac{r(x^k + \Delta x_l) - r(x^k)}{\Delta x_l} \tag{5.6}$$

The process proceeds with updated design variables obtained from the conventional optimization loop is then fed back to the nonlinear analysis domain. Nonlinear analysis constraint functions are calculated based on the original geometrical nonlinear simulation. Termination criteria are then evaluated. There are several ways to define the stopping criteria including objective convergence, design variable convergence or equivalent static loads convergence. The deployed stopping criterion based on the design objective ($f(x)$) can be formulated as in equation 5.7. Should the convergence criterion be violated, a new set of equivalent static loads is constructed for the new design and are supplied to the inner design loop. The entire process continues until the defined convergence criterion is met i.e. threshold ε is respected. Relatively relaxed convergence threshold of 1% was set in our case to avoid inefficient detail search. The value was however appropriate given preliminary design phase was considered. Due to 1% tolerance in applied load precision (section 5.2.1), maximum nonlinear analysis constraint violation allowed at the converged solution of the outer-loop optimization was relaxed to 2% from 1% specified in the inner-loop optimization.

$$\left| \frac{f(x)^{k-1} - f(x)^k}{f(x)^{k-1}} \right| \leq \varepsilon \tag{5.7}$$

5.3. Response-Surface based Optimization Techniques

For a very expensive system analysis, a surrogate model offers an economical design response usable for a subsequent optimization task. Constructing a sufficiently accurate surrogate model is however computationally demanding. An efficiency trade-off must be carried out before an official method selection is made. Response-surface based optimization techniques however deem a better choice than evolutionary algorithms in terms of speed but less affirmation on the global optimality. An efficiency comparison against the proposed optimization process involving ESLM was done in sub-chapter 9.1.1.

5.3.1. Global Response Surface Method

Altair's Global Response Surface Method (GRSM)[40] is a good compromise between surrogate model efficiency and global search capability. Appropriate for non-convex optimization problems and relatively expensive system analysis, GRSM is capable of obtaining global or close-to-global optimal solution with less number of system evaluations than that of evolutionary algorithms. Illustrated in figure 5.5, two parallel searches: response-surface based optimization and global sampling, are conducted simultaneously within GRSM. Before that, initial sample points via Latin Hypercube sampling and system evaluations are executed. Next, an initial Hyper Kriging meta model is constructed for the response-surface based optimization. The best design is reported as the solution of this unique iteration one. The gradient-based optimization problem is then solved on the created surface and the optimized design variables found are used in the next iteration. After the second iteration, GRSM globally generates a few sample points to avoid sub-optimal solution as well as locally to increase surrogate model accuracy. Locally, the meta model is adaptively updated in each iteration, obtaining more precise approximation. Gradient-based optimization continues on this adaptive surface. Iteration's optimized solution and the best global sample point are then compared against each other. The winner of the two is used to modify the adaptive response surface in the next iteration. The scheme continues until one of the stopping criteria met. GRSM will conclude if either maximum number of sample points is reached, or normalized distance between the newly sampled design and any of existing designs is less than user's specified value. Parallel model evaluations can be executed to reduce the run time, as sampled designs are completely independent. Ungwattanapanit and Baier[51] reported identical optimal solution obtained from GRSM and Genetic Algorithm (GA), in the case of a straight-fiber design. Highly agreeable results, with less than 2% deviation, were observed in the case of a variable stiffness design.

Although initial number of sample points of 11 (equal to no. of design variables+2) is suggested by default, 50 initial sample designs were conservatively generated in light of high multi-modality caused by fiber orientation parameterization. Convergence criterion for normalized distance was set to 0.0005 compared to 0.001 default value as close-to global optimum was targeted. Agreeable results when verified against genetic algorithm optimums affirmed the reliability of the chosen GRSM parameters. GRSM parameters specification is shown in table 5.3.

Table 5.2.: Design Optimization Parameters (DOPTPRM)[36]

Parameter	Description	Value
DESMAX	Maximum number of design cycles	40
CONV1	Convergence criterion: Relative change in design objective	0.5%
GMAX	Maximum constraint violation allowed at the converged optimum	1.0%

Table 5.3.: Global Response Surface Method Parameters

Parameter	Value
Max. evaluations	500
Min. evaluations	25
Initial sample points	50
Sampled designs per iteration	5
Convergence distance	0.0005

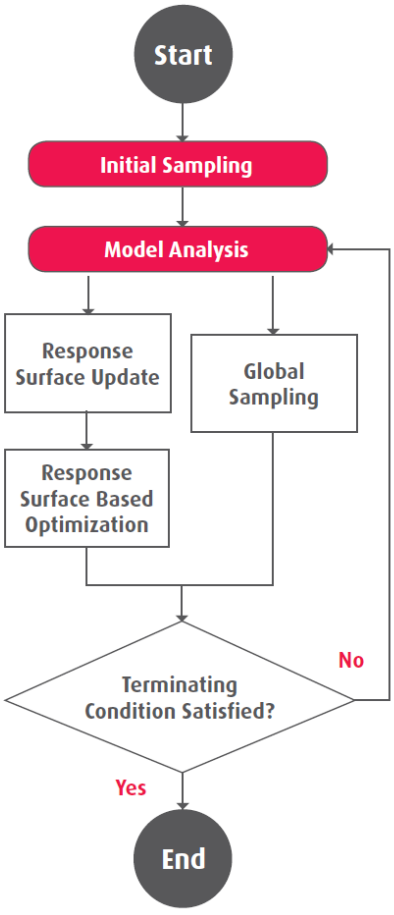

Figure 5.5.: Global Response Surface Method flowchart[40]

6

Optimization of Steered-Fiber Fuselage Panels via Equivalent Static Loads

This chapter explains the application of the proposed methodology. The proposed equivalent static loads method for postbuckling responses optimization is demonstrated in this chapter via two composite fuselage stiffened panels: keel and side sections. Relevant panels geometry, finite element models, design responses analysis and optimization problems formulation are provided.

6.1. TUM-LLB Flieger Fuselage

Shown in figure 6.1, cylindrical fuselage was taken from an in-house, single-aisle airliner model ”LLB Flieger”. Keel and side stiffened panels were used as demonstration examples in this research work. The original aluminum structure was replaced by a CFRP material. The only exception was to maintain aluminum window frame in the side panel. Moreover, J-stringers were substituted by Omega-stringers commonly used in the latest composite fuselage constructions as can be seen in Airbus A350 XWB or Boeing 787 Dreamliner.

6.1.1. Baseline Fuselage Keel Panel

A keel panel section was taken out of the whole fuselage barrel, and was utilized as a demonstration application. High compression load expected during the take-off entitled the panel as a suitable candidate for load-tailored, steered-fiber laminates. Structures subject to a single dominating load are expected to exploit steered-fiber laminates' weight benefit the most. Details of the chosen panel are shown in the following subsections.

Computer Aided Deign Model

Shown in figure 6.2, a stiffened fuselage keel panel located between two consecutive circumferential frames is of interest. Panel geometry data is presented in table 6.1.

Figure 6.1.: LLB-Flieger Fuselage

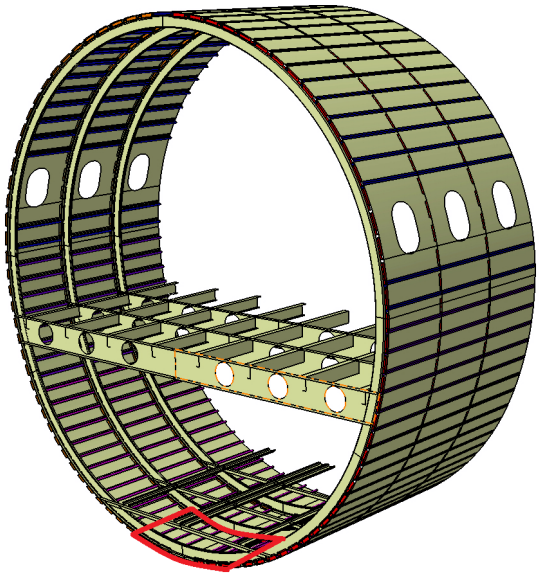

Figure 6.2.: Fuselage keel panel: CAD Model

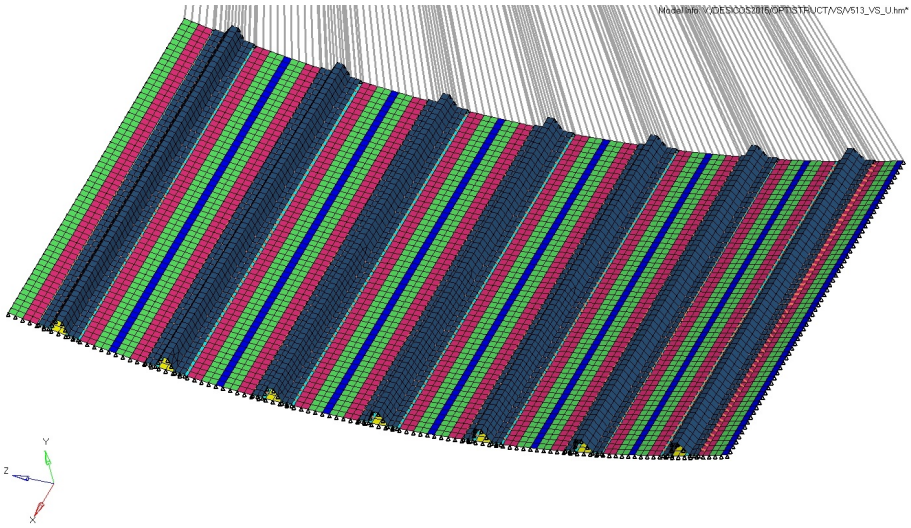

Figure 6.3.: Fuselage keel panel: FE Model

Finite Element Model

The keel panel was meshed by MSC Nastran three- and four-node 2D shell elements (CTRIA3, CQUAD4). 10-mm element width was chosen as it was found to be sufficiently accurate for eigen bifurcation buckling and geometrical nonlinear simulation. Connection between fuselage skin and omega stringers was idealized to be one-dimensional (1D) rigid bar elements (RBAR). The ideal bonding assumption was supported by first-ply failure constraints. Adhesive failure is judged unlikely when first-ply failure index is restricted to be less than unity. Verification of adhesive stress of optimized panels was anyway conducted afterwards as stringers will experience relatively concentrated force in optimized steered-fiber laminates. Furthermore, 1D rigid elements (RBE2) were deployed to transfer applied compressive force at cylinder center into uniform panel shortening, and transform torsional moment to uniform rotation. Shown in figure 6.3, the keel panel finite element model comprises almost 14500 elements in total. Longitudinal segmentation of skin elements facilitates the modeling of linearly-varied fiber pattern described in subsection 2.2.

Material and Properties

The fuselage panel was all-CFRP design. Orthotropic carbon-epoxy IM8/E8552 prepreg properties were referred in the presented work. The choice of common composite fuselage material brought the presented work even closer to a real-world scenario. Corresponding material properties are tabulated in table 6.2. There were however no properties distinction between straight-fiber and steered-fiber lamina in this research, despite prepreg properties being somewhat optimistic for steered-fiber layers. Identical material properties would make the subsequent comparison on structural performance and structural weight between the two types of laminates solely based on the stiffness tailoring ability. Inconsiderable properties difference can be anyway expectable (see sub-chapter 1.2.1 for more info). Besides, material nonlinearity was not foreseen as first-ply failure criteria were applied. Properties reductions

due to the damage tolerance and the environmental requirements are not taken into account.

The reference keel panel consisted of only conventional $\pm 45°$, $0°$ and $90°$ fiber orientations. Its performance served as the baseline and would then be compared with that of optimized counterparts, both straight-fiber and steered-fiber. Its laminates definition is specified in table 6.3.

Loads and Boundary Conditions

Loadcases for the keel section described in subsection 3.1.2 are briefly summarized here. Load magnitudes shown are design limit loads. Safety factor of 1.5 applies to all cases except for internal pressure load where safety factor of 2.0 applies.

1. Pure Axial Compression = 642 N/mm (376747 N compression)

2. Pure Shear = 55 N/mm (128150-Nm torsion)

3. Internal Pressure = 0.06481 MPa

Regarding the boundary constraints, panel's curved edges were clamped to reflect frames' stiffening condition, while panel's straight edges located at the middle of the outward bays between two stringers were simply supported.

6.1.2. Baseline Fuselage Window Panel

A fuselage window panel section was taken out of the whole fuselage barrel, and was utilized as another demonstrating application. Subject to high torsion and combined shear-compression due to aircraft yaw and roll moments, steered-fiber laminates were investigated when shear and combined buckling loads were to be withstood. Under shear load, post-buckled skin sustains applied shear load through diagonal tension and stiffeners contribute only a little compared to compression scenario. Details of the chosen panel are shown in the following subsections.

Computer Aided Deign Model

Shown in figure 6.4, a stiffened fuselage window panel located between two consecutive circumferential frames is interested. Panel geometry data is presented in table 6.4.

Table 6.1.: Reference Keel Panel Geometry Data

Parameter	Value
Radius [mm]	1975
Arc length [mm]	1140
Frame pitch [mm]	587
Omega stringer height [mm]	22
Omega stringer foot width [mm]	15
Omega stringer crown width [mm]	10
Omega stringer width excluding feet [mm]	30
Stringer pitch [mm]	164
Stringer thickness [mm]	2.5
Skin thickness [mm]	2.0
Total panel mass [kg]	3.521

Table 6.2.: CFRP IM8/E8552 UD-prepreg material properties[14;6]

Material Property	Value
E11 [MPa]	157000
E22 [MPa]	12000
Poisson's ratio	0.32
G12,G13,G23 [MPa]	5929
S1T [MPa]	2724
S1C [MPa]	1690
S2T [MPa]	64
S2C [MPa]	286
S12 [MPa]	120
S23 [MPa]	137
Density [kg/m^3]	1570

Table 6.3.: Reference keel panel's stacking sequence

Component	Stacking Sequence	Ply Thickness	Total Thickness
Skin	[+45/-45/0/90]2s	0.125 mm	2.00 mm
Stringer	[0/90/+45/-45/0/90/-45/+45/90/0]s	0.125 mm	2.50 mm

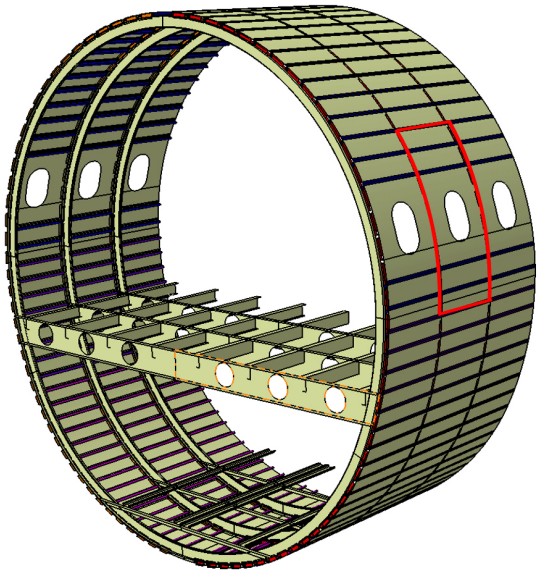

Figure 6.4.: Fuselage side panel: CAD Model

Table 6.4.: Reference Side Panel Geometry Data

Parameter	Value
Radius [mm]	1975
Arc length [mm]	1301
Frame pitch [mm]	587
Omega stringer height [mm]	22
Omega stringer foot width [mm]	15
Omega stringer crown width [mm]	10
Omega stringer width excluding feet [mm]	30
Stringer pitch [mm]	164
Stringer thickness [mm]	2.5
Window frame flange (skin side) [mm]	2.50
Window frame flange (hole side) [mm]	2.00
Window frame web [mm]	4.00
Cut-out skin arc length [mm]	656
Cut-out skin thickness [mm]	2.75
Skin thickness [mm]	2.75
Total panel mass [kg]	4.422

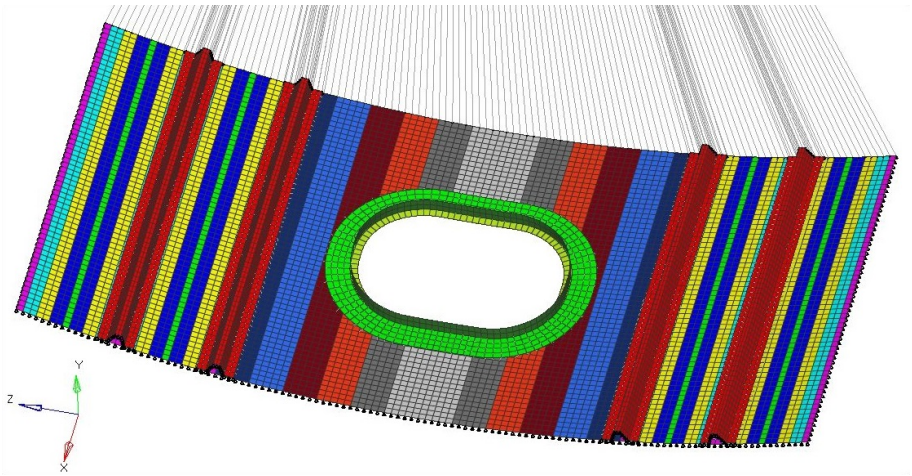

Figure 6.5.: Fuselage side panel: FE Model

Finite Element Model

Similar to the keel panel, the window side panel was meshed by MSC Nastran shell elements (CTRIA3, CQUAD4). 10-mm element width was also chosen. Connection of skin to stringers, and skin to window frame was idealized with rigid bar elements (RBAR). Verification of adhesive stress would be conducted afterwards. Furthermore, 1D rigid elements (RBE2) were deployed to transfer applied loads at cylinder center into uniform panel shortening or rotation, depending on the loading type. Shown in figure 6.5, the side panel finite element model comprises almost 12500 elements in total. Longitudinal segmentation of skin elements facilitates the modeling of linearly-varied fiber pattern described in subsection 2.2.

Material and Properties

Similar to the keel panel, the window panel was made from carbon composite except aluminum-alloy window frame. IM8/E8552 carbon-epoxy composite and Aluminum 7075-T73 was utilized respectively. Corresponding material properties are tabulated in table 6.2 and 6.5.

The reference side panel consisted of only conventional $\pm 45°$, $0°$ and $90°$ fiber orientations and homogeneous aluminum window frame. Its performance served as the baseline and would then be compared with that of optimized counterparts, both straight-fiber and steered-fiber. Its laminates definition is specified in table 6.6.

Loads and Boundary Conditions

Loadcases for the window section described in subsection 3.1.2 are briefly summarized here. Load magnitudes shown are design limit loads. Safety factor of 1.5 applies to all cases except for internal pressure load where safety factor of 2.0 applies.

1. Pure Shear = 100 N/mm (260000-Nm torsion)

2. Combined Compression-Shear = 294 N/mm (190877 N compression) & 40 N/mm (100360-Nm torsion)

3. Internal Pressure = 0.06481 MPa

Regarding the boundary constraints, panel's curved edges were clamped to reflect frames' constraint, while panel's straight edges were simply supported to reflect omega stringers' restraining effect.

6.2. Optimization Problems Formulation

Both aforementioned fuselage stiffened panels were to be studied. Each of the panel was designed by two different configurations: straight-fiber and linearly-varied fiber, with the aim to study the weight benefit offered by the latter. Relevant design optimization problem formulations are shown as follows.

6.2.1. Fuselage Keel Panels

Before formulating the optimization problems, laminates definition had to be prescribed as optimized fiber angles and ply thickness were sought after. Thin-ply, 60-layer skin laminate, either straight-fiber or steered-fiber, was to be simultaneously optimized with its ply thickness, which was made identical throughout the laminate. Both straight-fiber and steered-fiber designs consist of three independent design plies; fair comparison could thus be made later on. Simultaneous optimization of individual ply angles and individual ply thickness would have offered a better optimized solution, but at the cost of extreme non-convex design space and sluggish optimization convergence rate. In terms of stringers laminate, original reference stacking sequence was kept and only a common ply thickness of 0°, 90°, and 45° layers were to be optimized. Table 6.7 and 6.8 reveals straight-fiber and steered-fiber laminate definition of the keel panel respectively. Shown in figure 2.3, fiber angle was linearly varied from skin bay center between two successive stiffeners with an angle α_1 to an angle α_2 at stringer center for instance.

In order to study the weight saving benefit steered-fiber pattern is able to offer, optimized panels constrained by strength and stability requirements outlined in chapter 3 were sought after. In terms of strength, maximum strain failure criteria were applied to all loadcases. Elemental failure indexes must be less than or equal to unity before design ultimate loads are reached. Geometrical stability requirements divided into local panel linear buckling, global panel collapse, stringer linear buckling, and stringer crippling were applied against buckling loads only. As proposed, non-catastrophic local panel buckling can be allowed to occur below design limit load level in order to yield lighter structure. For simplicity, this design approach was only applied to the shortening load. Corresponding buckling eigenvalue was constrained

Table 6.5.: Aluminum 7075-T73 material properties[30]

Material Property	Value
E [MPa]	73000
Poisson's ratio	0.33
G [MPa]	26000
ST [MPa]	435
SC [MPa]	435
SS [MPa]	305
Density [kg/m^3]	2780

Table 6.6.: Reference side panel's stacking sequence

Component	Stacking Sequence	Ply Thickness	Total Thickness
Skin	$[(+45/-45/0/90)_2/+45/-45/0]$s	0.125 mm	2.75 mm
Stringer	[0/90/+45/-45/0/90/-45/+45/90/0]s	0.125 mm	2.50 mm

Table 6.7.: Keel panel: Straight-fibre design stacking sequence

Component	Stacking Sequence
Skin	[+D/-D/+E/-E/+F/-F]5s
Stringer	[0/90/+45/-45/0/90/-45/+45/90/0]s

Table 6.8.: Keel panel: Steered-fibre design stacking sequence

Component	Stacking Sequence
Skin	$[+\langle\alpha_1\vert\alpha_2\rangle/-\langle\alpha_1\vert\alpha_2\rangle/+\langle\beta_1\vert\beta_2\rangle/-\langle\beta_1\vert\beta_2\rangle/+\langle\gamma_1\vert\gamma_2\rangle/-\langle\gamma_1\vert\gamma_2\rangle]$5s
Stringer	[0/90/+45/-45/0/90/-45/+45/90/0]s

to be no less than 0.5 (50% limit load). For much less critical shear load, buckling eigenvalue was restricted to be no less than 1.5; nonlinear buckling analysis for this load could therefore be omitted. Final panel failure modes, i.e. panel collapse and stringer crippling, were also concerned. Panel collapse caused by stiffener global buckling and stiffener local crippling were not permitted below 120% the design ultimate load level or 1.8 times limit load. Like local panel buckling constraint, premature local stiffener buckling was to be avoided prior to the limit load. To be conservative, seven stiffening omega-shaped columns were assumed to solely absorb applied shortening load after the limit load was reached. Uniform load distribution to all stiffeners was presumed. Subject to applied ultimate loads, respective optimization problem formulation is as follows.

Design Objective:	To minimize panel $Mass$
Design Variables:	
Straight-fiber:	Ply thicknesses: t_{sk}, t_{str}
	Ply angles: D, E, F
Steered-fiber:	Ply thicknesses: t_{sk}, t_{str}
	Ply angles: α_1, β_1, γ_1, α_2, β_2, γ_2
Subject to:	Failure indexes, $FI_e \leq 1.0$
	Local panel buckling factor, $\lambda_{local,comp} \geq 0.334$
	Global panel buckling factor, $\lambda_{global,comp} \geq 1.200$
	Local stringer buckling factor, $\lambda_{str,local} \geq 0.667$
	Stringer crippling factor, $\lambda_{str,cripp} \geq 1.200$
	Panel shear buckling factor, $\lambda_{local,shear} \geq 1.000$
	Ply thicknesses:
	$0.01 \leq t_{sk} \leq 0.1$ mm
	$0.01 \leq t_{str} \leq 0.5$ mm
	Ply angles, $0° \leq D, E, F, \alpha, \beta, \gamma \leq 90°$
Loadcases:	Pure Axial Compression - Ultimate
	Pure Shear - Ultimate
	Internal Pressure - Ultimate

(6.1)

6.2.2. Fuselage Window Panels

Similar to the keel panel, thin-ply skin laminates were to be simultaneously optimized with a common ply thickness. However, normal stiffened skin and skin with window cutout were allowed to have different thickness due to different size of unstiffened areas. The straight-fiber design shared the same laminate stacking sequence between the two skins. The steered-fiber design allowed two different laminate definitions but identical laminate had to be shared at the border location between these two skins to ensure smooth fiber path transition. The

original stringer reference laminate was maintained, and aluminum window frame geometry was fixed. They were not part of the optimization. Table 6.9 and 6.10 reveals straight-fiber and steered-fiber design laminate definition of the side panel, respectively. For instance, fiber angle was linearly varied from skin bay center between two successive stiffeners with an angle α_1 to an angle α_2 at stringer center. The orientation variation continued to the center of cutout skin with an angle α_3. Anti-symmetry fiber path was enforced to form a balanced symmetric laminate.

Optimized window panels constrained by strength and stability requirements outlined in chapter 3 were sought after. There were however two dominant buckling loadcases instead of a single driving load in this application. Maximum strain failure criteria were applied to all loadcases. Since the structure was more critical in terms of strength under the torsion loadcase than the combined case, geometrical nonlinear analysis was only performed under torsion. Verification of failure indexes induced by the combined loadcase was done after the optimization. Geometrical stability requirements were applied against buckling loads only. In this case, non-catastrophic local panel buckling was allowed to occur only after design limit loads. Corresponding buckling eigenvalues were constrained to be no less than 1.0 (100% limit load). Subject to applied ultimate loads, respective optimization problem formulation is as follows.

Design Objective:	To minimize panel $Mass$
Design Variables:	
Straight-fiber:	Ply thicknesses: t_{sk}, $t_{sk,win}$
	Ply angles: D, E, F
Steered-fiber:	Ply thicknesses: t_{sk}, $t_{sk,win}$
	Ply angles: α_1, β_1, γ_1, α_2, β_2, γ_2, α_3, β_3, γ_3
Subject to:	Failure indexes, $FI_e \leq 1.0$
	Combined compression-shear buckling factor,
	$\lambda_{local,comb} \geq 0.667$
	Shear buckling factor, $\lambda_{local,shear} \geq 0.667$
	Ply thicknesses:
	$0.01 \leq t_{sk}, t_{sk,win} \leq 0.1$ mm
	Ply angles, $0° \leq D, E, F, \alpha, \beta, \gamma \leq 90°$
Loadcases:	Pure Shear - Ultimate
	Combined Compression-Shear - Ultimate
	Internal Pressure - Ultimate

(6.2)

6.3. Design Response Analysis

Having defined the optimization problem formulations, reliable mean of retrieving interested design responses e.g. failure indexes, buckling factors must be outlined. Versatile finite element software package MSC Nastran 2014 was employed to extract most of the design responses. Two exemptions were semi-analytical collapse and crippling formulations due to time consumption concern. Details for each analysis and respective design response are described.

6.3.1. Linear Static Finite Element Analysis

Linear static analysis subcase was calculated in the optimization process using commercial finite element solver MSC Nastran 2014 solution 101. Recalling static equilibrium matrix equation 5.2 and 5.3, the constrained stiffness matrix and the load vector are generated before the resulting displacements matrix can be calculated through stiffness matrix inversion.

Maximum Strain Failure Index

After obtaining nodal displacements, engineering elemental strains can be determined as shown in equation 3.3. Subsequently, elemental first-ply failure index of each lamina is computed via coordinate transformation and equation 3.4. Classical lamination theory[21] was referred.

6.3.2. Linear Buckling Finite Element Analysis

See sub-chapter 7.1.

6.3.3. Geometrical Nonlinear Static Finite Element Analysis

See sub-chapter 7.2.

6.3.4. Semi-Analytical Formulations for Postbuckling Failure Load

See sub-chapter 7.3.

6.4. Design of Experiments of Thin-Ply laminates

Until now design responses extraction methods have been described. As outlined in sub-chapter 5.1, a preparatory step through design of experiments was conducted to determine the best initial designs to be optimized afterwards. Latin-Hypercube sampling available inside a commercial optimization suite, HyperStudy 14.0, was deployed. No nonlinear analysis failure indexes were computed as it would have been prohibitive. Linear analysis responses were only included. Table 6.11 summarizes number of Latin-Hypercube samples and penalty multiplier r value in equation 5.1 for each optimization task. The penalty power p was always taken as 1.0 since every normalized constraint was equally important.

6.4.1. Fuselage Keel Panels

Regarding the keel panels, total number of independent design variables were five and eight for straight-fiber and steered-fiber, respectively. Number of sampling points were adjusted according to number of design variables. Shear buckling response and nonlinear analysis failure indexes were not computed so as to limit computational cost. Unfitness function determined the design ranking per equation 5.1.

6.4.2. Fuselage Window Panels

As for the window panel, only design angles were parameterized. Reference skin thicknesses were maintained and were not part of DOE since skin thickness parameterization is generally much less non-convex compared to the fiber orientation parametrization. Resulting independent number of design variables for straight-fiber and steered-fiber were three and nine respectively. As panel mass was not varied and constraint functions were all feasible, the unfitness function was not able to rank sampled designs as initially proposed in sub-chapter 5.1. The product of the first buckling eigenvalues from the two buckling loadcases: shear and combined cases were ranked instead. The ranking was based on the equivalent design fitness; the higher the product value, the fitter the design is. Due to time constraint, only 100 sampling points were generated for both fiber patterns. This also emphasizes deficiency of DOE when numerous non-convex design variables are to be simultaneously considered.

Table 6.9.: Window panel: Straight-fibre design stacking sequence

Component	Stacking Sequence
Skin w/o cutout	[+D/-D/+E/-E/+F/-F]5s
Skin w/ cutout	[+D/-D/+E/-E/+F/-F]5s

Table 6.10.: Window: Steered-fibre design stacking sequence

Component	Stacking Sequence
Skin w/o cutout	[+$\langle\alpha_1\|\alpha_2\rangle$/-$\langle\alpha_1\|\alpha_2\rangle$/+$\langle\beta_1\|\beta_2\rangle$/-$\langle\beta_1\|\beta_2\rangle$/+$\langle\gamma_1\|\gamma_2\rangle$/-$\langle\gamma_1\|\gamma_2\rangle$]5s
Skin w/ cutout	[+$\langle\alpha_3\|\alpha_2\rangle$/-$\langle\alpha_3\|\alpha_2\rangle$/+$\langle\beta_3\|\beta_2\rangle$/-$\langle\beta_3\|\beta_2\rangle$/+$\langle\gamma_3\|\gamma_2\rangle$/-$\langle\gamma_3\|\gamma_2\rangle$]5s

Table 6.11.: Design of experiments parameters value

Parameter	Keel Panel		Side Panel	
	Straight-fiber	Steered-fiber	Straight-fiber	Steered-fiber
Samples	250	400	100	100
Penalty multiplier, r	3	3	-	-

7

Validation of Buckling and Postbuckling Analyses

As buckling and postbuckling responses are of paramount importance in this dissertation, this chapter shows the validation of their analysis and corresponding validation results. Despite lack of experimental results correlation, obtained buckling and postbuckling finite element responses have been verified against the responses calculated by other implicit nonlinear Finite Element (FE) solvers including industry's de facto standard like Abaqus/Standard. Furthermore semi-analytical formulations for postbuckling failure load prediction have also been compared against detailed, implicit nonlinear FE results. Overall highly agreeable results have been shown; in other words optimization results presented in this dissertation were based on reliable structural response analyses.

7.1. Linear Buckling Finite Element Analysis

Lanczos eigenbuckling analysis in MSC Nastran 2014 was chosen to estimate the critical bifurcation buckling load. A good stiffened panel configuration would see local skin buckling modes prevailing global panel buckling ones. It has been observed that linear eigenbuckling analysis is sufficiently accurate in predicting the critical buckling eigenvalue when verified against FE geometrical nonlinear analysis results. Less than 5% discrepancy has been reported [52;53] when the initial imperfection was marginal. However, sufficient buckling modes must be requested and included in the optimization to avoid the mode-switching phenomenon. Twenty buckling modes were requested per analysis run in our case. The buckling load (P) can be computed by multiplying the obtained eigenvalue (λ) to applied load (F) per equation 7.1.

$$P = \lambda F \tag{7.1}$$

7.1.1. Panel Eigenbuckling Factor

The first panel's local buckling eigenvalue was interested. Under compression, the critical buckling marks the first locally geometrical instability of a stiffened panel. As mentioned earlier, this local instability does not suddenly crumble the whole panel as stiffeners still remain straight and are able to hold the applied load until the skin loses all of its stiffness

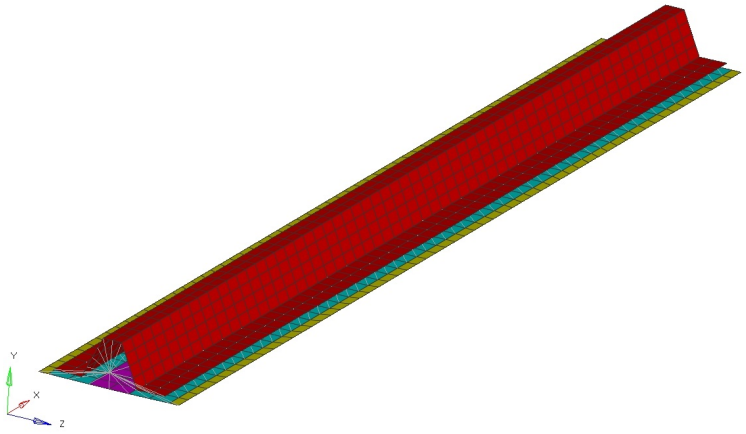

Figure 7.1.: Stringer section: FE Model

and stiffeners buckle or cripple. The linear buckling subcase was only necessary in buckling loadcases i.e. axial compression, torsion, or combined compression-shear as internal pressure load would exert in-plane tension force to the cylindrical fuselage skin.

7.1.2. Stiffener Eigenbuckling Factor

In order to determine stiffener's critical buckling load, a separate FE model of the omega stiffener section (figure 7.1) was created and embedded into the global panel FE model. The model consisted of an omega stringer and an adjacent longitudinal skin section. As local stiffener buckling modes were focused, finite element mesh size was refined from 10-mm element width to 5-mm element width resulting into 1647 elements- 1298 of which were 2D shell elements. Cross-sections were clamped, longitudinal skin edges were simply supported. Seven stiffeners were conservatively assumed to solely absorb applied compression after the limit load was reached. Therefore, uniform shortening displacement caused by 53820-N force (limit load) was applied.

7.2. Geometrical Nonlinear Static Finite Element Analysis

Postbuckling responses, e.g. displacement, engineering stress/strain, failure index, were retrieved from a geometrical nonlinear static analysis solved by MSC Nastran 2014 Solution 106. Slow fuselage loading rate justified the quasi-static load assumption. Taking panel geometrical nonlinearity into account, the finite element software package simulated panels' structural behavior in both pre- and postbuckling regimes until the maximum buckling load is reach; ultimate loads were applied in this case. The chosen quasi-static nonlinear solver is more efficient than closer-to-reality nonlinear dynamic solvers. Nonetheless, scheme convergence and robustness are perhaps more important aspects. A single divergent nonlinear analysis simply leads to premature optimization process termination despite the need of nonlinear scheme robustness in covering the whole range of design exploration during the optimization process. Initial geometrical imperfection was not taken into account in this

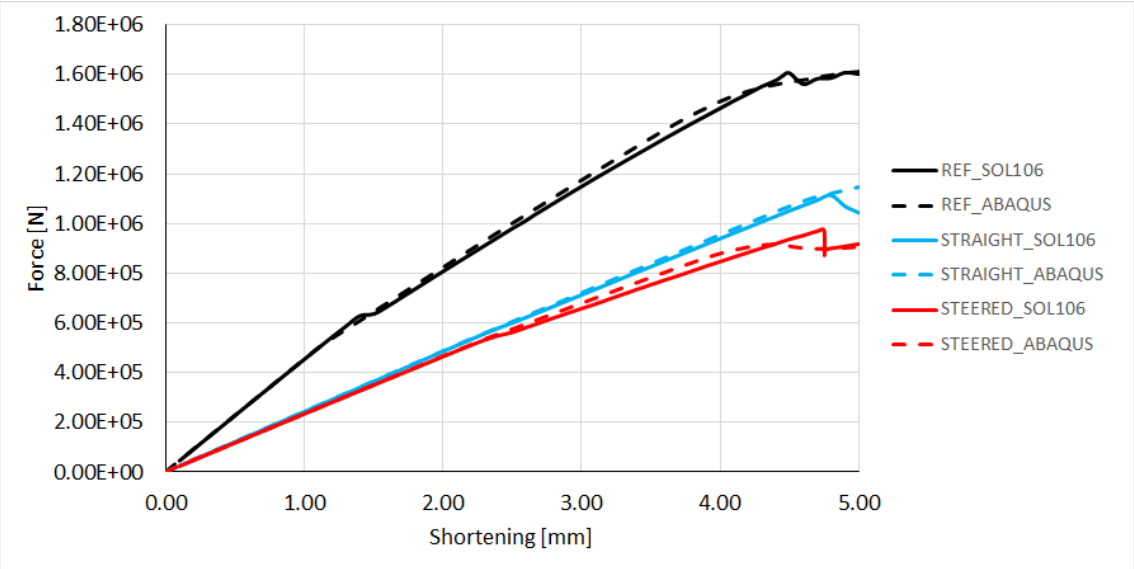

Figure 7.2.: Nastran SOL106 - Abaqus/Standard Benchmarking

dissertation but considerable drop in buckling load was not expected to be as significant as in the non-stiffened panels. Previous study by the author[51] proved insignificant effect of geometrical imperfection on a stiffened fuselage window panel, when 10% of linear static analysis transverse displacement was imposed as an initial imperfection.

A robust set of nonlinear static analysis parameters were eventually found. The Newton's method of iteration coupling with arc-length Riks method for time step control was utilized. According to MSC Nastran 2014 Quick Reference Guide[35], engineering precision level of load (P) and work (W) error tolerance criteria were chosen. Conservative time step control parameters were specified by limiting maximum allowable arc-length adjustment ratio between increments ($MAXALR$) to 1.0. The chosen set of nonlinear analysis parameters set in MSC Nastran solution 106 is summarized in table 7.1.

Reliability of the chosen nonlinear static solver was also successfully benchmarked against the de facto standard nonlinear FE solver Abaqus/Standard. Abaqus 6.13 static stabilization with 5% viscous damping tolerance was employed. The benchmarking samples were the reference, a straight-fiber and, a steered-fiber panel. The straight-fiber design's skin laminate was [±73/±75/±76]5s with total skin and stringer thickness of 1.32mm and 1.846mm, respectively. The curvilinear fiber design's skin laminate was [±⟨81|4⟩/±⟨73|90⟩/±⟨88|4⟩]5s with total skin and stringer thickness of 1.47mm and 1.204mm, respectively. Abaqus/Standard shell elements with reduced integration (S4R and S3R) were modeled. Shown in figure 7.2, highly agreeable results in terms of panel stiffness as well as panel's peak collapse load were observed. Although not shown here, comparable buckling modes were also seen. The study only considered geometrical nonlinearity; no material degradation model was included. Results after the first-ply failure therefore do not represent realistic progressive failure physics.

7.3. Semi-Analytical Formulations for Postbuckling Failure Load

Detailed FE panel failure simulation would have consumed too much computational time and resource, and still accurate panel failure load would have not been guaranteed since experimental data was not available for correlation. Besides, design responses between the first-ply failure and the panel maximum load were not interested. Highly efficient semi-analytical panel failure formulations justified the time limitation normally striven for, in a preliminary design phase. A closed-form formulation providing the failure estimation can be integrated in the optimization suite MSC Nastran solution 200 via the second-level design response (DRESP2) and equation (DEQATN) feature[36].

7.3.1. Global Panel Collapse

The closed-form formulation was based on a global buckling formulation for a compressed hat-stiffened panel[26]. Based on the fact that the derived formulation was based on a circumferentially continuous stiffening pattern, the global buckling estimation could have been too optimistic. However, correlation of the analytical approximation to finite element results of several straight-fiber and steered-fiber panels revealed to be agreeable. One of the reasons behind this might be favorable compression load distribution of the optimized panels; the expected over-estimation was offset. Less than 10% average error with respect to finite element nonlinear static analysis results was reported in sub-chapter 8.1.3; the error was on the conservative side. Note that the FE simulations did not take into account material degradation and skin-stiffener debonding. Comparative study between the best straight-fiber and curvilinear fiber design was anyway preferred to getting realistic panels' collapse load. The complete formulation is provided in appendix A.1.

7.3.2. Stiffener Crippling

The semi-empirical formulations based on no-edge-fee and one-edge-free normalized crippling data documented in MIL-HDBK-17-3F[8] were referred (figure 7.3 and 7.4). Illustrated in figure 7.5, omega stringer's cross section with an adjacent skin were referred in the crippling load estimation. Its symmetric cross section comprises a single one-edge-free section and three non-edge-free sections. Being idealized, the one-edge-free section combines skin and stringer into a single laminate. Steered-fiber pattern was circumferentially linearized and was taken into account in the formulation as several straight-fiber laminates. Correlation to finite element Nastran SOL106 results suggested a correction factor of 1.05 to be applied to the original formulation. Less than 10% average error, on the conservative side, with respect to finite element nonlinear static analysis results was reported in sub-chapter 8.1.3. Note that the FE simulations did not take into account material degradation and skin-stiffener debonding. A comparative study between the best straight-fiber and curvilinear fiber design was preferred to getting realistic panels' collapse load. The complete formulation is provided in appendix A.2.

Table 7.1.: Nonlinear static analysis parameters in MSC Nastran SOL106[35]

NLPARM	Value
NINC	50
KMETHOD	ITER
KSTEP	5
MAXITER	25
CONV	PW
EPSP	1.0E-2
EPSW	1.0E-2
MAXLS	20
NLPCI	**Value**
TYPE	RIKS
MINALR	0.25
MAXALR	1.00

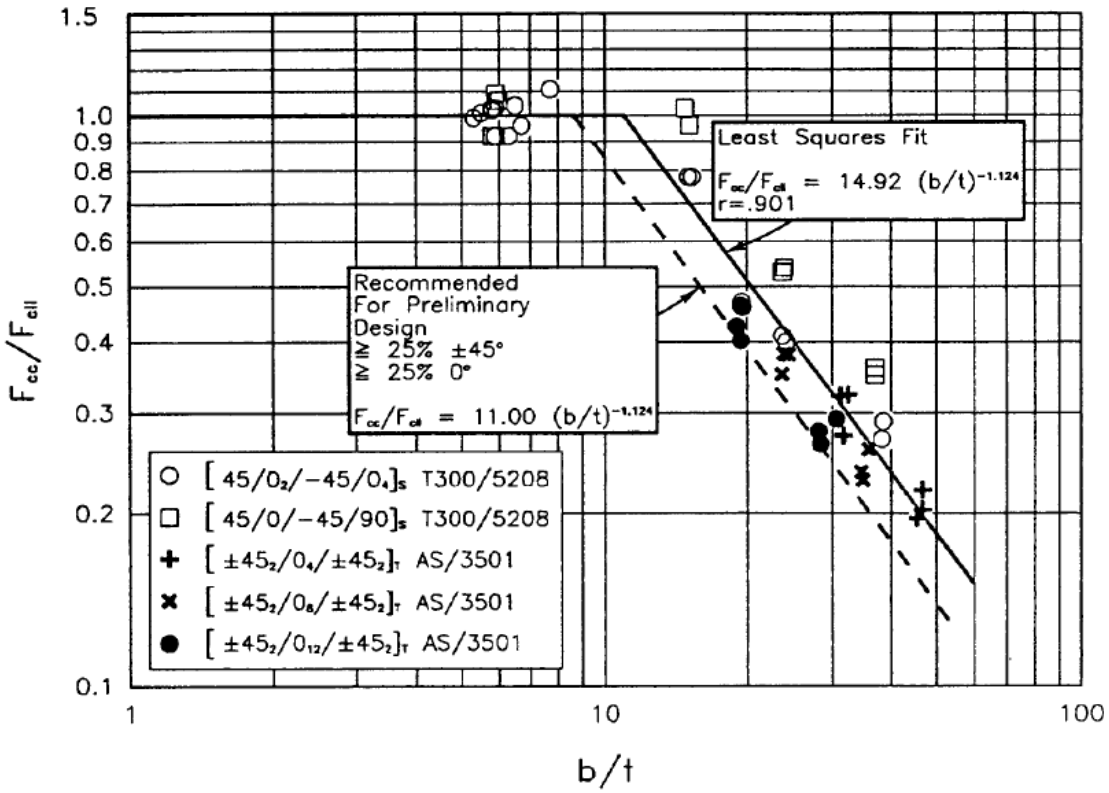

Figure 7.3.: Normalized crippling data - No Edge Free[8]

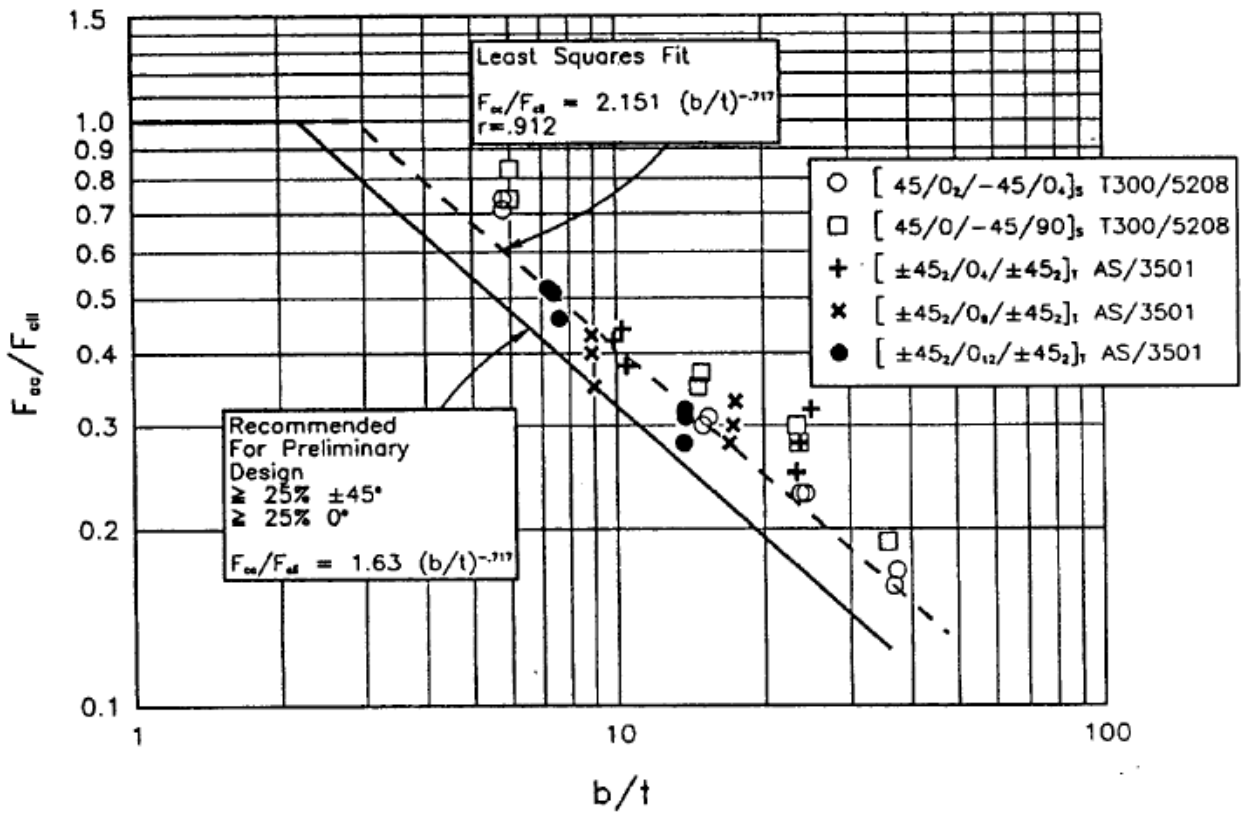

Figure 7.4.: Normalized crippling data - One Edge Free[8]

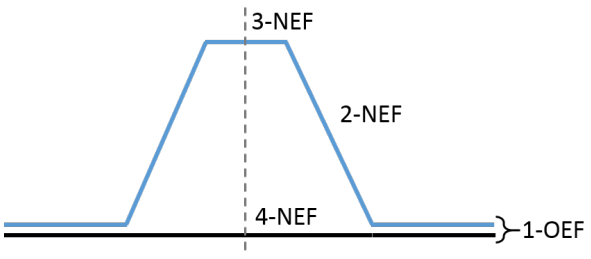

Figure 7.5.: Omega stringer and adjacent skin cross section used in crippling semi-empirical formulation

8

Results and Discussions

Following optimization problems outlined in chapter 6, results and discussions of selected examples are presented in this chapter. Benefits and limitations of optimized steered-fiber patterns with respect to optimized straight-fiber patterns are discussed.

8.1. Fuselage Keel Panels

8.1.1. Design of Experiments Results

Design of experiments results in terms of unfitness function distribution is plotted in figure 8.1. Number of sampling points was used to normalize the occurrence frequency so that fair comparison could be made. A comparable unfitness frequency and distribution between straight-fiber and steered-fiber configurations were found. Based on the design exploration by DOE, little mass-saving benefit was provided by the use of steered-fiber design in this preparatory design phase. The best five designs, i.e. those with the least unfitness, of each configuration were elected and were then fed to the proposed optimization scheme. The chosen five fittest designs are listed in table 8.1 and 8.2. Curvilinear candidates offered slightly lighter panel weight at the end of this preparatory step.

8.1.2. Optimization Results

The chosen five designs from section 8.1.1 were deployed as initial starting points of the proposed optimization with equivalent static loads method. As design starting vectors were all independent from each other, parallel optimization runs could be simultaneously executed, given a sufficient resource. Only the best optimized design's result is revealed and discussed in this chapter. Complete details of the optimization results are shown in appendix A.4.

Straght-Fiber Panels

From the five starts, the fifth best design obtained from DOE gave the best optimized straight-fiber keel panel with 2.469 kg, equivalent to 30% reduction from the reference panel mass. Excluding the initial iteration, it took only three iterations to achieve the converged solution. The converged design was also the best feasible design. Failure index from the shortening, global buckling constraints were active at the converged solution, while stiffener crippling, bifurcation shear, compression and stiffener buckling constraints were inactive. Though

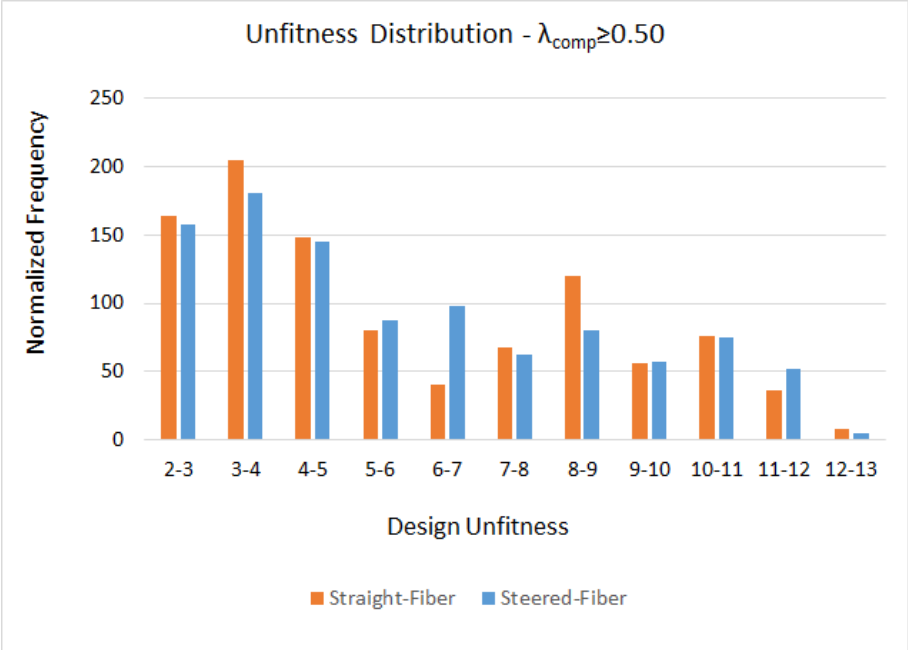

Figure 8.1.: DOE: Keel Panel: Unfitness distribution with λ_{comp} ≥0.50

Table 8.1.: DOE Results: Straight-fiber keel panel ranking

Ranking - ID	1^{st} - 41	2^{nd} - 172	3^{rd} - 147	4^{th} - 90	5^{th} - 238
Unfitness [kg]	2.406	2.411	2.427	2.486	2.509
Mass [kg]	2.202	2.411	2.427	2.486	2.509
D [°]	81	74	75	29	78
E [°]	81	86	76	61	11
F [°]	87	43	56	77	45
t_{sk} [mm]	0.021	0.025	0.021	0.024	0.029
t_{str} [mm]	0.076	0.075	0.098	0.084	0.060

Table 8.2.: DOE Results: Steered-fiber keel panel ranking

Ranking - ID	1^{st} - 253	2^{nd} - 354	3^{rd} - 290	4^{th} - 396	5^{th} - 93
Unfitness [kg]	2.303	2.327	2.426	2.433	2.465
Mass [kg]	2.218	2.327	2.348	2.380	2.150
α_1 [°]	46	86	71	27	73
α_2 [°]	60	5	30	3	72
β_1 [°]	84	69	73	80	37
β_2 [°]	7	63	51	58	81
γ_1 [°]	50	37	62	73	51
γ_2 [°]	64	12	42	63	4
t_{sk} [mm]	0.021	0.024	0.020	0.022	0.021
t_{str} [mm]	0.077	0.073	0.093	0.086	0.073

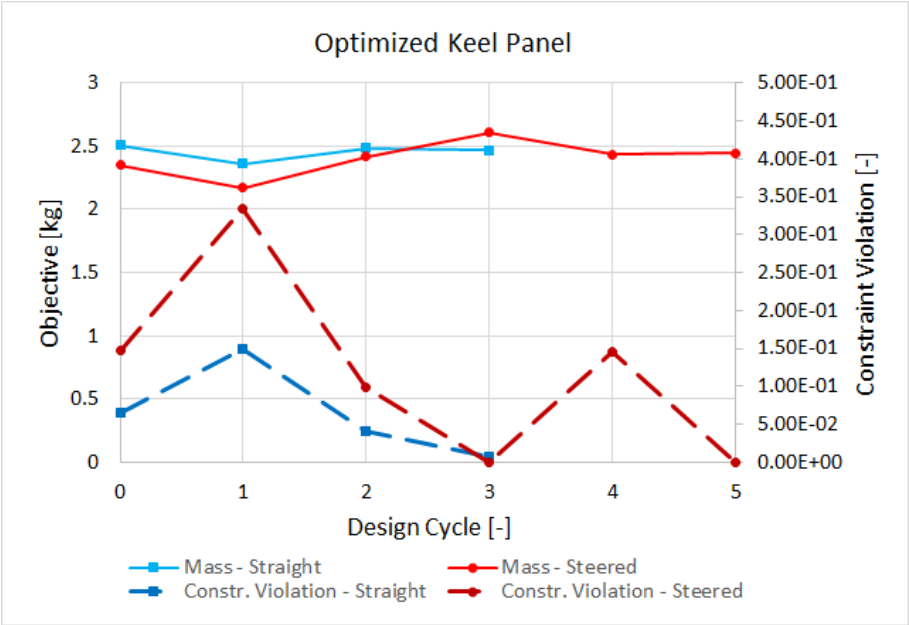

Figure 8.2.: The best optimized keel panels with λ_{comp} ≥0.50

having been inactive, the estimated stiffener crippling load was close to the constraint value specified. In other words, shear and internal pressure loadcases were noncritical. Note that the initial design was infeasible due to the nonlinear analysis failure index constraint. Matching failure index constraints solved by nonlinear analysis and linear analysis at the optimized solution suggest proper functionality of the proposed optimization method. The figure 8.2 shows corresponding optimization history and comparison to the steered-fiber counterpart. Detailed design variables optimization history is shown in table 8.3. Convergence of design variables as well as design objective can be observed.

Table 8.5 summarizes optimized panel mass from each starting design. Brackets indicate infeasible design. Standard deviation was calculated based on the feasible panels. Coefficient of variation, indicating standardized measure of a probability distribution dispersion with respect to samples mean, is as well tabulated. Small coefficients of variation shown indicate low degree of objective (mass) function's multi-modality, although the optimized steered-fiber designs suggest higher level of starting vector dependency than their straight-fiber counterparts.

Steered-Fiber Panels

From the five starts, the third best design obtained from DOE gave the best optimized steered-fiber keel panel with 2.444 kg, or 31% mass saving from the reference panel. Compared to the best optimized straight-fiber keel panel, only marginal weight of almost 1% was spared. Excluding the initial iteration, it took only five iterations to achieve the converged solution. The converged design was also the best feasible design. Failure index, stiffener crippling, and compression buckling constraints were activated at the converged solution, while bifurcation shear buckling, stiffener buckling, and collapse constraints were inactive. In other words,

shear and internal pressure loadcases were noncritical. Though having been inactive, the estimated global buckling load was close to the constraint value specified. Similar to the best optimized straight-fiber panel, failure index, stiffener crippling and collapse load appeared to be the most relevant constraints for mass-optimized panels. This advocates the reliability and optimality of the proposed optimization scheme as it successfully minimized the failure load excess and at the same time fulfilled the failure index constraints of the optimized panels. Agreeable failure index constraints solved by nonlinear analysis and linear analysis at the optimized solution also suggest normality of the proposed optimization method.

Figure 8.2 shows corresponding optimization history and comparison to the straight-fiber counterpart. Detailed design variables optimization history is shown in table 8.4. The optimized fiber angle patterns were only slightly curvilinear with the maximum 21° fiber angle transition between two control points. Similar to the optimized straight-fiber skin laminate, the first and the third design plies were very similar and were separated by 90° layers.

Table 8.5 summarizes optimized panel mass from each starting design. It is observed that only a single initial panel was feasible, suggesting that the unfitness function conducted in DOE was too optimistic due to missing nonlinear analysis failure index responses.

8.1.3. Optimized Designs Verification

The optimized keel panels' structural performance is verified and compared in this subsection. Figure 8.3 compares load-shortening curves of the optimized panels to the reference design. Stiffness reduction is observed in the optimized panels due to relaxed panel buckling constraint from 100% to 50% limit load. Though buckling and stiffness requirements are obviously against each other, the reduction is however relatively minimal below the limit load. Besides, steered-fiber design exhibits less stiffness decrease than its straight-fiber counterpart. Critical loads where the secondary stiffness path starts are slightly dissimilar. The steered-fiber panel shortening stiffness reduces at 75% while almost 90% limit load is seen on the straight-fiber panel. The secondary stiffness for both optimized panels are however very similar. Restricted by 180% limit load threshold, the optimized panels must not fail prior to that point. Straight-fiber panel was a little over-designed in this regard. Assuming the first load drop, the semi-analytical failure load formulations over-predicted by 4%, despite load pick-up afterwards. Regarding the curvilinear-fiber panel, the panel failure mode was dominated by the stiffener crippling as evidenced by gentle stiffness decrease after the peak load. The semi-empirical crippling equation marginally under-predicted by 2%, therefore slightly missing the failure margin requirement.

Displacement and Failure Index

In figure 8.4 and 8.5, corresponding transverse displacements and failure indexes of the proposed optimums are illustrated at 50%, 100%,150% and 180% shortening limit load. Several observations can be made from the presented plots. The optimized steered-fiber panel's

Table 8.3.: The best optimized straight-fiber keel panel: Optimization History

Iteration	Linear-loop iterations	Mass [kg]	t_{sk} [mm]	t_{str} [mm]	D [°]	E [°]	F [°]
0		2.509	0.0289	0.0603	78	11	45
1	8	2.362	0.0297	0.0433	83	22	18
2	3	2.486	0.0318	0.0426	90	22	19
3	**2**	**2.469**	**0.0314**	**0.0432**	**90**	**25**	**22**

Table 8.4.: The best optimized steered-fiber keel panel: Optimization History

Iteration	Linear-loop iterations	Mass [kg]	t_{sk} [mm]	t_{str} [mm]	α_1 [°]	β_1 [°]	γ_1 [°]	α_2 [°]	β_2 [°]	γ_2 [°]
0		2.348	0.0204	0.0932	71	73	62	30	51	42
1	21	2.171	0.0233	0.0615	52	90	38	26	90	19
2	19	2.416	0.0281	0.0568	57	89	34	34	90	23
3	14	2.605	0.0302	0.0615	61	67	33	84	90	23
4	5	2.435	0.0299	0.0484	17	80	13	40	90	17
5	**3**	**2.444**	**0.0306**	**0.0454**	**10**	**89**	**10**	**31**	**90**	**25**

Table 8.5.: Standard Deviation of Optimized Keel Panels

Design	M_1 [kg]	M_2 [kg]	M_3 [kg]	M_4 [kg]	M_5 [kg]	Std. Deviation	Coeff. of Variation
Straight-fiber	(2.461)	(2.358)	2.489	2.528	2.469	2.45×10^{-2}	0.98%
Steered-fiber	2.600	2.702	2.444	2.809	(2.171)	13.5×10^{-2}	4.67%

*() = infeasible design

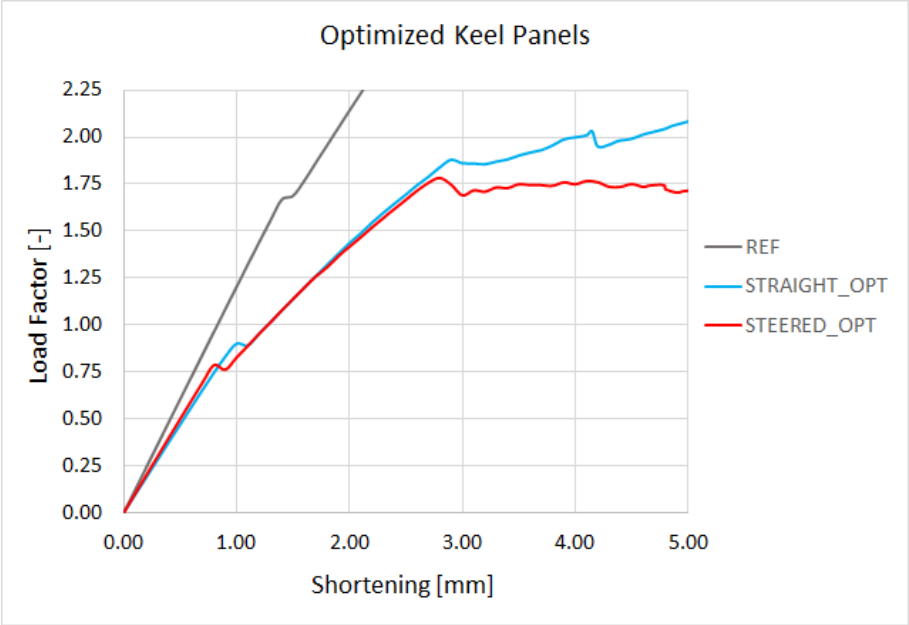

Figure 8.3.: Optimized keel panels: Load-shortening curves, λ_{comp} ≥0.50

shortening load had its peak at 175% limit load as stated earlier.

In terms of buckling mode, both configurations buckled with five longitudinal half-waves. Skin buckling mode changing from one load level to another was hardly noticed. Above the design ultimate load level, i.e. L.F.=1.5, global buckling and stiffener crippling started to evolve, and higher panel transverse displacement was induced.

Critical location where failure index first reached unity for both optimized panels was skin strips under the omega stringers. This could be explained by the fact that stiffeners attracted multitude of applied load in the postbuckling regime. As the skin strips between two stringer feet were the thinnest member of the load introduction area; they thus became the most stressed region. Specifically, skin strips and stringer feet circumferentially aligned to buckling wave anti-nodes had to restrain the buckled skin even further. As a result, failure index was highest at these locations due to bending stress. Failure indexes at outer skin edges were intentionally omitted because simplified boundary condition did not reflect similar buckling response shown at inner stiffened skin. Note that laminate progressive failure and skin-stiffener debonding mechanism were not considered in the analysis after maximum failure indexes reached unity.

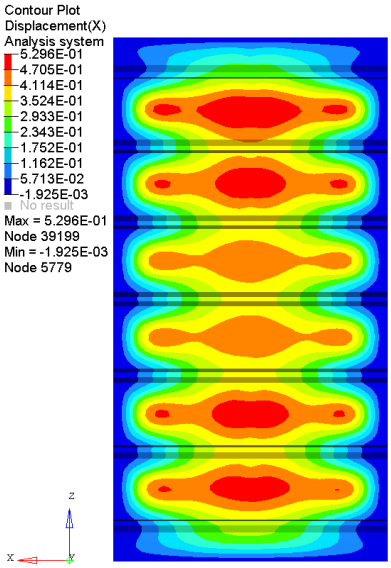

(a) w, L.F.=0.5

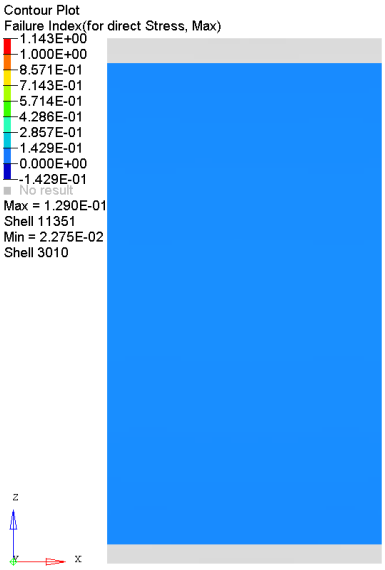

(b) F.I., L.F.=0.5

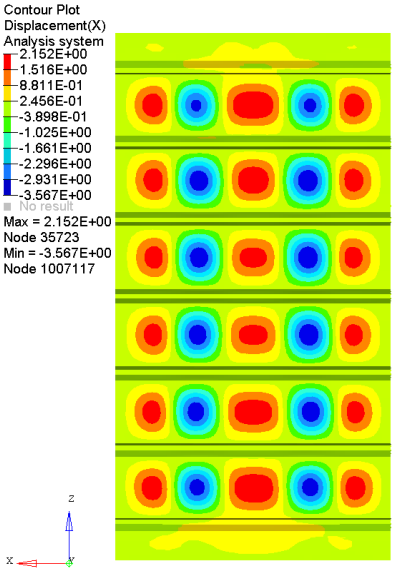

(c) w, L.F.=1.0

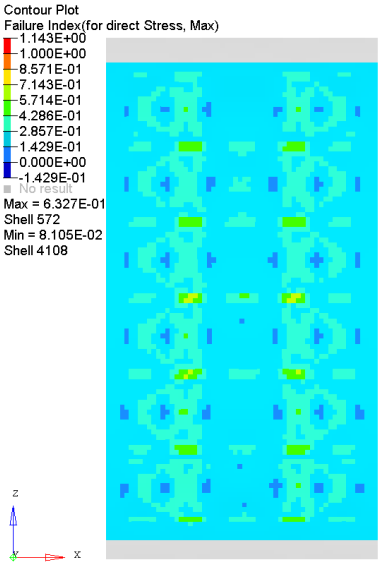

(d) F.I., L.F.=1.0

Figure 8.4.: Optimized straight-fiber keel panel: transverse displacement w [mm] and failure index plots

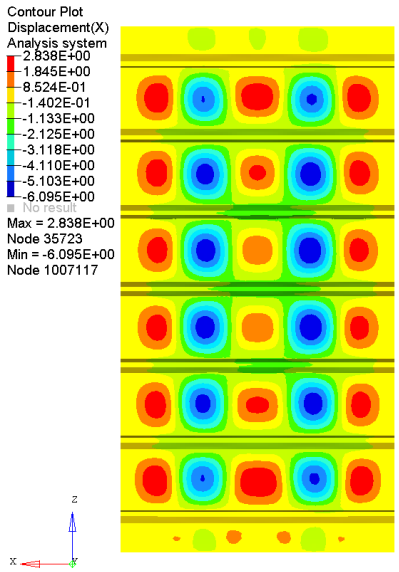

(e) w, L.F.=1.5

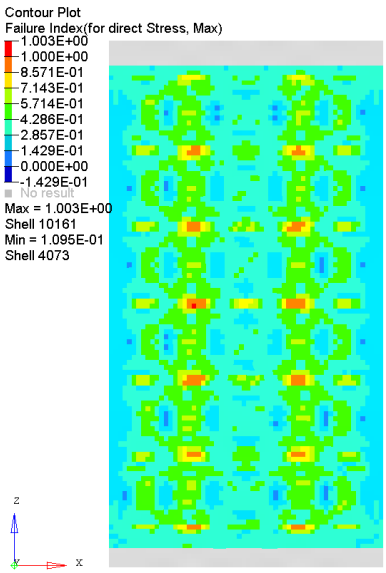

(f) F.I., L.F.=1.5

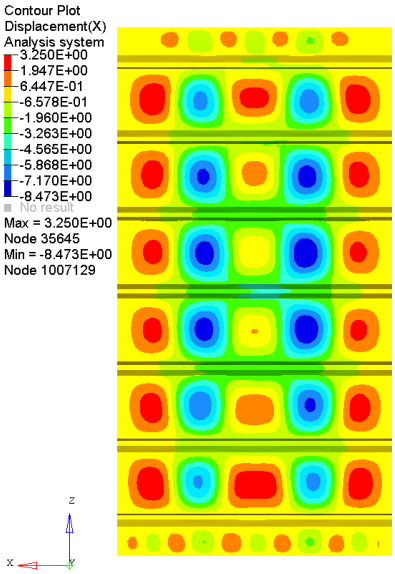

(g) w, L.F.=1.8

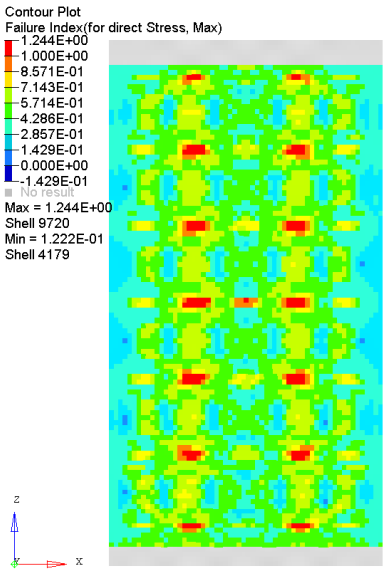

(h) F.I., L.F.=1.8

Figure 8.4.: Optimized straight-fiber keel panel: transverse displacement w [mm] and failure index plots (cont.)

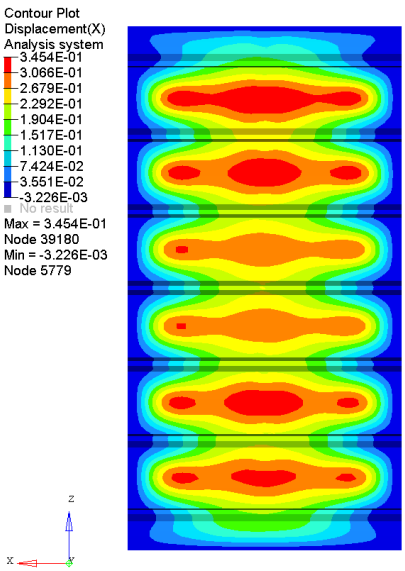

(a) w, L.F.=0.5

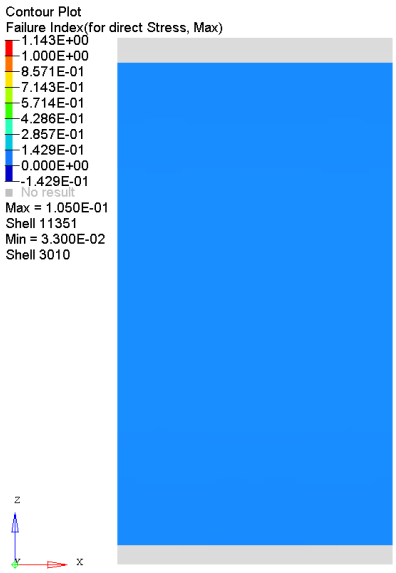

(b) F.I., L.F.=0.5

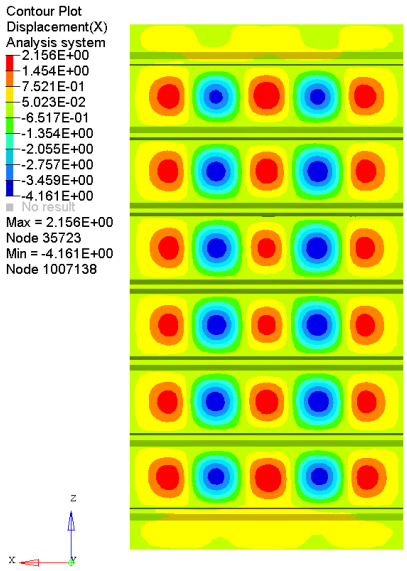

(c) w, L.F.=1.0

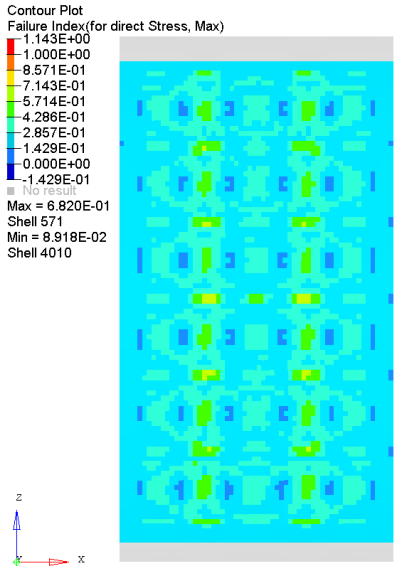

(d) F.I., L.F.=1.0

Figure 8.5.: Optimized steered-fiber keel panel: transverse displacement w [mm] and failure index plots

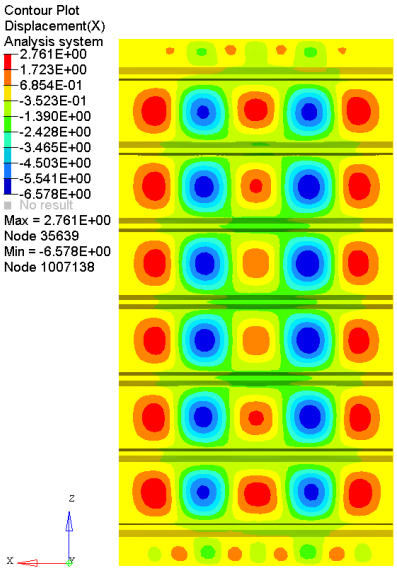

(e) w, L.F.=1.5

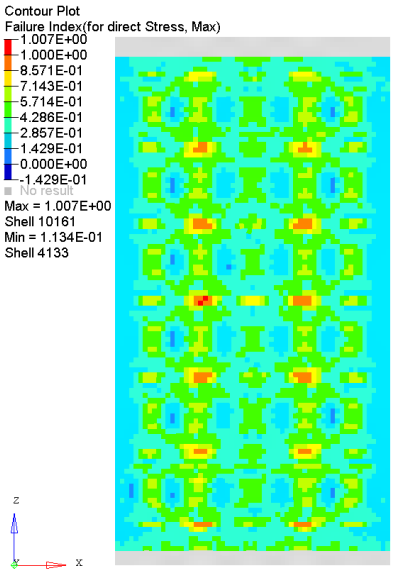

(f) F.I., L.F.=1.5

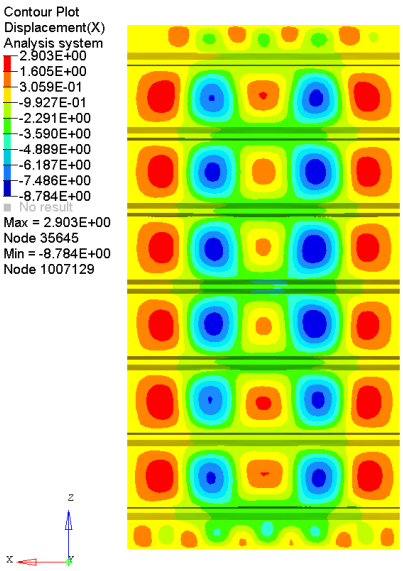

(g) w, L.F.=1.75

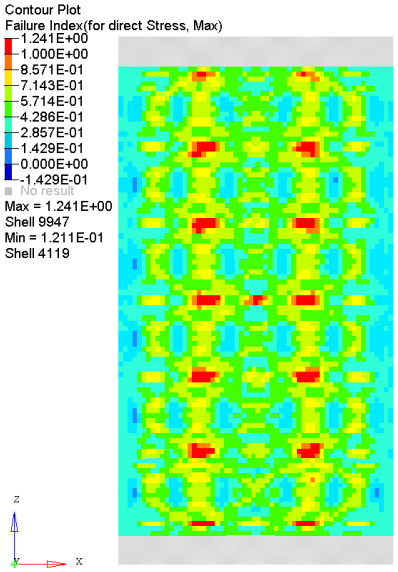

(h) F.I., L.F.=1.75

Figure 8.5.: Optimized steered-fiber keel panel: transverse displacement w [mm] and failure index plots (cont.)

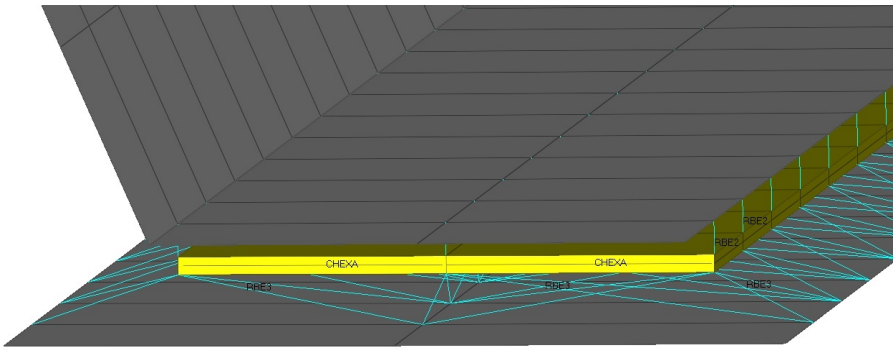

Figure 8.6.: Optimized keel panels: finite element model of the adhesive between skin and stiffeners

Bonding Shear Stress

Another strength verification was done on the adhesive bonding between the skin and stiffeners as concentrated load after skin buckling was proven in this area but the adhesive was not incorporated in the optimization model. 1D rigid elements between the two components were replaced by 8-node three-dimensional (3D) solid elements (CHEXA). They were attached to the skin by displacement coupling elements (RBE3) and to stiffeners by rigid elements (RBE2) as shown in figure 8.6. Table 8.6 declares adhesive material properties referred in the bonding analysis. The updated finite element model was undergone a geometrical nonlinear analysis by MSC Nastran solution 106. Verified against the optimization finite element model, structural responses comparison based on the optimized keel panels at the ultimate load level was made. Highly agreeable outcomes in terms of displacement were found. Less critical skin failure indexes were shown by the updated, more detailed FE model since the adhesive layer helped relieve the load previously carried by the skin. Finally, maximum shear stress in the adhesive layer was checked against the allowable value of 38 MPa. No adhesive debonding was expected in the optimized panels at least up to 150% shortening limit load. Although both straight-fiber and steered-fiber panels were successfully verified, fringe plots of the optimized variable-stiffness panel were only chosen to be displayed in figure 8.7.

Panel Failure Loads

Accuracy of panel collapse load and stiffener-crippling load predicted by semi-analytical formulations was as well verified against finite element results. Optimized straight-fiber and steered-fiber keel panels' peak loads and mode of failure were reviewed. Once again, laminate progressive failure was not considered in the panel failure analysis. Less than 8% load error average was reported, suggesting a good correlation. The closed-form solutions tended to conservatively under-predict the finite element results. More details can be found in table 8.7. Figure 8.8 plots deformation of the best optimized panels (CS-5 and VS-3) when subject to 5-mm shortening displacement. Combined behavior of the global buckling and crippling of stiffeners' inclined flanges, which were the widest member, was observed in both optimized panels.

Table 8.6.: 3M^{TM} Scotch-Weld^{TM} EC-9323 B/A material properties at 23°C[1]

Material Property	Value
E [MPa]	5972
Poisson's ratio	0.40
ST [MPa]	80
SC [MPa]	80
SS [MPa]	38
Density [kg/m^3]	1153

Table 8.7.: Keel panels: Failure loads verification

Design ID	Semi-analytical Collapse [N]	Semi-analytical Crippling [N]	FE Load [N]	FE Mode	Error [%]
CS-1	678170	702820	711898	combined	-4.74
CS-2	771980	687730	705609	combined	-2.53
CS-3	683700	689580	815960	combined	-16.21
CS-4	690780	685790	812050	combined	-15.55
CS-5	679850	703970	707995	combined	-3.98
VS-1	680660	687460	718059	combined	-5.21
VS-2	inactive	inactive		inactive	
VS-3	721900	679990	663944	combined	+2.42
VS-4	687530	988210	767869	combined	-10.46
VS-5	789030	677840	718845	collapse	-5.70
				Average	**-7.42**

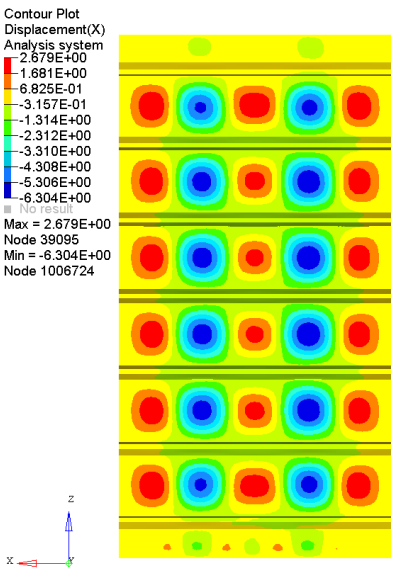

(a) w, detailed model

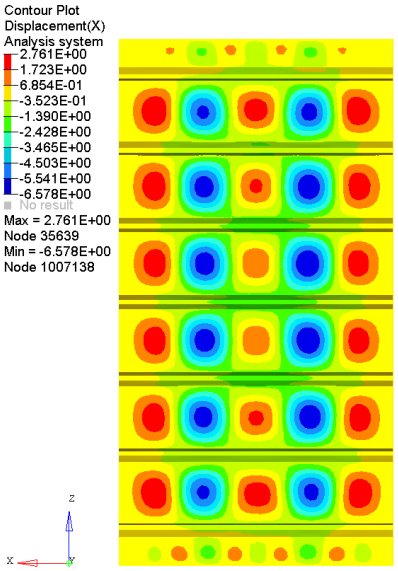

(b) w, optimization model

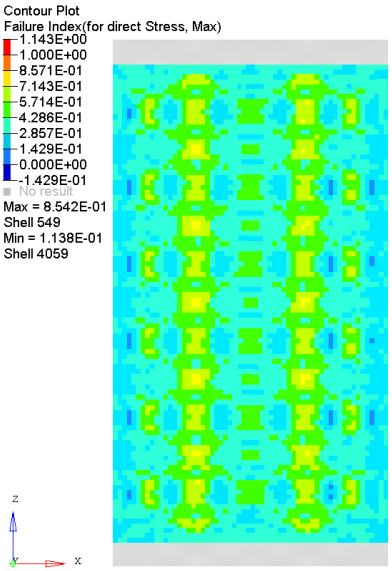

(c) F.I., detailed model

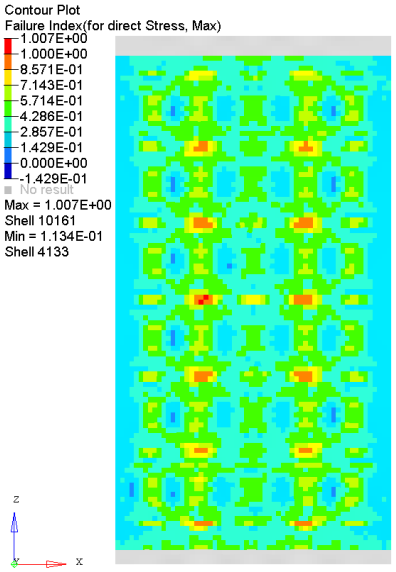

(d) F.I., optimization model

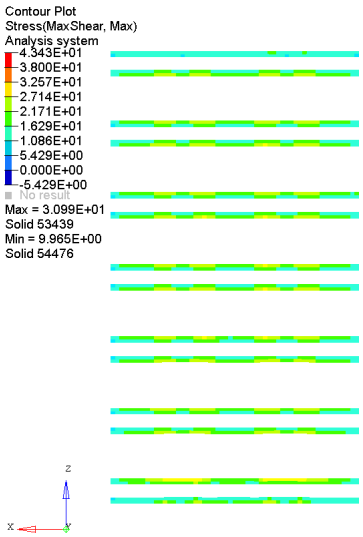

(e) max. shear stress, detailed model

Figure 8.7.: Optimized steered-fiber keel panel: transverse displacement w [mm], failure index, and bonding shear stress verification

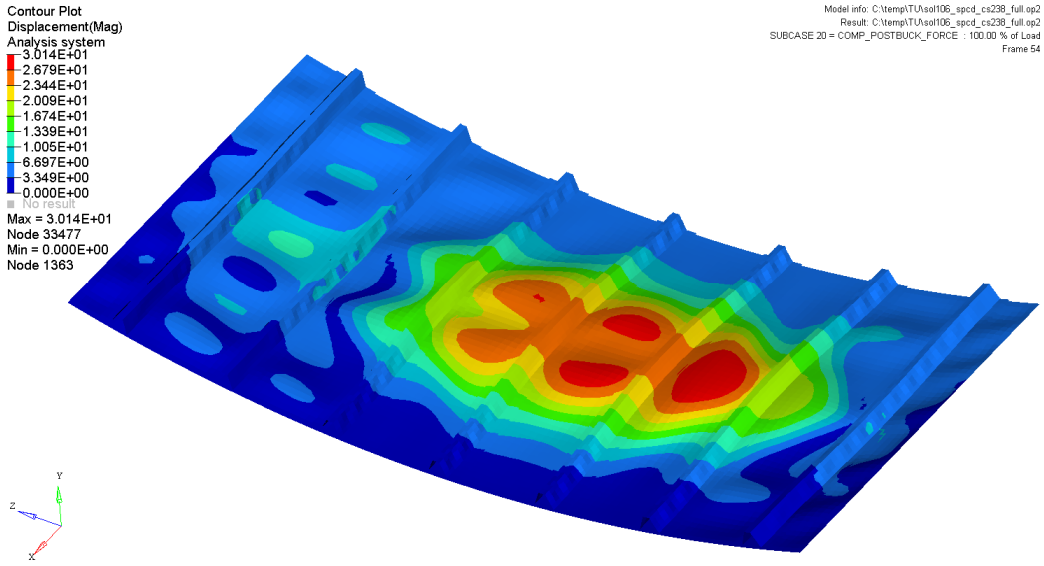

(a) straight-fiber CS-5

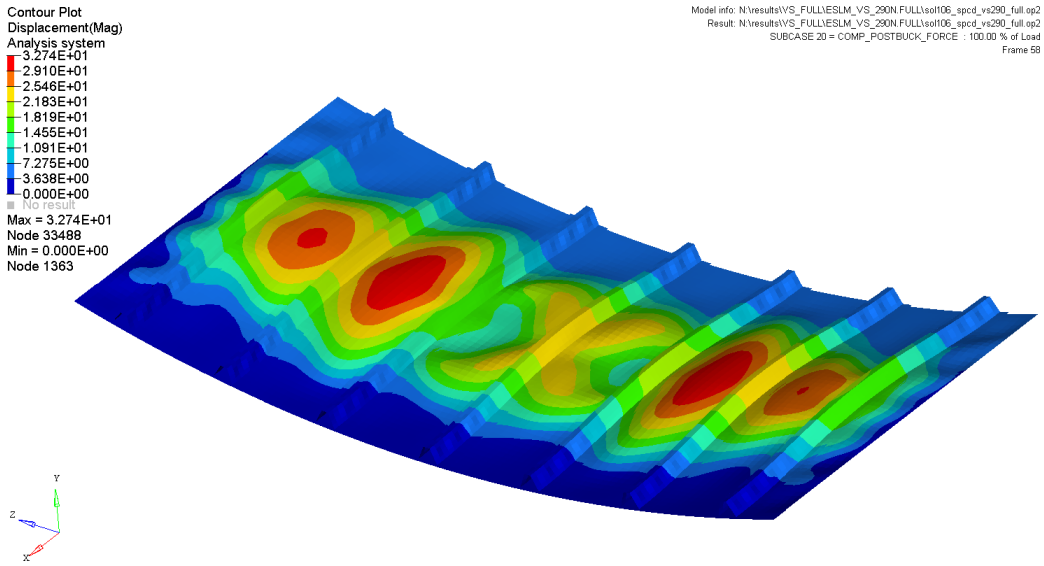

(b) steered-fiber VS-3

Figure 8.8.: The best optimized keel panels: displacement plot at 5-mm shortening

8.2. Effect of Compression Buckling Constraint towards Optimized Mass

So far, hardly weight benefit by the use of steered-fiber laminates has been witnessed. The author suspected that relaxed keel panel buckling load constraint from 100% to 50% limit load was the main reason. More stringent buckling constraint would make the compression load a very dominant loadcase; a situation where curvilinear-fiber laminates are likely to outperform conventional counterparts. More restricted requirement however also means less overall weight saving with respect to the reference design. The following investigation was conducted to demonstrate weight benefit improvement in comparison to optimized straight-fiber keel panels. In reality, the more stringent buckling constraint can be found, for example, in an aircraft wing panels where buckling deformation is not allowed under the limit load due to affected aerodynamic performance.

8.2.1. Optimization Problem Formulation

The original optimization equation 6.1 was modified into equation 8.1. Basically, only the panel bifurcation buckling load constraint was changed to 66.7% design ultimate load, or 100% limit load. Given design ultimate loadcases, the corresponding optimization problem can be formulated as follows.

Design Objective:	To minimize panel $Mass$
Design Variables:	
Straight-fiber:	Ply thicknesses: t_{sk}, t_{str}
	Ply angles: D, E, F
Steered-fiber:	Ply thicknesses: t_{sk}, t_{str}
	Ply angles: α_1, β_1, γ_1, α_2, β_2, γ_2
Subject to:	Failure indexes, $FI_e \leq 1.0$
	Local panel buckling factor, $\lambda_{local,comp} \geq 0.667$
	Global panel buckling factor, $\lambda_{global,comp} \geq 1.200$
	Local stringer buckling factor, $\lambda_{str,local} \geq 0.667$
	Stringer crippling factor, $\lambda_{str,cripp} \geq 1.200$
	Panel shear buckling factor, $\lambda_{local,shear} \geq 1.000$
	Ply thicknesses:
	$0.01 \leq t_{sk} \leq 0.1$ mm
	$0.01 \leq t_{str} \leq 0.5$ mm
	Ply angles, $0° \leq D, E, F, \alpha, \beta, \gamma \leq 90°$
Loadcases:	Pure Axial Compression - Ultimate
	Pure Shear - Ultimate

Internal Pressure - Ultimate

(8.1)

8.2.2. Design of Experiments

Followed the same procedure, design of experiments were conducted based on the new buckling criterion. Resulting unfitness distribution is shown in figure 8.9. As shown in the chart, only a small number of candidates are able to deliver in the best fitness group. Steered-fiber designs show a sign of superiority by presenting more samples in that fitness group. Shown in figure 8.10, steered-fiber panels exploitation is even better when the panel buckling load constraint increases to 150% limit load, confirming the assumption validity.

8.2.3. Optimization Results

Three fittest straight-fiber and steered-fiber designs retrieved from DOE were optimized by the proposed optimization process with ESLM. Resulting optimization history of the best optimized panels is presented in figure 8.11. Corresponding optimal design objective and variables are shown in table 8.8. Corresponding optimized fiber paths are shown in figure 8.12. Two-third of the optimized steered-fiber paths eventually ended up being a straight-fiber pattern. The remaining curvilinear fiber pattern however resulted in a significant performance improvement or weight saving over the pure straight-fiber panel.

Both optimized straight-fiber and steered-fiber panels reached linear compression buckling and global collapse load threshold, while failure index along with other buckling constraints were inactive. As expected, doubling buckling constraint led to 12% and 22% mass reduction for straight-fiber and steered-fiber configurations respectively; a significant drop from c.a. 30% saving in the original problem (equation 6.1). On the other hand, weight benefit from steered-fiber pattern utilization considerably increased from barely 1% to 10%, underlining its high dependency on loadcase orthotropicity. An alternative design scenario where steered-fiber design would be advantageous over its straight-fiber counterpart is to relax shear buckling constraint down from 150% limit load. The dominance of compression buckling will be again restored, but postbuckling response consideration of shear loadcase must be included in the ESLM optimization, incurring more computational cost.

Additional optimization task was done on buckling-free keel panels to reaffirm the buckling constraint influence on the weight saving benefit. Compression buckling load constraint was raised to 150% limit load while the original applied loads were still maintained. In this problem, a conventional gradient-based optimization procedure could be directly employed as there was no interest in postbuckling responses. subsequent optimized panel masses along with optimized fiber angles were summarized together with the previous results in table 8.9. Weight benefit of the curvilinear fiber pattern did not follow the same trend but would rather stay at around 10% when the compression buckling load constraint was increased from 100% to 150% limit load. Looking into optimized fiber orientations,

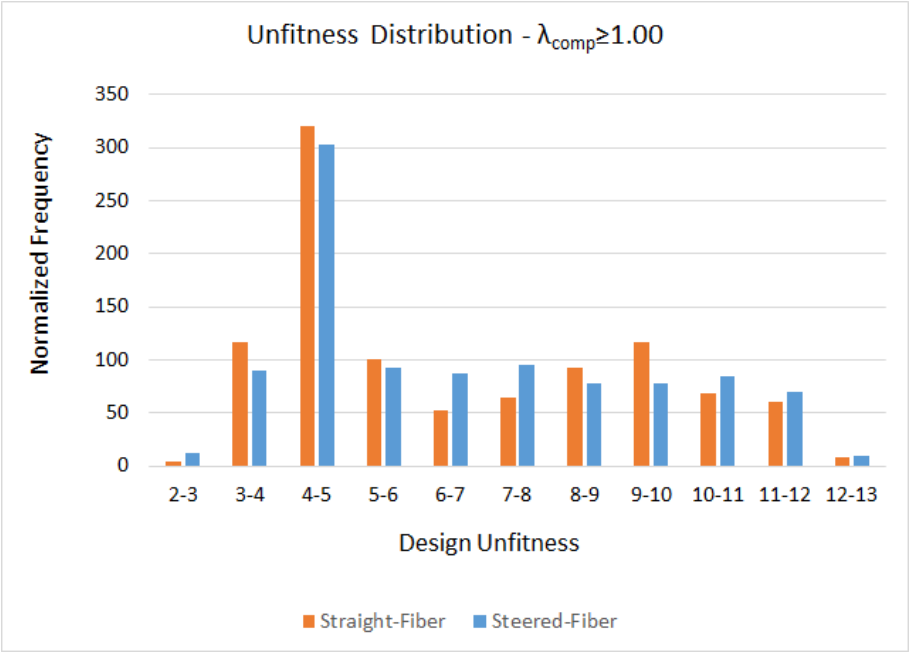

Figure 8.9.: DOE: Keel Panel: Unfitness distribution with λ_{comp} ≥1.00

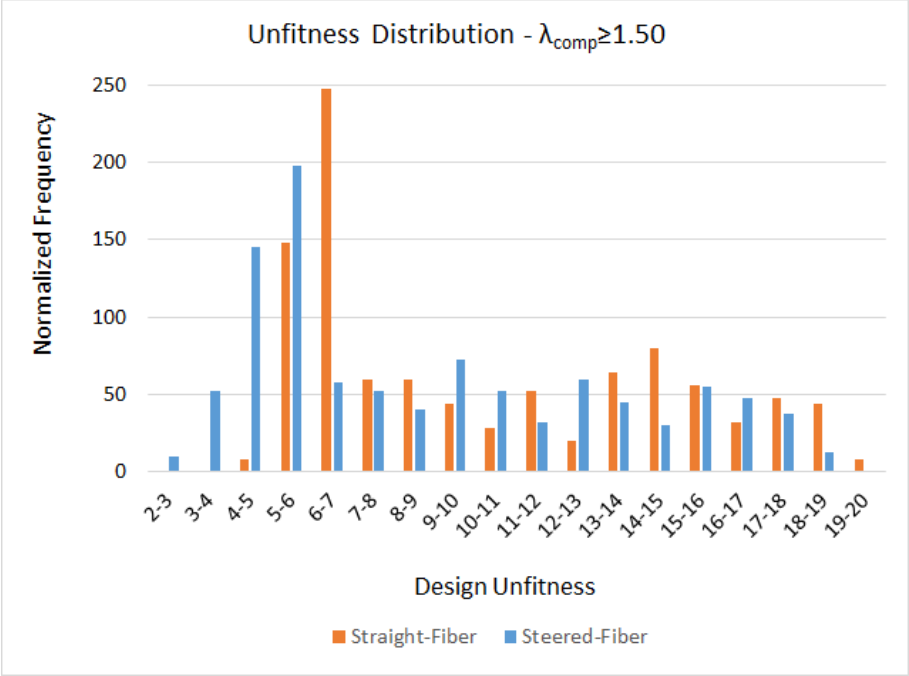

Figure 8.10.: DOE: Keel Panel: Unfitness distribution with λ_{comp} ≥1.50

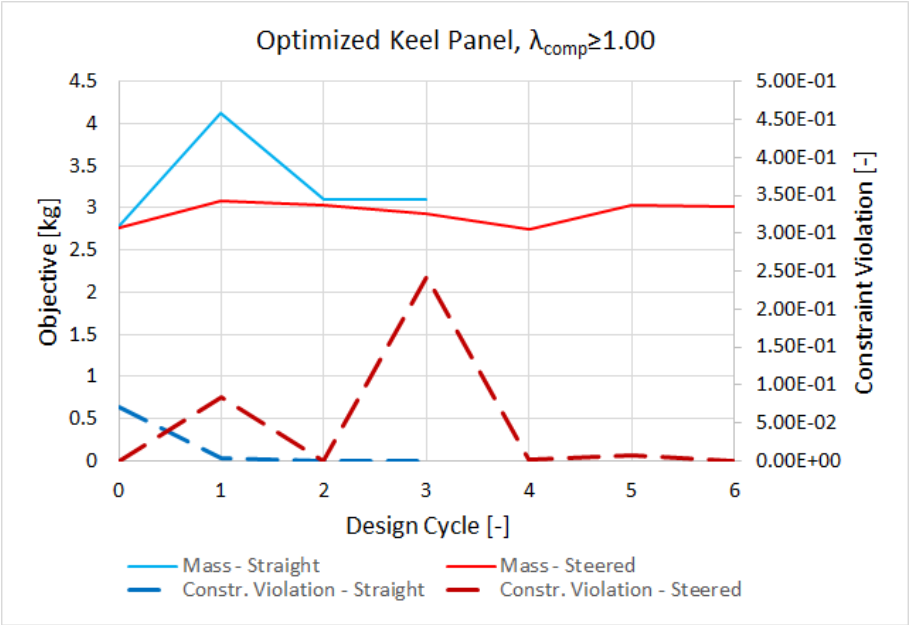

Figure 8.11.: The best optimized keel panels with λ_{comp} ≥1.00

almost straight-fiber paths were suggested when the buckling constraint was relaxed. When the buckling constraint was tightened to 150% limit load, two third of the laminate was governed by high fiber angles at skin bay center and almost parallel fibers along the stiffeners. This fiber pattern transferred applied load towards the stiff stringers, effectively delaying skin local buckling.

8.3. Fuselage Window Panels

8.3.1. Design of Experiments Results

Design of experiments results in terms of equivalent fitness function distribution is plotted in figure 8.13. Comparable fitness distribution between straight-fiber and steered-fiber configurations was found until fitness value of 1.2. Beyond that point, only steered-fiber laminates are able to exhibit higher buckling loads. However, the nonlinear analysis failure index requirement was not taken into account. It still remained to be seen whether the outstanding steered-fiber panels would be really able to offer mass saving potential. The best three designs of each configuration were selected and were fed to the proposed optimization scheme. The chosen designs are listed in table 8.10 and 8.11.

8.3.2. Optimization Results

The chosen three designs from section 8.3.1 were initial starting points of the proposed optimization with equivalent static loads method. As mentioned before, parallel optimization runs could be simultaneously computed to save computational time. Only the best optimized

Table 8.8.: The best optimized keel panes with λ_{comp} ≥1.00 : Optimized objective and design variables

Straight-Fiber Panel								
Mass [kg]	t_{sk} [mm]	t_{str} [mm]	D [°]	E [°]	F [°]			
3.092	0.0412	0.0436	90	90	10			
Steered-Fiber Panel								
Mass [kg]	t_{sk} [mm]	t_{str} [mm]	α_1 [°]	β_1 [°]	γ_1 [°]	α_2 [°]	β_2 [°]	γ_2 [°]
2.751	0.0354	0.0458	47	90	38	40	90	75

Table 8.9.: The best optimized keel panels: Mass effect of compression buckling constraint

λ_{comp}	Steered-Fiber Mass [kg]	Reference Mass [kg]	Δm [%]	Straight-Fiber Mass [kg]	Δm [%]	α_1 [°]	β_1 [°]	γ_1 [°]	α_2 [°]	β_2 [°]	γ_2 [°]
≥0.50	2.444		31	2.469	1	10	89	10	31	90	25
≥1.00	2.751	3.521	22	3.092	11	47	90	38	40	90	75
≥1.50	3.074		13	3.398	10	77	29	61	8	89	6

Table 8.10.: DOE Results: Straight-fiber window panel ranking

Ranking - ID	1^{st} - 83	2^{nd} - 36	3^{rd} - 61
Fitness [-]	1.195	1.187	1.182
D [°]	18	15	5
E [°]	68	88	51
F [°]	74	51	88

Table 8.11.: DOE Results: Steered-fiber window panel ranking

Ranking - ID	1^{st} - 80	2^{nd} - 75	3^{rd} - 71
Fitness [-]	1.303	1.248	1.237
α_1 [°]	70	36	41
α_2 [°]	80	1	80
α_3 [°]	85	87	29
β_1 [°]	27	49	26
β_2 [°]	9	57	21
β_3 [°]	86	67	13
γ_1 [°]	23	82	30
γ_2 [°]	53	87	89
γ_3 [°]	64	47	59

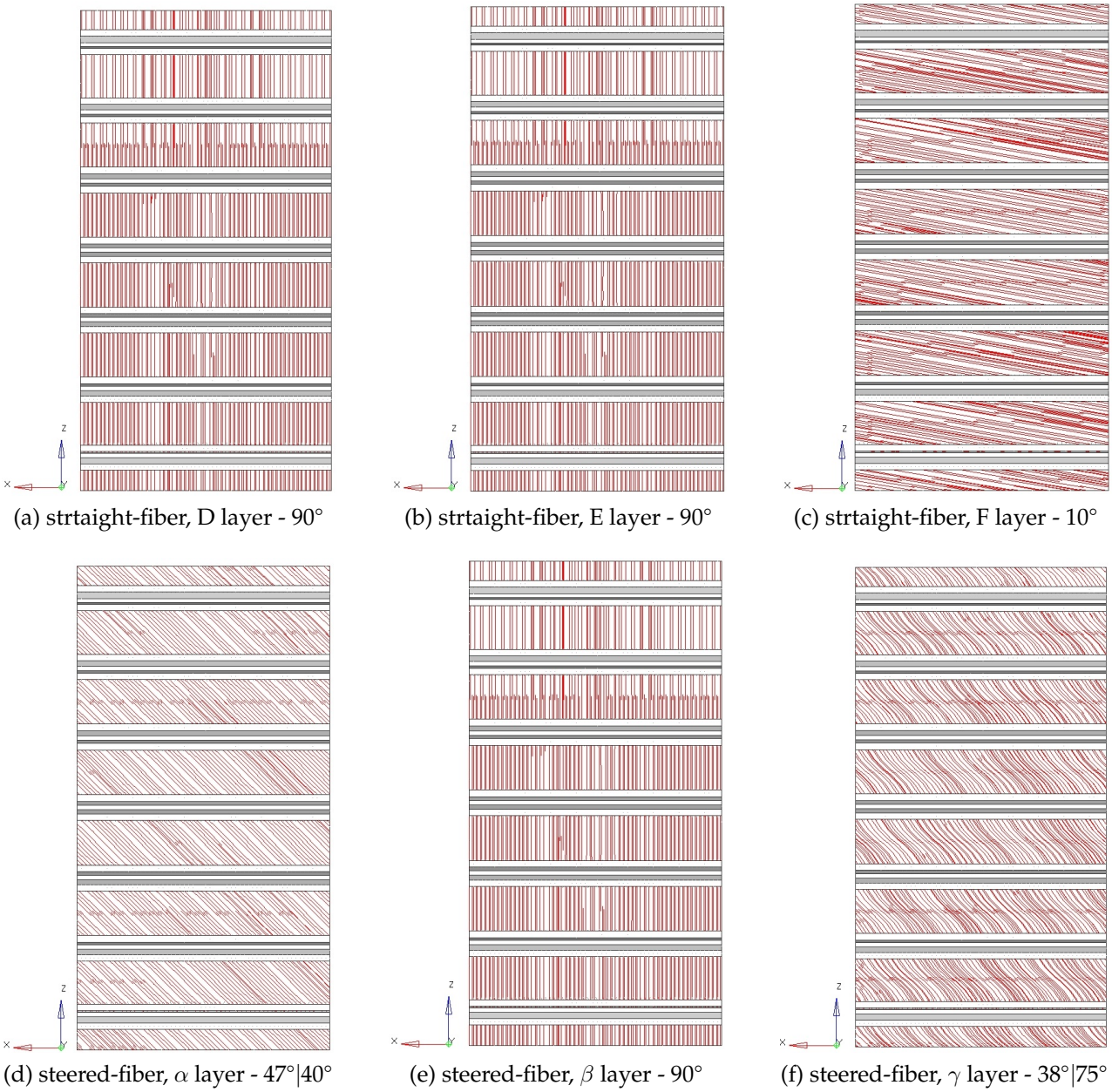

(a) strtaight-fiber, D layer - 90° (b) strtaight-fiber, E layer - 90° (c) strtaight-fiber, F layer - 10°

(d) steered-fiber, α layer - 47°|40° (e) steered-fiber, β layer - 90° (f) steered-fiber, γ layer - 38°|75°

Figure 8.12.: Optimized keel panel fiber path comparison, λ_{comp} ≥1.00

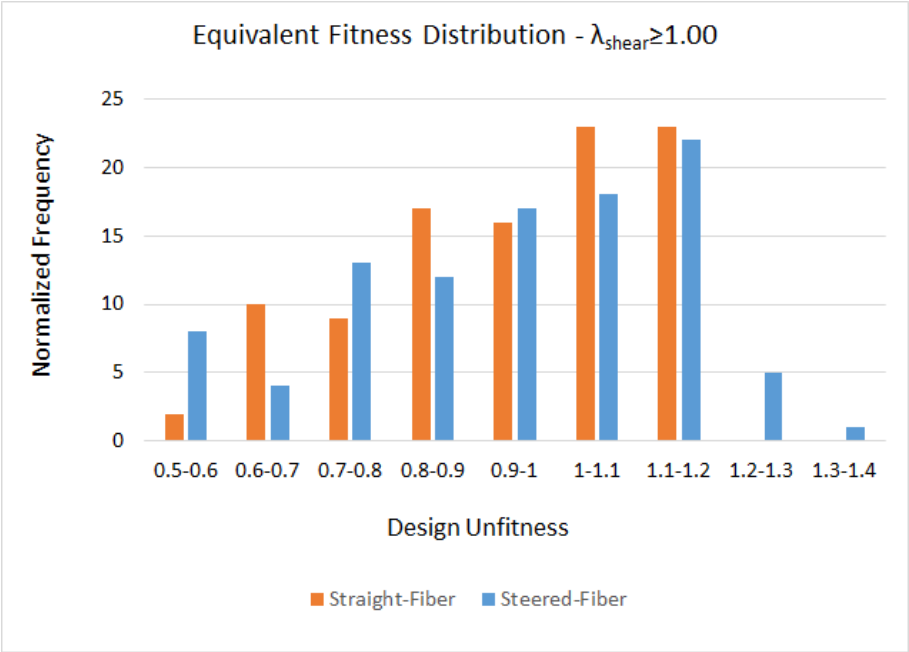

Figure 8.13.: DOE: Side Panel: Equivalent Fitness distribution with λ_{shear} ≥1.00

design's result is revealed and discussed in this chapter. Complete details of the optimization results are shown in appendix A.4.

Straght-Fiber Panels

From the three starts, the first best design obtained from DOE gave the best optimized straight-fiber window panel with 3.678 kg, saving 17% mass from the reference panel. Excluding the initial iteration, it took three design cycles to achieve the converged solution. The converged design was however not the best feasible design as the latter was already found from the first iteration. This is considered typical for an optimization via equivalent static loads, given that the best feasible design and the converged solution are only slightly apart. It was observed that the active constraints were buckling load from the combined loadcase and failure index from the pure shear loadcase. Agreement in maximum failure index determined by the nonlinear analysis and linear analysis also underlined the introduced scheme's applicability in all type of buckling loads. Internal pressure loadcase appeared to be noncritical even though the window cutout's stress concentration could have raised a concern.

Figure 8.14 shows corresponding optimization history and comparison to the steered-fiber counterpart. Detailed design variables optimization history is shown in table 8.12. As expected, optimized panel's skin was thicker around the window cutout and thinner where the cutout did not exist. Convergence of design variables and design objective can be as well observed. However, number of linear-loop design cycles did not converge but would rather stay relatively constant. As design objective had more or less settled after the first iteration, significant improvement was not expected should the scheme have been allowed to continue. Convergence difficulty occurred in the linear optimization loops perhaps was

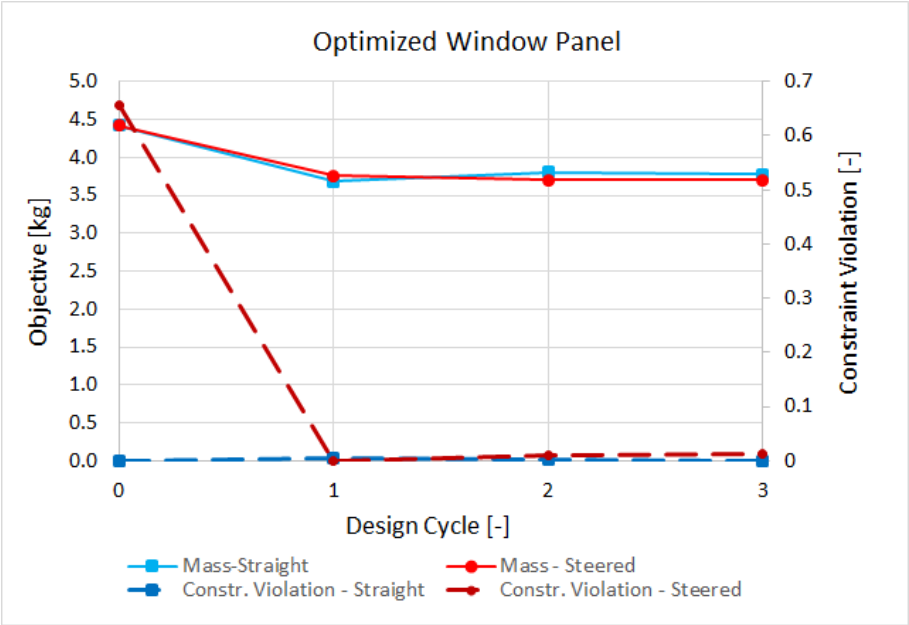

Figure 8.14.: The best optimized window panels with λ_{shear} ≥1.00

caused by mode switching behavior originated from eigenbuckling constraints[10;50].

Table 8.14 summarizes optimized panel mass from each starting design. Standard deviation was calculated based on the feasible optimized panels. Both straight-fiber and steered-fiber panels' standard deviation were of the same order of magnitude. Coefficient of variation indicating standardized measure of a probability distribution dispersion is as well tabulated. Very small coefficients of variation shown indicate low degree of objective (mass) function's multi-modality.

Steered-Fiber Panels

From the three starts, the first best design obtained from DOE led to the best optimized straight-fiber window panel with 3.698 kg. Compare to the best straight-fiber window panel mass of 3.678 kg, these two figures are almost identical. In other words, no weight benefit was yielded by the use of curvilinear fibers. While there was no mass saving, the optimized steered-fiber window panel had one plus point against the straight-fiber solution: lower stress level. The steered-fiber optimum experienced the maximum failure index of 0.85 which is 15% lower than that of straight-fiber optimum. The design drivers in this case were shear buckling and combined buckling load constraints. The proposed process with ESLM took only three design cycles to achieve the converged solution. The converged design was however not the best feasible design as the latter was already found from the second iteration. As already mentioned, this is considered typical for an optimization via equivalent static loads, given that the best feasible design and the converged solution are only slightly apart. Although being lighter, the last iteration's design violated the combined load buckling constraint. Highly agreeable maximum failure index determined by the nonlinear analysis

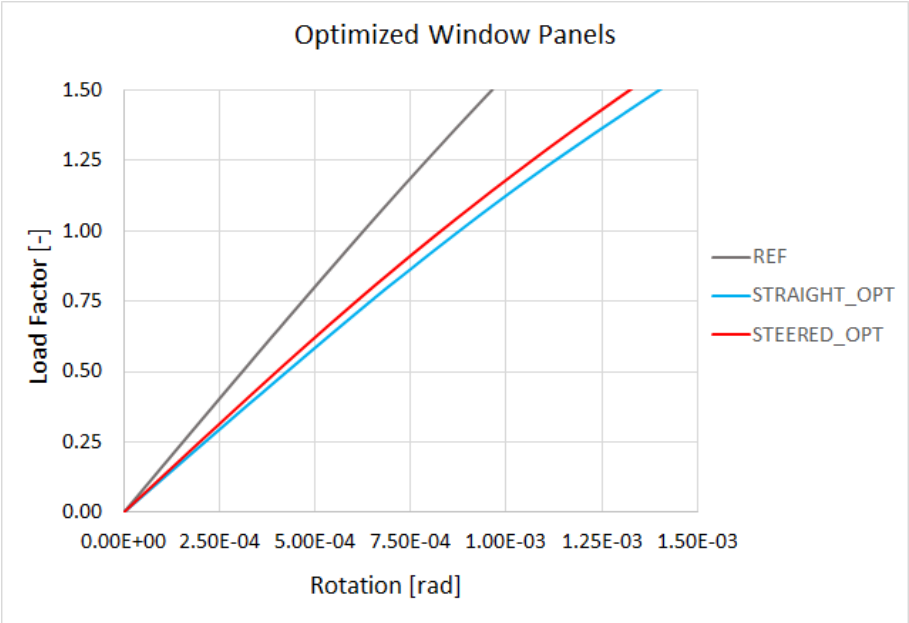

Figure 8.15.: Optimized window panels: Torsion-rotation curves, λ_{comp} ≥1.00

and linear analysis was also found. Internal pressure loadcase appeared to be sub-dominant.

Figure 8.14 shows corresponding optimization history and comparison to the straight-fiber counterpart. Detailed design variables optimization history is shown in table 8.13. In general, optimized fiber paths were not much curvilinear except the first layer where 15° fiber at the skin bay center needed to steer to 88° at stringers. As expected, optimized panel's skin was thicker around the window cutout and thinner where the cutout did not exist. Convergence of design variables and objective can be observed. Similar to straight-fiber problem, number of linear-loop design cycles did not converge. As design objective had converged since the first iteration, considerable weight saving was not expected should the scheme have been allowed to continue. Compared to the straight-fiber panel optimization, higher number of inner-loop iterations came from greater number of design variables, but convergence difficulty due to mode switching behavior was also believed to be one of the root causes.

8.3.3. Optimized Designs Verification

The optimized window panels' structural performance is verified and compared in this subsection. Figure 8.15 compares torsion-rotation curves of the optimized panels to the reference design. Torsional stiffness reduction is observed in the optimized panels due to relaxed panel buckling constraint from 150% to 100% limit load. Comparable rotation curves are observed although the curvilinear-fiber panel was slightly stiffer, both in pre- and post-buckling. Compared to panels under shortening load, smooth and almost linear postbuckling stiffness curves can be seen in the torsion loadcase. Structural responses up to only 150% limit load was of interest.

Table 8.12.: The best optimized straight-fiber window panel: Optimization History

Iteration	Linear-loop iterations	Mass [kg]	t_{sk} [mm]	$t_{sk,win}$ [mm]	D [°]	E [°]	F [°]
0		4.420	0.0458	0.0458	18	68	74
1	**24**	**3.678**	**0.0324**	**0.0368**	**12**	**73**	**40**
2	20	3.807	0.0331	0.0403	12	45	47
3	21	3.775	0.0336	0.0387	9	53	47

Table 8.13.: The best optimized steered-fiber window panel: Optimization History

Iteration	Linear-loop iterations	Mass [kg]	t_{sk} [mm]	$t_{sk,win}$ [mm]	α_1 [°]	β_1 [°]	γ_1 [°]	α_2 [°]	β_2 [°]	γ_2 [°]	α_3 [°]	β_3 [°]	γ_3 [°]
0		4.420	0.0458	0.0458	70	27	23	80	9	53	85	86	64
1	21	3.761	0.0357	0.0356	23	41	22	82	4	30	52	77	29
2	**33**	**3.698**	**0.0341**	**0.0356**	**15**	**48**	**15**	**88**	**4**	**32**	**48**	**71**	**29**
3	40	3.697	0.0338	0.0359	16	51	17	84	5	31	59	76	22

Table 8.14.: Standard Deviation of Optimized Window Panels

Design	M_1 [kg]	M_2 [kg]	M_3 [kg]	Std. Deviation	Coeff. of Variation
Straight-fiber	3.678	3.723	3.783	4.30×10^{-2}	1.15%
Steered-fiber	3.698	3.742	3.718	1.80×10^{-2}	0.48%

Displacement and Failure Index

In figure 8.16 and 8.17, corresponding transverse displacements and failure indexes of the proposed optimums are illustrated at 50%, 100% and 150% torsional limit load. Several observations can be made from the presented plots.

In terms of buckling mode, both configurations buckled with agreeable shear buckling mode shape. As revealed by the smooth stiffness curves, skin buckling mode did not change around the window cutout, and only local buckling waves started to take place at stiffened bays when the ultimate load was being reached.

Critical location where failure index first exceeded unity for both optimized panels was skin around the window frame (omitted in the figures). Twisting stress caused by buckling deformation coupled by stress concentration due to abrupt thickness change were the rationale behind this stress peak. Aluminum window frame's von mises stress was crossed-checked, and less than material yield strength values were confirmed from the verifying analysis. As reported earlier, steered-fiber panel experienced 14% lower strain than the best straight-fiber counterpart at the shear ultimate load. Failure indexes at outer skin edges were intentionally omitted because simplified boundary condition did not reflect similar buckling response shown at inner stiffened skin. Failure indexes from the combined compression-shear load were not crucial as compression insignificantly stressed the skin.

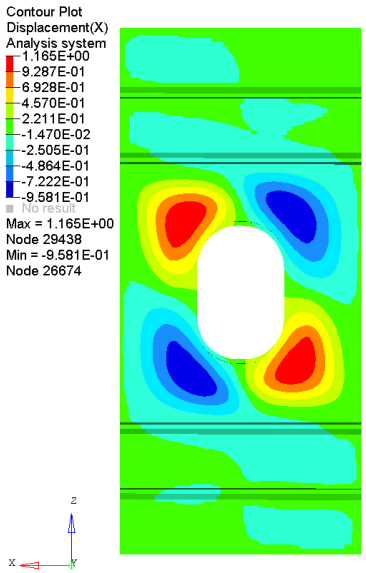

(a) w, L.F.=0.5

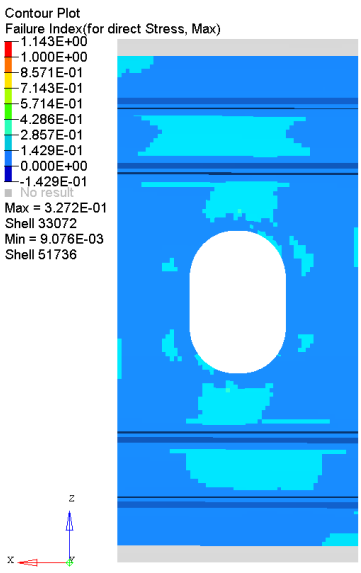

(b) F.I., L.F.=0.5

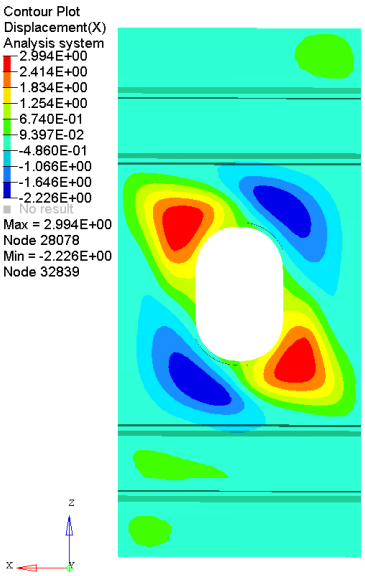

(c) w, L.F.=1.0

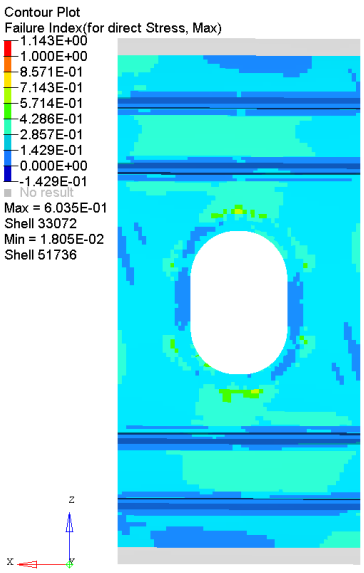

(d) F.I., L.F.=1.0

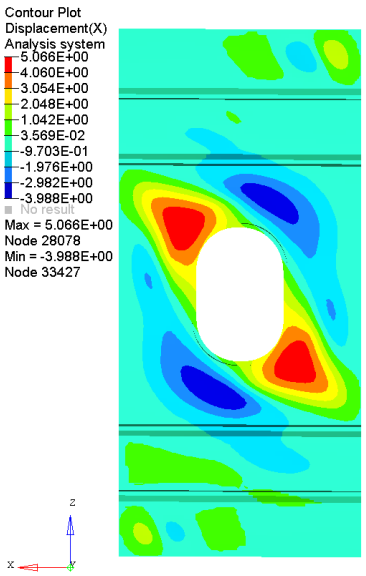

(e) w, L.F.=1.5

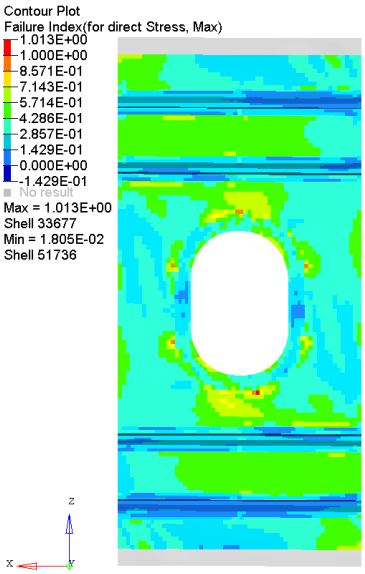

(f) F.I., L.F.=1.5

Figure 8.16.: Optimized straight-fiber window panel: transverse displacement w [mm] and failure index plots

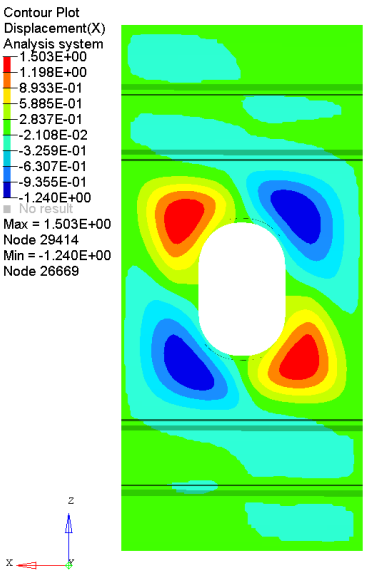

(a) w, L.F.=0.5

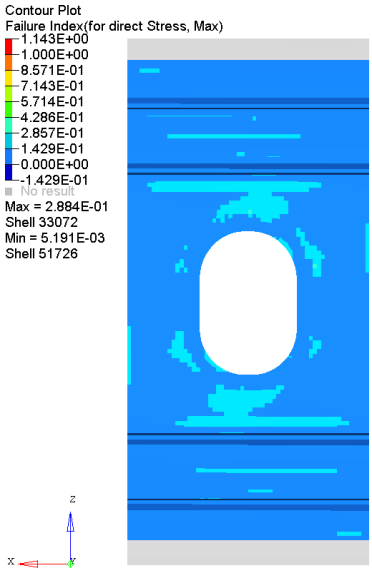

(b) F.I., L.F.=0.5

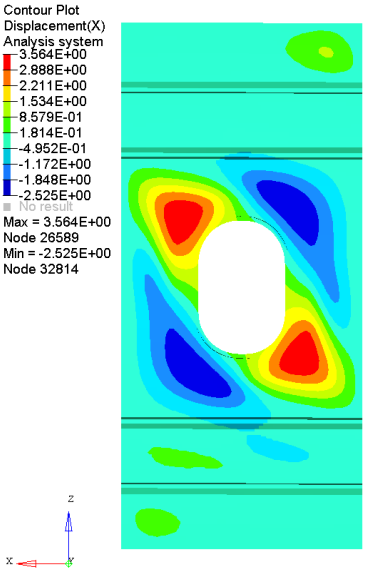

(c) w, L.F.=1.0

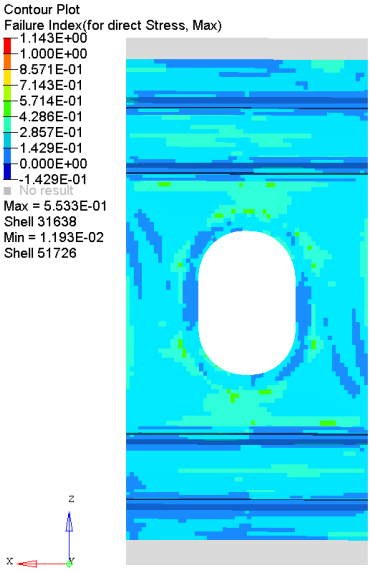

(d) F.I., L.F.=1.0

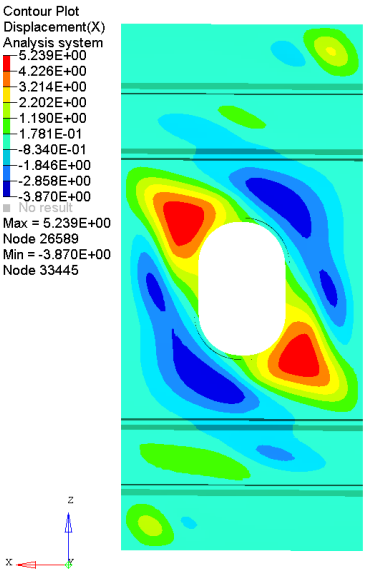

(e) w, L.F.=1.5

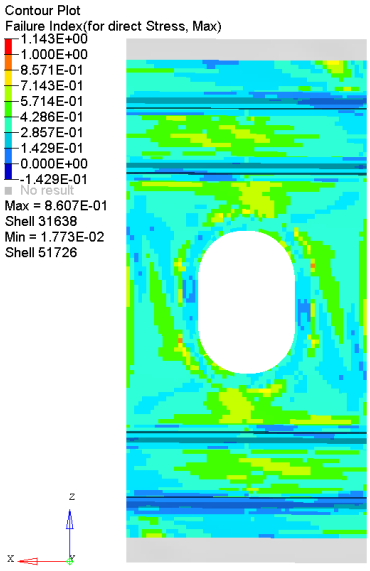

(f) F.I., L.F.=1.5

Figure 8.17.: Optimized steered-fiber window panel: transverse displacement w [mm] and failure index plots

9

Equivalent Static Load Method Charcteristics and Parametric Study

This chapter discusses optimization behavior of the proposed optimization process involving ESLM as compared to other applicable optimization processes. Computational efficiency comparison is especially focused. In order to demonstrate the comparison, the fuselage panel optimization problem previously discussed is used as study example. The chapter also provides a closer look to optimality verification of the proposed optimization method. Influence of important ESLM parameters was also studied and presented herein. Effect of different optimization stopping criteria and different number of equivalent static loads is in particular described. Verification of nonlinear responses, i.e. displacement and lamina failure index, represented by equivalent static loads was also conducted.

9.1. Characteristics of Optimization Process with ESLM as compared to other Optimization Processes

As outlined in chapter 5, several optimization techniques are applicable to solve a structural optimization problem where postbuckling responses are included. Besides the proposed ESLM as part of the full optimization process, advanced response surface-based optimization GRSM was also utilized by the author to investigate and compare optimization performances, i.e. computational efficiency and solution's optimality. Discussion and comparison with respect to traditional optimization methods, e.g. conventional gradient-based optimization and genetic algorithm, are as well a part of this sub-chapter.

9.1.1. Computational Efficiency Verification

Efficiency directs to duration the scheme requires to obtain the optimized result. Optimization computational efficiency becomes one of the top priorities once dealing with a real-world, large-scale problem where time and budget constraints are stringent. The efficiency of ESLM per se and as part of a gradient-based process, when compared to other applicable optimization processes, is discussed using fuselage panel problems previously studied as verification specimens. Although only the fuselage panels' results are studied here, but the verification outcome should indicate the validity of the proposed method in a more generic application .

Example: Fuselage Keel Panels

Optimization efficiency in terms of number of design analyses and computation duration was evaluated based on the optimized keel panels constrained by 50% compression buckling load (equation 6.1). Table 9.1 summarizes the number of design iterations and nonlinear analyses of both optimized steered- and straight-fiber keel panels. For each ESLM design cycle including the initial one, three displacement-based nonlinear analyses were computed so as to reach prescribed applied compressive force. Approximated average duration of the geometrical nonlinear analysis by MSC Nastran solution 106 on a Dual CPU Intel Xeon X5550 - 2.67 GHz was 150 seconds. Total optimization duration was a matter of a couple of hours. Not to underestimate, computation time spent on design of experiments must be included in the efficiency calculation. For instance, DOE on steered-fiber keel panel sampled 400 design points. Each point required 75 seconds on the same machine, but parallel processing helped alleviate the computational burden as much as quadruple the time spent on a sequential analysis run. Altogether, DOE analysis took two to three hours before the proposed ESLM could commence.

From the table, quick optimization convergence of the best optimized designs can be observed whereas tedious optimizations led to sub-optimal solutions. The observation highlights initial design sensitivity of the presented gradient-based optimization scheme. More design angle variables in steered-fiber panels also raised number of total linear-loop iterations considerably.

Example: Fuselage Window Panels

Optimization efficiency in terms of number of design analyses and computation duration was evaluated based on the optimized window panels (equation 6.2). Table 9.2 summarizes number of design iterations and nonlinear analyses of both optimized steered- and straight-fiber side panels. For each ESLM design cycle including the initial one, three rotation-based nonlinear analyses were computed so as to reach prescribed applied torsional moment. Approximately average duration of the geometrical nonlinear analysis by MSC Nastran solution 106 on a Dual CPU Intel Xeon X5550 - 2.67 GHz was 85 seconds. Shear load produces much smoother pre- to postbuckling stiffness transition than shortening load; nonlinear shear analysis thus converges faster. Subsequently, total optimization duration completed within an hour. As aforementioned, computation time spent on design of experiments must be included in the efficiency calculation. DOE on window panel sampled 100 design points. Each point required 100 seconds on the same machine. With a help from parallelization, almost an hour was required before the proposed ESLM could commence.

From the table, only few design cycles were required to meet prescribed convergence criterion, optimized design masses were as well comparable. Significantly higher number of design variables in steered-fiber panels insignificantly affected number of total linear-loop iterations. Difficulty in inner-loop optimization convergence owed to buckling mode switching phenomenon. The issue was exaggerated further by having two competing critical

buckling loadcases.

Computational Efficiency Comparison

Although outstanding efficiency improvement was expected, computational cost comparison against the response-surface based Global Response Surface Method outlined in sub-chapter 5.3.1 was conducted to give an impression of how large the number of nonlinear analyses reduction was. Efficiency of the optimization process with ESLM was based on a nonlinear displacement optimization on a fuselage keel panel conducted by the author[53]. Optimization efficiency of GRSM was based on an analogous optimization problem except that the specimen was a fuselage window panel (Ungwattanapanit and Baier[51]). As the computational efficiency can be roughly indicated by nonlinear analysis burden, table 9.3 summarizes the number of nonlinear analyses required by each optimization strategy. The computational performance of the proposed gradient-based ESLM is clearly demonstrated. The efficiency margin shown by ESLM of course will be reduced when the global optimum is to be found, e.g. by the proposed DOE outlined in sub-chapter 5.1. However, efficiency superiority by at least a factor of five is still very well expectable by the use of ESLM. Figure 9.1 illustrates corresponding optimization history comparison. ESLM clearly exhibits typical gradient-based optimization behavior where optimization convergence and solution are efficiently found, while GRSM seems to be dominated by GA characteristic, but to a lessor extent.

A comparison to an evolutionary algorithm performance would be even more contrasting especially when more design variables are involved, like, in the case of steered-fiber laminates. Benchmarking study conducted by Luo[32] showed GRSM superiority over traditional GA in all examples of single-objective problem. In terms of a comparison to conventional gradient-based optimization algorithm where nonlinear analysis response is directly used to derive design sensitivities, it was found infeasible to do so for this type and scale of structural problem as accurate gradients calculation could not be provided by an iterative nonlinear implicit finite element solver. This on the other hand underlines the advantage of the proposed ESLM once again. Nevertheless, Park[42] conducted a comparative study between an optimization process with ESLM and conventional gradient-based method based on a ten-bar truss problem, where geometric and material nonlinearity were considered. It was found that the number of nonlinear analysis required by the conventional method ranged from 256 to 301, while the scheme assisted by ESLM needed only 5 to 11 nonlinear analyses, depending on what type of nonlinearity was included.

9.1.2. Local-Global Search Capability

As the proposed ESLM is based on a gradient-based optimization in the inner loop, care must be taken when obtaining an optimum as it may highly depend on initial design variables. As suggested in sub-chapter 5.1, DOE of thin-ply laminates enhances the global search capability of the proposed optimization procedure when design space multi-modality is to be dealt with. Demonstration of the whole optimization process can be found in chapter 8. Optimized solutions as directly compared to those from other non-gradient methods, e.g. GRSM and

Table 9.1.: Optimized Keel Panels: Number of design iterations and nonlinear analyses

Straight-Fiber Panels					
Initial Design ID	41	172	147	90	238
Optimized Mass [kg]	(2.461)	(2.358)	2.489	2.528	**2.469**
No. of ESLM iterations	4	2	4	5	**3**
No. of nonlinear analyses	15	9	15	18	**12**
No. of linear-loop iterations	35	22	25	15	**13**
Steered-Fiber Panels					
Initial Design ID	253	354	290	396	93
Optimized Mass [kg]	2.600	2.702	**2.444**	2.809	(2.171)
No. of ESLM iterations	6	10	**5**	5	1
No. of nonlinear analyses	21	33	**18**	18	6
No. of linear-loop iterations	98	300	**62**	90	5

*() = infeasible design

Table 9.2.: Optimized Window Panels: Number of design iterations and nonlinear analyses

Straight-Fiber Panels			
Initial Design ID	83	36	61
Optimized Mass [kg]	**3.678**	3.723	3.783
No. of ESLM iterations	**3**	3	2
No. of nonlinear analyses	**12**	12	9
No. of linear-loop iterations	**65**	83	62
Steered-Fiber Panels			
Initial Design ID	80	75	71
Optimized Mass [kg]	**3.698**	3.742	3.718
No. of ESLM iterations	**3**	2	3
No. of nonlinear analyses	**12**	9	12
No. of linear-loop iterations	**94**	50	64

Table 9.3.: Number of nonlinear analyses required by ESLM and GRSM optimization strategy

	ESLM[53]	GRSM[51]
Straight-Fiber Panels		
No. of design variables	3	3
No. of nonlinear analyses	7	261
Steered-Fiber Panels		
No. of design variables	6	9
No. of nonlinear analyses	6	171

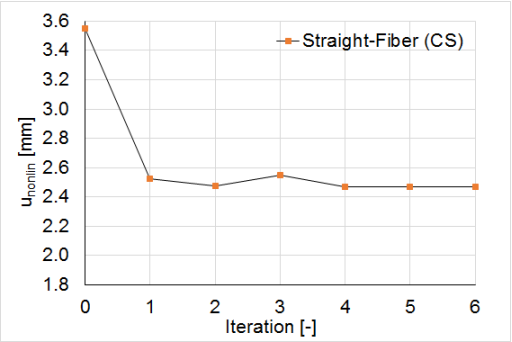

(a) ESLM, Straight-fiber

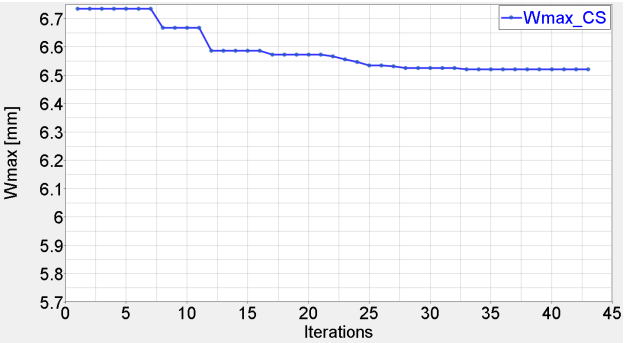

(b) GRSM, Straight-fiber

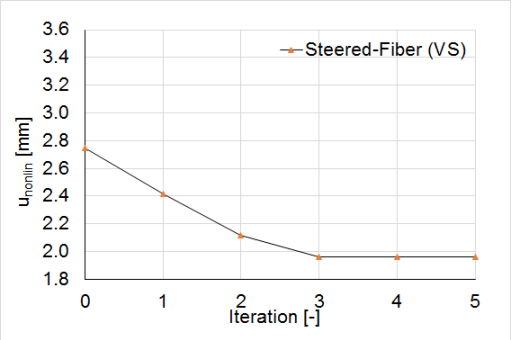

(c) ESLM, Steered-fiber

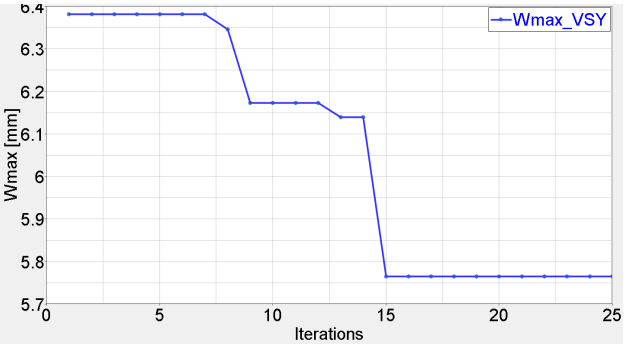

(d) GRSM, Steered-fiber

Figure 9.1.: Optimization history: Equivalent Static Load Method[53] vs Global Response Surface Method[51]

GA, would be interesting, but would as well require tremendous computational resource for real-world problems presented herein. Indirect global-optimality verification can be done by measuring coefficient of variation of obtained results. The coefficient of variation is defined as the ratio between standard deviation and mean value. The lower the coefficient, the less dependency on initial design values the problem is. Presented in table 8.5 and 8.14, 0.5% - 5% coefficient of variation is reported, indicating low degree of initial design vector dependency on mass. In other words, the obtained optimized design masses can be regarded as close-to-global optimal solution. Beside, the optimality criteria verification of the obtained results can be found in sub-chapter 9.2.

9.1.3. Usability Comparison

Usability is the degree to which a software tool can be used to achieve quantified objectives with effectiveness, efficiency, and satisfaction. In the more informal definition, usability is interchangeable with the term "user-friendliness". Although a systematic study would have to be conducted if software usability was to be indicated and compared, a qualitative discussion is provided here to give the reader a first impression on how usable the proposed ESLM is.

Assuming that the reader is familiar with conventional optimization techniques, an optimization process involving ESLM is very analogous to other well-known gradient-based

methods, e.g. SQP, MFD. In addition to optimization parameters required to setup such a method in the ESLM inner loop, the user requires to specify only two more parameters in the outer loop. Firstly, number of equivalent static loads, depending on how nonlinear the response in a temporal scale is, must be defined. Influence of number of equivalent static loads is presented in sub-chapter 9.4. Secondly, ESLM stopping criteria must be defined. Either convergence of design objective or convergence of design variables can be chosen. Corresponding convergence threshold then must be specified. What makes an optimization with ESLM different to conventional gradient methods is that the converged design at the last iteration may not be the best (optimal) design among all of calculated outer-loop iterations. Results presented in chapter 8 however suggest that the last design iteration is typically the best feasible design. Influence of different stopping criteria is presented in sub-chapter 9.3. Compared to non-gradient optimization methods where a number of setup parameters and sub-processes involve, an optimization scheme with ESLM is obviously more usable. Unlike in conventional gradient-based optimization, repeatability of optimized solution cannot be guaranteed by a process assisted by ESLM since iterative nonlinear analysis may be not 100% repetitive. Nevertheless highly similar optimized solutions are still expected as long as the respective starting design vectors are identical.

9.2. Optimality Verification

Optimization optimality of the optimized designs obtained is one of the most important aspects to be verified when a new optimization scheme is introduced. Optimality indicates how optimal the optimized design is with respect to Karush Kuhn Tucker (KKT) optimality conditions[4]. Although optimization optimality cannot promise global optimality of the solution, it is indeed necessary as the solution's optimality, either local or global, is affirmed.

Though direct comparison between the proposed ESLM optimized design and conventional gradient-based optimized solution was prohibitive due to difficult computation of accurate nonlinear analysis response sensitivities, optimality of the optimized designs could nevertheless still be testified. Karush-Kuhn-Tucker (KKT) optimality conditions consists of stationarity requirements, complementary requirements, and primal and dual feasibility. The KKT criteria are shown in equation 9.2 through 9.4 with an introduction of the Lagrange function L and Lagrange multiplier λ. Slightly violated KKT stationarity requirements leading to close-to-optimal solution in engineering optimization problems sometimes exist. However the solution is generally considered acceptable in practice as more detailed analysis of the obtained solution would have to be conducted afterwards anyway.
Given the Lagrange function:

$$L(x, \lambda_j) = f(x) + \sum_j \lambda_j g_j(x) \tag{9.1}$$

The KKT conditions are the stationarity requirements:

$$\nabla_x L = \nabla_x f + \sum_j \lambda_j \nabla_x g_j = 0 \tag{9.2}$$

the complementarity requirements:

$$\sum_j \lambda_j \nabla_x g_j = 0 \quad j = 1, ..., p \tag{9.3}$$

and the primal and dual feasibility:

$$\begin{aligned} x &\in X \\ g_j &\leq 0 \quad j = 1, ..., p \\ \lambda_j &\geq 0 \quad j = 1, ..., p \end{aligned} \tag{9.4}$$

In 2003, Park and Kang[41] proved that the stationarity conditions for a dynamic problem and a static problem are identical when the optimization involving ESLM terminates. However, Stolpe[48] later disproved the claim by Park and Kang and suggested an alternative algorithm which satisfied the KKT criteria by adding the gradients calculation step to the original nonlinear analysis response. The gradients computation of nonlinear analysis responses tremendously undermines the optimization efficiency originally promoted for. Optimality of the best optimized stiffened panels derived from equation 6.1 therefore had to be verified. The optimality of the proposed nonlinear analysis response optimization scheme is evaluated as the following, using fuselage panel problems previously discussed as demonstrators. Although only the fuselage panels' results are presented, but the verification outcome should indicate the validity of the proposed method in the more generic level.

9.2.1. Example: Fuselage Keel Panels

Table 9.4 reveals constraint function value of each type of response. Note that there could be more than one active failure index constraints, but only the minimum constraint values are shown. The best optimized straight-fiber and steered-fiber panels both activated the nonlinear analysis failure index constraints. Besides the failure index constraints, they were constrained by global panel collapse and stiffener crippling load respectively.

In lieu of direct but tedious KKT optimality evaluation, correlation of active nonlinear analysis failure indexes and those of linear static analysis would implicitly justify the optimality conditions of the structure actively constrained by nonlinear analysis failure indexes since the design optimality was already satisfied in the linear-loop optimization. Table 9.4 already shows a very close correlation of the minimum failure index constraint retrieved from the two types of analysis, promising justifiable optimality conditions at the optimized solutions. More detailed verification can be found in section 9.5.

9.2.2. Example: Fuselage Window Panels

Table 9.5 reveals constraint function value of each type of response. Note that there could be more than one active failure index constraints, but only the minimum constraint values are shown. The best optimized steered-fiber window panel did not activate the nonlinear

analysis failure index constraints. Compliance of KKT conditions can be therefore assumed as they were already evaluated in the linear-loop optimization[36]. The attention now turns to the optimized straight-fiber panel as nonlinear analysis failure indexes were at the critical threshold. Besides the failure index constraints, combined load buckling was also activated by the optimized straight-fiber panel.

Instead of direct KKT optimality evaluation, correlation of active nonlinear analysis failure indexes and those of linear static analysis would implicitly justify the optimality conditions of the optimized structure since the design optimality was already satisfied in the linear-loop optimization. Compared to the straight-fiber keel panel, the optimized window panel showed larger deviation in failure index correlation as shown in table 9.5. Still, good agreement was observed with approximately 6% failure index discrepancy between linear and nonlinear analysis. More detailed verification can be found in section 9.5.

9.3. Stopping Criteria

Influence of different ESLM stopping criteria were investigated. Note that the investigation did not vary stopping criteria deployed in the conventional linear optimization loop. While the presented study opted convergence of design objective to be the termination criterion, convergence of design variables, which also means convergence of equivalent static loads, between two consecutive ESLM design cycles is an alternative stopping strategy. Equation 9.5 shows the design object convergence criterion. The objective convergence of two consecutive iterations is satisfied if a relative change in design objective is less than 1%. Equation 9.6 declares the design variable convergence criteria used in this study. The convergence of every design variable in two successive iterations is satisfied if a relative change in every design variable is less than 1%.

$$\left| \frac{f(x)^k - f(x)^{k-1}}{f(x)^{k-1}} \right| \leq 0.01 \tag{9.5}$$

$$\left| \frac{x_i^k - x_i^{k-1}}{x_i^{k-1}} \right| \leq 0.01 \tag{9.6}$$

Two keel panel case studies were conducted to observe the influence of both kinds of stopping criteria. Straight-fiber and steered-fiber keel panels under axial shortening were optimized. Linear buckling load was constrained at the limit load level. Shortening stiffness in the form of axial deformation was also required not to exceed 120% shortening of the reference panel at the ultimate load. Shear and internal pressure loadcases were not considered. The corresponding optimization formulation is written in equation 9.7. Both convergence criteria were implemented in Altair HyperMath script in conjunction with ESLM suite available in Altair OptiStruct 13.0[3]. Radioss implicit dynamic nonlinear analysis was chosen for the geometrical nonlinear analysis instead of OptiStruct nonlinear static analysis (NLGEOM) thanks to the former's scheme stability and robustness. Radioss implicit dynamic nonlinear solver was verified against Abaqus 6.13 nonlinear static solver; agreeable

load-shortening curves, buckling modes, collapse mode shape, and critical global buckling load were observed[52].

Design Objective:	To minimize panel $Mass$
Design Variables:	
Straight-fiber:	Ply thicknesses: t_{sk}, t_{str0}, t_{str45}, t_{str90}
	Ply angles: D, E, F
Steered-fiber:	Ply thicknesses: t_{sk}, t_{str0}, t_{str45}, t_{str90}
	Ply angles: α_1, β_1, γ_1, α_2, β_2, γ_2
Subject to:	Failure indexes, $FI_e \leq 1.0$
	Local panel buckling factor, $\lambda_{local,comp} \geq 0.667$
	Shortening (nonlinear analysis), $\bar{u}_{nonlin} \leq 1.20$
	Ply thicknesses:
	$0.01 \leq t_{sk} \leq 0.1$ mm
	$0.05 \leq t_{str0}, t_{str45}, t_{str90} \leq 0.5$ mm
	Ply angles, $0^\circ \leq D, E, F, \alpha, \beta, \gamma \leq 90^\circ$
Loadcases:	Pure Axial Compression - Ultimate

(9.7)

9.3.1. Straight-Fiber Panel

Table 9.6 demonstrates the influence of different stopping strategies towards the optimized straight-fiber keel panel. Convergence δ_{obj} and δ_{var} was defined by the left side of equation 9.6 and 9.5 respectively. If the design objective criterion was to be chosen, the optimized panel mass of 2.999 kg would be found within only three iterations. It would instead take nine iterations if the design variable criteria were to be selected. Although longer optimization duration would be required, the best feasible design, obtained from the sixth iteration, revealed only slightly lighter panel mass at 2.992 kg. Note that the optimization governed by design variables relative change did not offer the lightest panel in the last iteration where the prescribed criteria were complied. Nevertheless, mass deviation between the last design cycle and the best feasible design was negligible.

Resulting panel masses from two different convergence criteria differed from each other by only seven grams; it was clearly too little to be credited. Optimized design variables of both panels were also very similar. Optimized stacking sequence may seem to be different but as thin-ply laminates were utilized, stacking sequence effect became almost nullified. Optimized ply angles from both designs were in fact comparable with the following pairing ply orientations: 71° - 66°, 47° - 49°, and 12° - 0°. From this particular study, It is fair to state that the design variables convergence induced unnecessary additional design iterations without purposeful objective improvement.

9.3.2. Steered-Fiber Panel

Table 9.6 demonstrates the influence of different stopping strategies towards the optimized steered-fiber keel panel. Unlike the straight-fiber problem, both stopping conditions led to identical optimized panel. The best feasible panel also came from the last design iteration where stopping criteria were satisfied. Relatively quick convergence was as well observed as only five optimization iterations were carried out. Compared to the optimized straight-fiber panels, steered-fiber laminates exhibited superior weight performance in this particular loading condition by being almost 20% lighter.

Table 9.4.: Optimized Keel Panels: Constraint value g_j

Panel	F.I. Nonlinear	F.I. Linear	$\lambda_{local,comp}$	$\lambda_{global,comp}$	$\lambda_{str,local}$	$\lambda_{str,cripp}$	$\lambda_{local,shear}$
Straight-Fiber	0.0080	-0.0081	inactive	-0.0025	inactive	inactive	inactive
Steered-Fiber	0.0070	-0.0015	-0.0076	inactive	inactive	-0.0027	inactive

Table 9.5.: Optimized Window Panels: Constraint value g_j

Panel	F.I. Nonlinear	F.I. Linear	$\lambda_{local,comb}$	$\lambda_{local,shear}$
Straight-Fiber	0.0130	-0.0601	0.0045	inactive
Steered-Fiber	inactive	inactive	0.0095	-0.0196

Table 9.6.: The optimized straight-fiber keel panel: Optimization convergence history

Iteration	Linear-loop Iterations	Mass [kg]	δ_{obj} [%]	t_{sk} [mm]	t_{str0} [mm]	t_{str90} [mm]	t_{str45} [mm]	D [°]	E [°]	F [°]	$\delta_{var,max}$ [%]
0		3.521		0.0333	0.125	0.125	0.125	45	45	45	
1	6	3.033	**13.9**	0.0347	0.132	0.05	0.05	63	35	27	**60.0**
2	3	2.979	**1.8**	0.0344	0.122	0.05	0.05	80	53	20	**50.9**
3	3	**2.999**	**0.7**	0.0345	0.126	0.05	0.05	71	47	12	**41.6**
4	4	3.004		0.0342	0.131	0.05	0.05	59	59	0	**100.0**
5	2	3.004		0.0337	0.141	0.05	0.05	51	66	0	**12.3**
6	2	2.992		**0.0350**	**0.114**	**0.05**	**0.05**	**49**	**66**	**0**	**19.6**
7	2	3.000		0.0356	0.106	0.05	0.05	47	73	0	**10.9**
8	2	3.003		0.0354	0.110	0.05	0.05	47	72	0	**4.0**
9	2	3.003		0.0354	0.110	0.05	0.05	47	72	0	**0.0**

Table 9.7.: The optimized steered-fiber keel panel: Optimization convergence history

Iteration	Linear-loop Iterations	Mass [kg]	δ_{obj} [%]	t_{sk} [mm]	t_{str0} [mm]	t_{str90} [mm]	t_{str45} [mm]	α_1 [°]	β_1 [°]	γ_1 [°]	α_2 °]	β_2 [°]	γ_2 [°]	$\delta_{var,max}$ [%]
0		3.521		0.0333	0.125	0.125	0.125	45	45	45	45	45	45	
1	6	2.886	**18.0**	0.0251	0.265	0.05	0.05	63	63	63	27	27	27	**112.4**
2	5	2.399	**16.9**	0.0213	0.192	0.05	0.05	81	81	81	9	9	9	**66.7**
3	6	2.341	**2.4**	0.0204	0.192	0.05	0.05	90	90	90	0	0	0	**100.0**
4	2	2.398	**2.4**	0.0196	0.223	0.05	0.05	90	90	90	0	0	0	**16.1**
5	2	**2.398**	**0.0**	**0.0196**	**0.223**	**0.05**	**0.05**	**90**	**90**	**90**	**0**	**0**	**0**	**0.0**

9.4. Number of Equivalent Static Loads

Although insignificant effect was expected due to constant shortening rate, influence of number of equivalent static loads used in the linear-loop optimization was studied to reaffirm the hypothesis. Three optimization runs with a single, five, and twenty equivalent static loads were performed on the straight-fiber keel panel. Commercial off-the-shelf ESLM suite available in Altair OptiStruct 13.0[3] was deployed together with Radioss implicit dynamic nonlinear analysis. Axial stiffness constraints was additionally specified, but no panel failure loads were considered. Shortening and rotation loadcases producing reference panel's critical buckling eigenvalues (λ = 1.0) were applied. The corresponding optimization formulation is written as in equation 9.8.

Design Objective:	To minimize panel $Mass$
Design Variables:	
Straight-fiber:	Ply thicknesses: t_{sk}, t_{str0}, t_{str45}, t_{str90}
	Ply angles: D, E, F
Subject to:	Failure indexes, $FI_e \leq 1.0$
	Local panel buckling factor, $\lambda_{local,comp} \geq 0.667$
	Shortening (linear analysis), $\bar{u}_{linear} \leq 1.000$
	Shortening (nonlinear analysis), $\bar{u}_{nonlin} \leq 1.000$
	Panel shear buckling factor, $\lambda_{local,shear} \geq 1.000$
	Ply thicknesses:
	$0.01 \leq t_{sk} \leq 0.1$ mm
	$0.05 \leq t_{str0}, t_{str45}, t_{str90} \leq 0.5$ mm
	Ply angles, $0° \leq D, E, F \leq 90°$
Loadcases:	Pure Axial Compression - Ultimate
	Pure Shear - Ultimate

(9.8)

Given identical initial design, design objective and variables optimized from three different runs reveal almost identical values as shown in table 9.8. Meager effect of number of equivalent static loads variation in this particular application was confirmed. Effect of number of equivalent static loads towards optimization efficiency is shown in table 9.9. As can be foreseen, number of equivalent static loads barely had an impact over computational performance. Agreeable observations were also reported in the case of flying-wing Unmanned Aerial Vehicle (UAV) structure[22].

9.5. Verification of Nonlinear Analysis Responses represented by Equivalent Static Loads

Nonlinear analysis responses i.e. displacement and laminate failure index were represented by equivalent static loads in the linear-loop optimization. Perfect correlation was enforced in every initial step but more deviation may have occurred down the road when the optimization proceeded further. Matching nonlinear analysis responses at an optimized design signal the ESLM optimization convergence and justifiable design's optimality conditions as previously mentioned. Comparison of original nonlinear analysis displacements and failure indexes to those of equivalent linear static analysis is demonstrated through fuselage panels previously discussed in the following subsections. Although only the best optimized panels' results are presented, but the verification outcome should indicate the validity of the proposed method in a more generic application.

As equivalent static loads were generated based on nonlinear analysis displacement, a displacement comparison of the best optimized panels both straight-fiber and steered-fiber was performed at the design ultimate load level or 150% limit load. Corrected failure indexes were also compared at the same load level.

9.5.1. Example: Optimized Keel Panels

Detailed in sub-chapter 5.2.3, a small failure index correction factor was necessary to make maximum linear static failure index exact to maximum nonlinear static failure index before a subsequent linear-loop optimization began. As a result, displacement-based equivalent static loads, in every initial linear-loop optimization iteration, produced the same displacement field and maximum failure index as seen in the original nonlinear analysis. Failure index correction factor of the optimized straight-fiber and steered-fiber panel was 1.113 and 1.130 respectively. Figure 9.2 and 9.3 show displacement and failure index comparison between linear analysis and geometrical nonlinear analysis. Only failure indexes at stringers and skin strips underneath them were considered and constrained as skin bay between stringers would produce wrong failure index responses due to unrotated Lagrangian coordinate system. As mentioned before the most stressed components were stiffeners and skin under their feet, the stationary coordinate system sufficed in this case.

In terms of displacement, very close correlation can be observed. The overall displacement plots take into account the shortening and transverse deformation. Larger discrepancy in terms of failure indexes can be seen. Still, less than 5% failure index discrepancy was found at the critical panel skin. Higher degree of error was found at stringers. The equivalent static load slightly underestimated failure index at the most critical stringer. Unmatched critical locations were also observed. The outer stringer slightly absorbed more loads than its counterparts due to differences in stringer pitch.

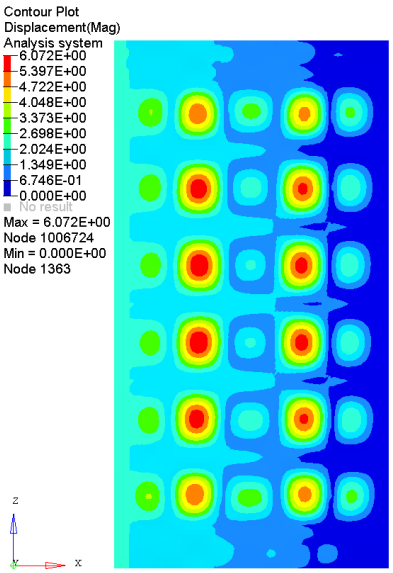

(a) Straight-fiber, Linear analysis

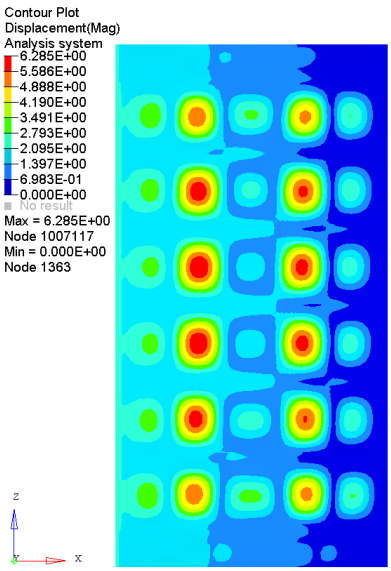

(b) Straight-fiber, Nonlinear analysis

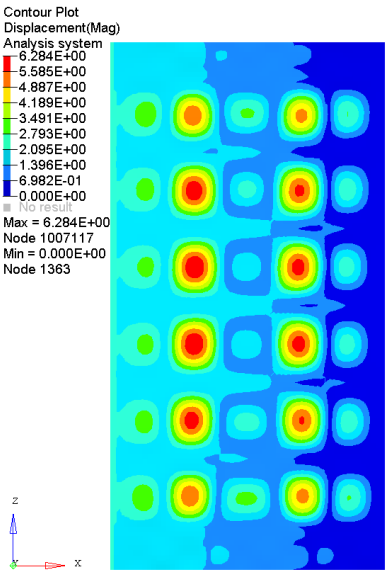

(c) Steered-fiber, Linear analysis

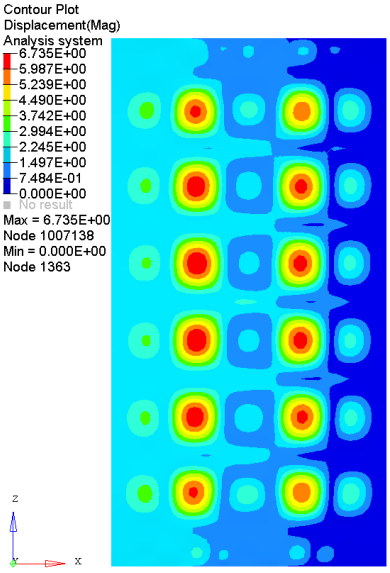

(d) Steered-fiber, Nonlinear analysis

Figure 9.2.: Optimized keel panels: Nonlinear analysis displacement verification

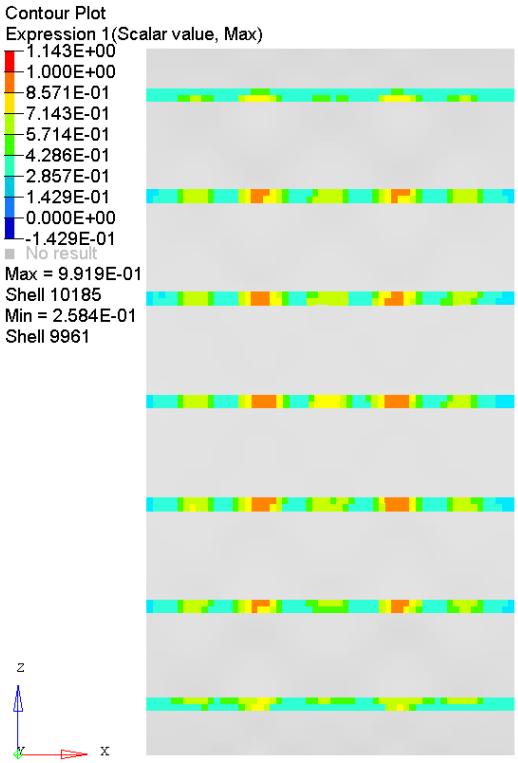

(a) Straight-fiber, Skin, Linear F.I.

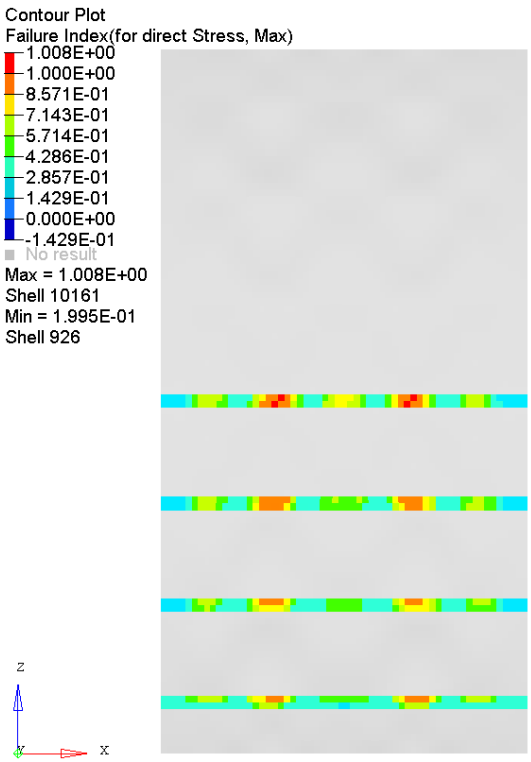

(b) Straight-fiber, Skin, Nonlinear F.I.

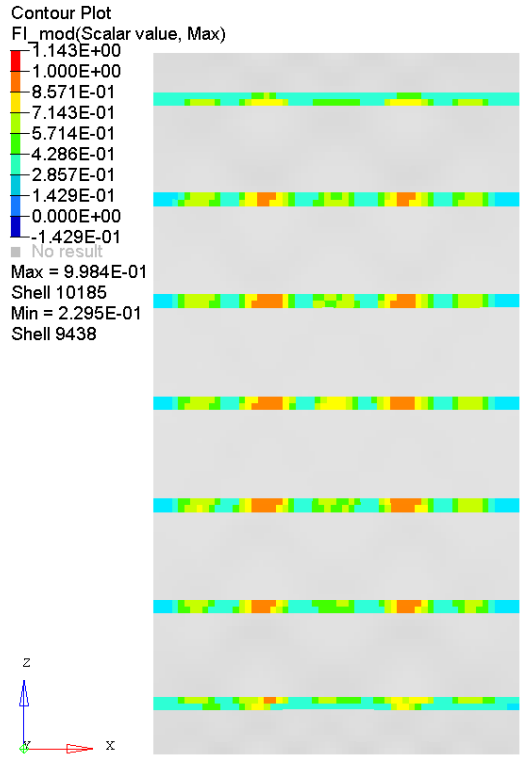

(c) Steered-fiber, Skin, Linear F.I.

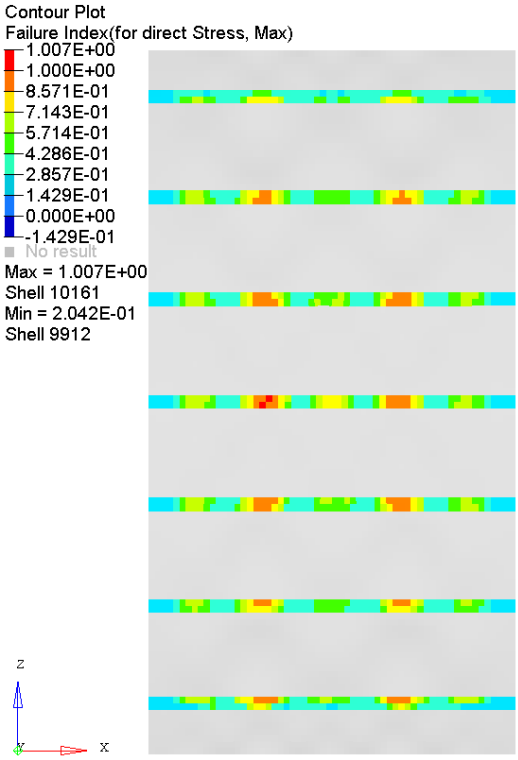

(d) Steered-fiber, Skin, Nonlinear F.I.

Figure 9.3.: Optimized keel panels: Nonlinear analysis failure index verification

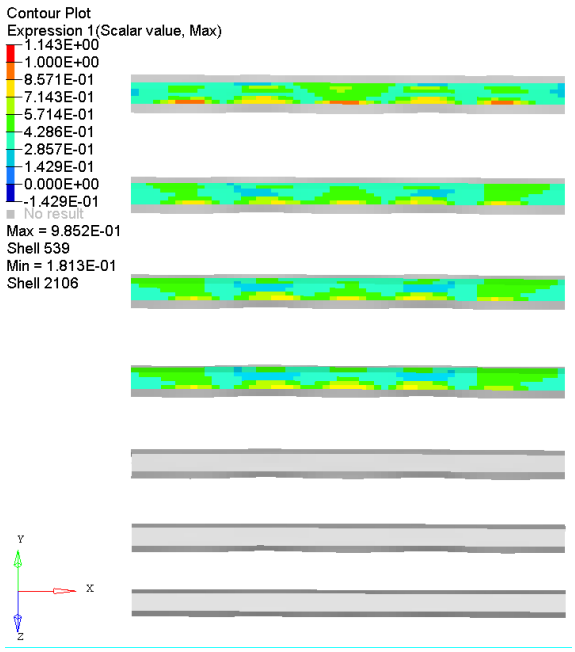

(e) Straight-fiber, Stringer, Linear F.I.

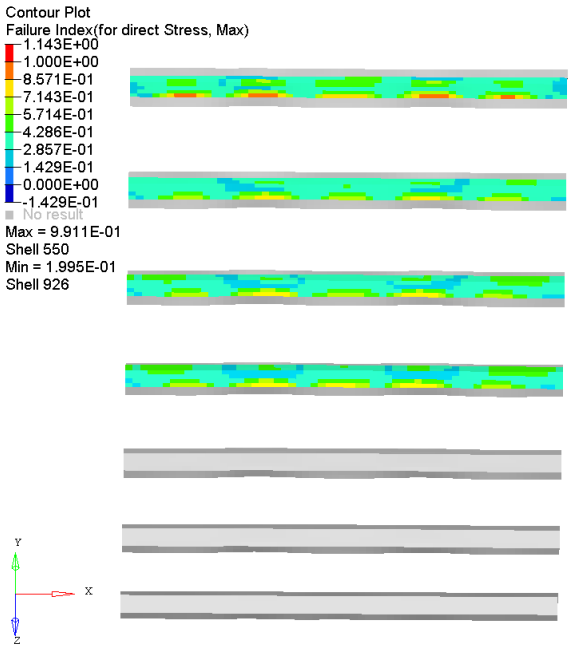

(f) Straight-fiber, Stringer, Nonlinear F.I.

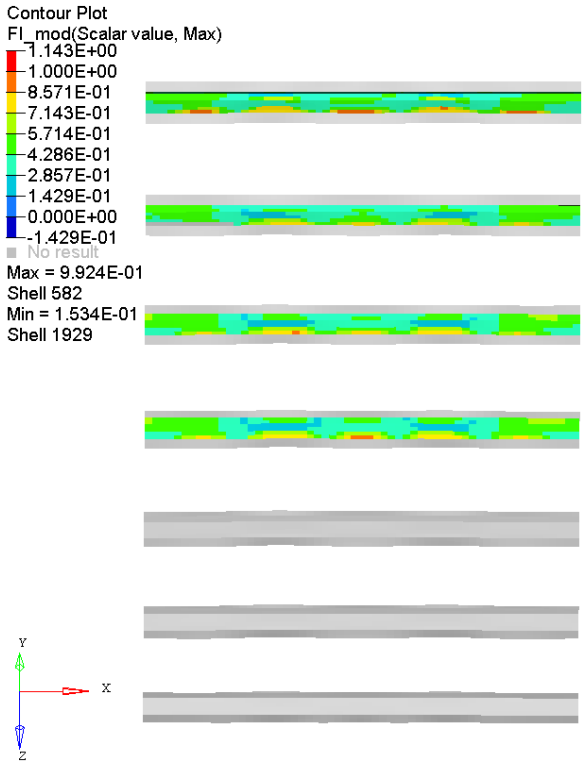

(g) Steered-fiber, Stringer, Linear F.I.

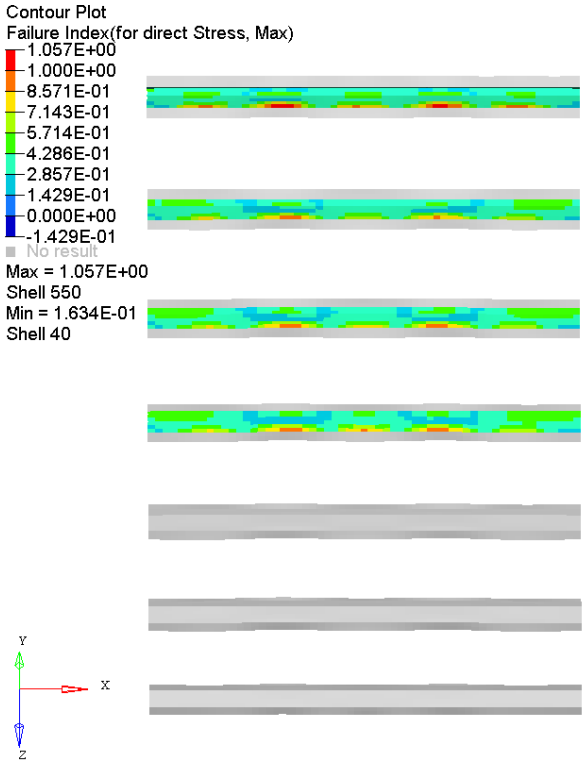

(h) Steered-fiber, Stringer, Nonlinear F.I.

Figure 9.3.: Optimized keel panels: Nonlinear analysis failure index verification (cont.)

Table 9.8.: Effect of no. of equivalent static loads to optimized design objective and variables

No. of ESL	Mass [kg]	tsk [mm]	tstr0 [mm]	tstr45 [mm]	tstr90 [mm]	D [°]	E [°]	F [°]
1	3.057	0.0395	0.050	0.050	0.050	69	18	8
5	3.061	0.0396	0.050	0.050	0.050	69	17	8
20	3.059	0.0395	0.050	0.050	0.050	70	18	4

Table 9.9.: Effect of no. of equivalent static loads to optimization iterations

No. of ESL	No. of ESLM Iterations	No. of linear-loop iterations						
		1	2	3	4	5	6	Total
1	6	7	4	3	2	2	3	21
5	6	7	4	3	2	2	4	22
20	6	7	4	3	2	3	2	21

9.5.2. Example: Optimized Window Panels

Similar to the optimized keel panels, a small failure index correction factor was applied to give equal maximum failure index response to that of nonlinear static analysis. Failure index correction factor of the optimized straight-fiber and steered-fiber window panel was 1.002 and 1.009 respectively. Linear analysis responses in this case were virtually the same as those of nonlinear analysis. Figure 9.4 shows displacement and failure index comparison between linear analysis and geometrical nonlinear analysis of the optimized window panels. Very good displacement agreement around the window cutout was observed but the straight-fiber panel's transverse displacement was under predicted at outer skin bays. As for failure index, highly correlated results were found. The critical area around window frame was correctly captured despite few missing stress peaks in the linear analysis result. Stringers were non-critical in this particular application.

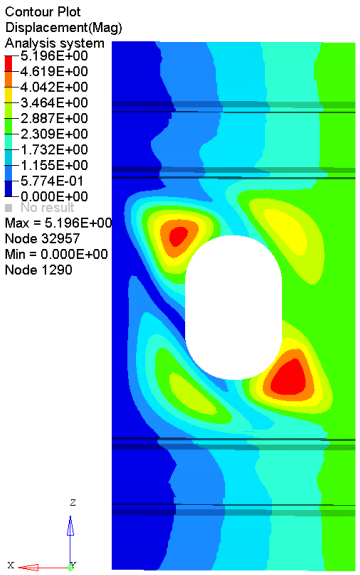

(a) Straight-fiber, Linear Displ.

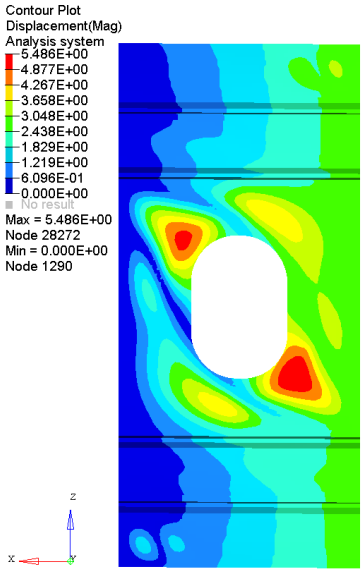

(b) Straight-fiber, Nonlinear Displ.

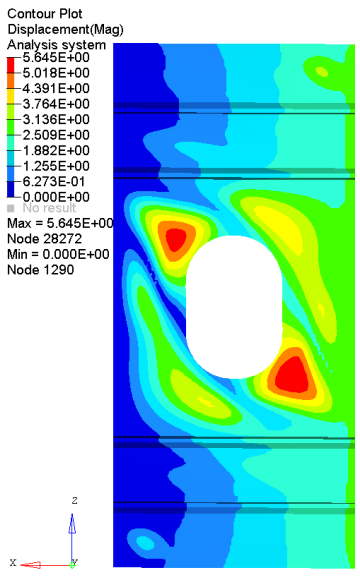

(c) Steered-fiber, Linear Displ.

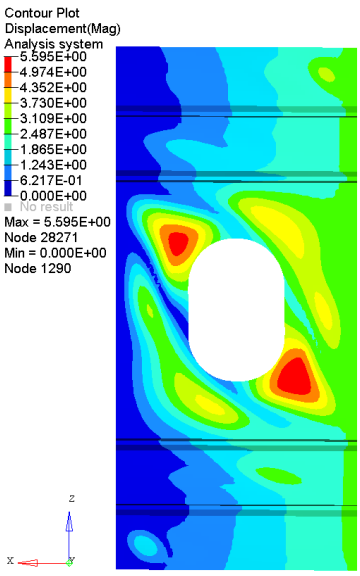

(d) Steered-fiber, Nonlinear Displ.

Figure 9.4.: Optimized window panels: Nonlinear analysis responses verification

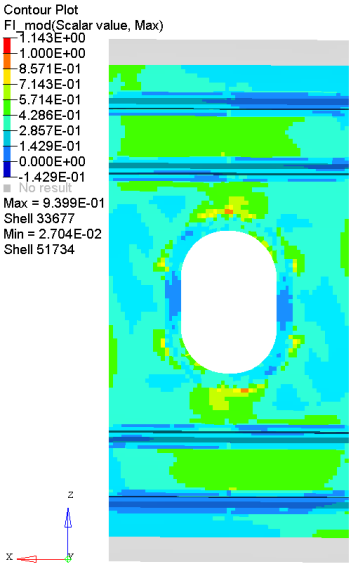

(e) Straight-fiber, Linear F.I.

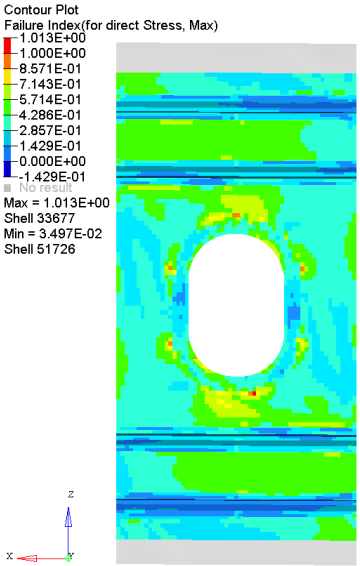

(f) Straight-fiber, Nonlinear F.I.

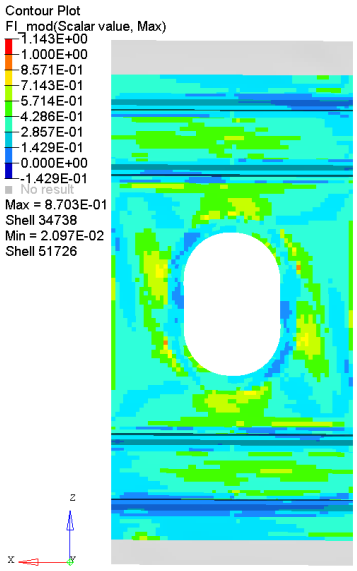

(g) Steered-fiber, Linear F.I.

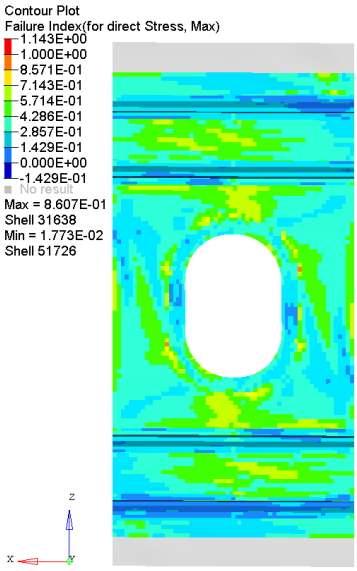

(h) Steered-fiber, Nonlinear F.I.

Figure 9.4.: Optimized window panels: Nonlinear analysis responses verification (cont.)

10

Conclusions and Outlook

This chapter summarizes key findings discovered from the presented dissertation through the investigation of two stiffened fuselage panels - keel and window panels. Head-to-head comparison of the best straight-fiber and steered-fiber panels were conducted to identify pros and cons of each design. The influence of important ESLM parameters described in chapter 9 is also summarized in this closing chapter. Finally, optimization guidelines are outlined for new optimizers who are interested in using ESLM for postbuckling responses optimization.

10.1. Results Summary

The proposed weight optimization with the consideration of geometrical nonlinear analysis constraints via equivalent static loads was successfully demonstrated through the application of two major examples - stiffened fuselage keel and window panels. The best optimized straight-fiber and steered-fiber paths along with ply thicknesses were successfully obtained from the proposed nonlinear response optimization process. Selected set of realistic aircraft loadcases, requirements, and materials were considered. Key findings of each application are summarized as follows.

10.1.1. Fuselage Keel Panels

Local compression buckling constraint was relaxed to 50% limit load to better exploit panel postbuckling load-carrying capability. The use of steered-fiber laminates was brought into action in light of further mass saving with respect to optimal straight-fiber counterpart. However, it was found that steered-fiber patterns did not perform as expected in this particular loading and constraints condition. Only 1% of mass was spared compared to the best straight-fiber panel mass. In any case, more than 30% weight reduction compared to the quasi-isotropic reference design was found. It was suspected that the relaxation of compression buckling constraint undermined the dominance of the shortening load, making the criticality of compression and shear buckling requirement closer to each other. Tighter compressive buckling restriction at 100% limit load affirmed the hypothesis by revealing 11% mass reduction. The improvement nevertheless did not increase further when the compression buckling constraint was raised to 150% limit load in a buckling-free design. Without postbuckling consideration below limit load, more than 20% weight reduction from the reference design was offered by the use of steered-fiber laminates; equivalent to around 10% drop from the postbuckled design. It can be concluded that a dominant loading scenario is very

essential for steered-fiber laminate performance. Note that under a single dominant loadcase, number of constraints does not affect the improvement offered by optimized steered-fiber laminates[52]. Non-stiffened thin-walled structures e.g. launch vehicle, where skin buckling load is extremely severe, seem to be a more suitable application of steered-fiber laminates. Another suitable candidate being an aircraft wing panel which is not permitted to buckle under a limit load condition.

Regarding the manufacturability of optimized fiber orientations, almost straight-fiber paths were suggested when the compression buckling constraint was specified at 50%. Degree of fiber steering was higher when a tighter buckling constraint was imposed. This observation was in line with mass reduction improvement over the optimized straight-fiber designs. When the buckling constraint was tightened to 150% limit load, two third of the laminate was patterned by high fiber angles at skin bay center and almost parallel fibers along the stiffeners. Maximum change in fiber orientation of 69° was reported in this case. This fiber path concentrated the shortening load towards the stiff stringers. Subsequently, skin local buckling was effectively delayed. The influence of pattern curvature limit was reported to be very decisive to resulting performance gain over the best conventional counterpart[16].

The optimized keel panels were found constrained by the laminate failure index, critical compression buckling load, stiffener crippling load, and global panel collapse load. This underlines the importance of postbuckling failure index inclusion. Without postbuckling responses consideration, the strength constraints would have been violated. The strength-critical regions were found to be skin strips underneath stiffeners. Furthermore, the activation of panel final failure constraints, i.e. stiffener crippling and collapse loads, indicated that untimely panel failure could have occurred if the final failure constraints had not been imposed. The consideration of failure indexes alone would be hardly useful in this regard as the failure behaviors were characterized by geometrical instability modes. Lack of final failure restrictions would have resulted into an optimization divergence due to panel failure mode switching.

Verification of finite element failure load peaks against those of semi-analytical formulations was conducted with a satisfactory agreement. Since steered-fiber patterns tend to concentrate applied force towards the stiffener sections, adhesive between stiffener feet and neighboring skin was concerning. Detailed stiffener-skin bonding shear stress was successfully verified. This was done as a cross-check after the optimization to save computational cost. Agreeable failure index results obtained from linear and nonlinear analysis were also observed.

10.1.2. Fuselage Window Panels

There were two comparable dominant loadcases in this window panel structure - shear and combined compression & shear. Both were buckling sensitive but the latter was more critical since uni-axial compression was involved, whereas the former was more relevant to strength constraints. Both critical buckling load limits were set to be 100% of respective limit load. It was found that the loading scenario with two different dominant loadcases

did not advocate the use of steered-fiber patterns as the best straight-fiber and steered-fiber panels shared almost the same weight. However, the optimized steered-fiber panel revealed 14% lower failure index than its straight-fiber counterpart. The most relevant failure indexes appeared around the aluminum window frame. The optimized steered-fiber window panel was constrained by both dominant buckling loads, indicating its sensitivity to conflicting buckling requirements.

Regarding the manufacturability of optimized fiber orientations, maximum change in fiber orientation of 73° between two control points was reported in this case. This fiber transition is beyond the current tow placement technology capability. After the optimization completion, aluminum window frames von mises stresses were successfully crossed-checked against the material yield strength. Agreeable failure index results obtained from linear and nonlinear analysis were as well observed.

10.2. Equivalent Static Load Method Charcteristics and Parametric Study

Chapter 9 studied several important behaviors and parameters of the proposed ESLM procedure. Findings of each parameter's influence are summarized as follows.

10.2.1. Characteristics of an Optimization Process involving ESLM as compared to other Optimization Processes

The proposed optimization procedure with ESLM including a preparatory design of experiments phase clearly demonstrated its efficiency superiority over other conventional methods including conventional gradient-based algorithms, surrogate-based optimization method, and undoubtedly evolutionary algorithms. Freedom from design sensitivity calculation of nonlinear analysis response is the biggest contributor to its efficiency performance. Normal optimization convergence similar to conventional gradient-based algorithms was observed, but the best feasible design could be found before the last iteration where convergence criteria were satisfied.

Its local-global search capability as compared to other optimization methods was also discussed. The preparatory DOE enhances the global search capability of the proposed gradient-based optimization procedure, when design space multi-modality is to be dealt with. The supplementary global search phase definitely affects the computational performance of the proposed ESLM, but considerable efficiency margin over non-gradient optimization methods has been successfully demonstrated.

Last but not least, the newly introduced method as a software tool must be friendly enough for users especially the beginners. Usability of ESLM was therefore qualitatively discussed. In sum, an optimization with ESLM is very analogous to gradient-based methods

but additionally requires a couple of parameters specifications i.e. number of equivalent static loads and stopping convergence criteria. Optimizers who are already familiar with conventional gradient-based optimization techniques should therefore experience a smooth transition.

10.2.2. Optimality Verification

While its optimization efficiency could be expected, the optimality of obtained designs may be put into question by many optimizers. The dissertation addresses this question indirectly due to foreseen complexity of direct determination of Kuhn-Tucker optimality conditions. The optimality verification was already evaluated for all linear analysis responses including those represented by equivalent static loads. Compliance of optimality conditions therefore could be presumed if nonlinear analysis responses i.e. failure indexes are identical to those estimated by equivalent static loads in linear static analysis. Shown in details in section 9.5, highly agreeable maximum failure index with less than 1% error was reported in optimized keel panels, while the optimized window panels showed up to 6% deviation. Close-to optimal solutions could thus be assumed.

10.2.3. Stopping Criteria

While keeping the same linear-loop termination criteria, two ESLM-loop stopping criteria were compared based on prescribed convergence condition. The present study utilized the convergence of design objective. A comparison with the design variables convergence was made. As can be expected, the design variables convergence criteria needed more design iterations to converge. Nonetheless, the best feasible designs obtained from both methods revealed almost identical mass despite slightly different design variables. Choice of design objective convergence criteria was therefore justified.

10.2.4. Number of Equivalent Static Loads

Thanks to quasi-static buckling load, the presented study fed only a single equivalent static load to represent the most critical nonlinear analysis responses at the last time step. Up to twenty equivalent static loads were generated to evaluate the chosen number of static load used in this dissertation. Highly agreeable optimized design objective and design variables were found regardless of how many static loads were generated. Only a single equivalent static load was therefore sufficient in this particular panel shortening example.

10.3. Optimizers' Guidelines: ESLM for Postbuckling Responses of Stiffened Panels

This section summarizes important considerations and limitations of postbuckling optimization using the proposed equivalent static loads method. Considering study cases conducted so far, there are obviously many aspects to be considered before a successful optimization run can be achieved. Even in the case of commercially ready ESLM package, an optimizer without prior experience would likely struggle to obtain the optimal design initially aimed for. Important optimization considerations can be listed as follows.

10.3.1. Dependency on initial design vector

Being a gradient-based optimization scheme, a local optimum trap is a well-known drawback inherited by nature of any gradient-based search algorithm. Verification by starting from several initial design vectors can be done to observe the degree of multi-modality if any. More complex measure may be required to alleviate the non-convexity issue like the use of thin-ply laminates in this dissertation. If numerous fiber orientation variables are to be dealt with, lamination parameters offer a convex optimization problem despite the need of constraints derivation as a function of lamination parameters. In addition, realistic ply angles interpretation from optimal set of lamination parameters is also required. As optimizing lamination parameters is much less sensitive to dimension of design space. Lamination parameters may be the only effective strategy for a very complex design problem.

10.3.2. Choices of nonlinear analysis

Fortunately, a buckling load can be assumed as a quasi-static load with constant loading rate. A geometrical nonlinear static or low-speed implicit dynamic scheme thus can be deployed instead of an extremely expensive transient explicit dynamic solver. In general, a nonlinear static scheme is more efficient as relatively larger time steps are applicable. It is however less stable and less robust compared to an implicit dynamic scheme. The fact that a single set of nonlinear scheme parameters are utilized over different designs throughout the optimization makes the choice of nonlinear analysis vital because a single scheme divergence would lead to premature termination of the whole optimization process. Automatically updated nonlinear analysis parameters and re-analysis option in case of unsuccessful analysis are workaround examples.

Another aspect of a nonlinear analysis is a trade-off between efficiency and accuracy through the choice of loading type - displacement or force. Force application according to prescribed loadcase magnitude is straight-forward and analogous to conventional practice in linear static response optimization. Due to laborious stiffness matrix inversion, computational efficiency is however affected. Moreover, nonlinear scheme divergence and instability frequently become a concern. Enforced displacement on the other hand diminishes the stiffness inversion step, leading to a quick convergence rate. However, an iterative procedure, similar to the presented approach, has to be implemented to achieve the prescribed force magnitude. As more than one iterations of nonlinear analysis are solved, the computational

expense is multiplied. A thorough study is therefore required before a logical decision can be made on the aforementioned choice of nonlinear analysis.

10.3.3. Buckling and failure load constraints

Critical local buckling constraint is necessary to avoid optimization convergence difficulty, even postbuckling responses are only of interest. Lack of bifurcation or linear buckling constraint would allow geometrical instability moves from one energy level to another, affecting postbuckling behavior. If panel's buckling deformation is to be optimized or constrained, shortening deformation is always preferred over transverse displacement as skin buckling mode switching may cause the gradient-based optimizer struggle to converge. Subject to compression load, inclusion of final panel failure load, whether the global panel collapse or stiffener crippling load, is as well of importance as premature panel failure may occur before constrained nonlinear analysis responses reach their threshold.

10.3.4. Lagrangian coordinate system

Unlike in a large-displacement nonlinear analysis, linear static analysis normally refers to stationary Lagrangian representation. Stress or strain of postbuckled components represented by equivalent static loads is therefore miscalculated due to non-following coordinate system in the linear analysis. Shown in figure 10.1, curved skin reveals incorrect failure indexes as compared to the original nonlinear analysis result. Straight skin strips underneath stringers on the other hand were not affected as system transformation was not needed. Automatically transformed coordinate system must be implemented if postbuckled areas marked by high finite element rotation deem critical.

10.3.5. Material nonlinearity

The inclusion of material nonlinearity, either in metallic or composite materials, will pose several challenges. First, geometrical nonlinear analysis will need more time to complete due to added material nonlinearity. Sophisticated progressive laminate failure analysis has to be performed in case of composite structure. Nonlinear stress or strain formulations, e.g. Cauchy stress, plastic strain, or creep strain, must be referred instead of their engineering values when material yield point is exceeded. Second, additional set of equivalent static loads specific to nonlinear stress or strain will be required. As outlined by Lee and Park[28], the derivation of stress-based equivalent static loads requires modified Young's moduli in all time steps. That means new stiffness matrix must be assembled at all time steps. The resulting scale of subsequent linear static response optimization can be very large, resulting into an extreme computation cost. Consideration of only time steps of the maximum stress or strain are recommended in this case. More simplified approach is employed by MSC Nastran[36]. Stress or strain ratio scheme is applied to correct linear analysis stress or strain results without modified material moduli. However, deviation of stress/strain results with respect to those of nonlinear analysis may grow as linear-loop optimization proceeds.

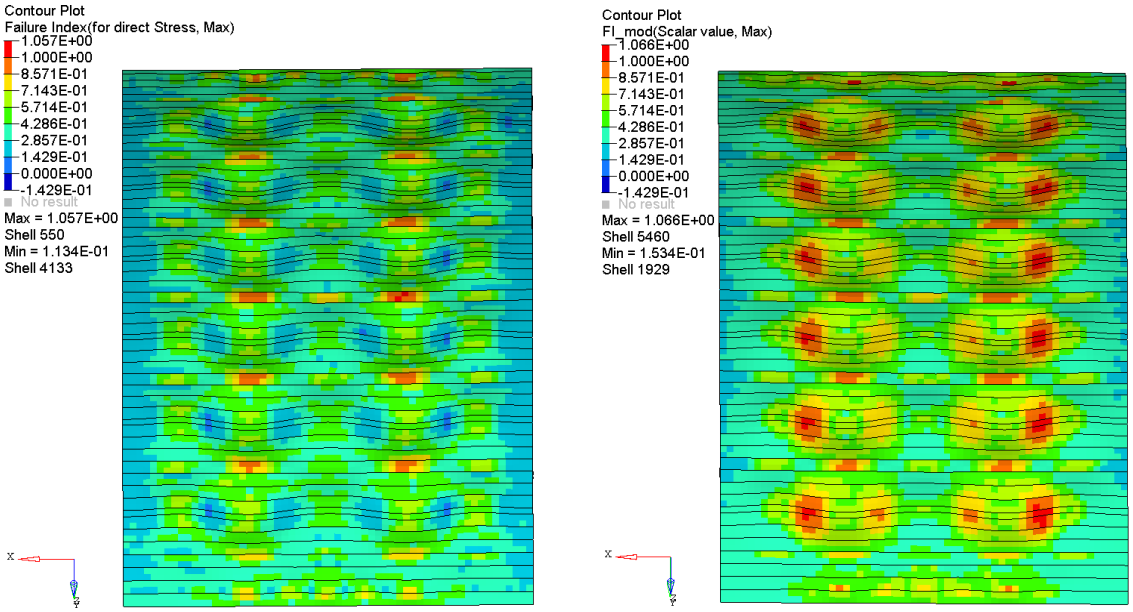

(a) Nonlinear analysis (b) Linear analysis

Figure 10.1.: Optimized keel steered-fiber panel's failure indexes: Incorrect representation due to non-rotated Lagrangian coordinate system in linear analysis

10.4. Closing Remarks

Based on the presented study, it can be concluded that the proposed nonlinear response optimization via equivalent static loads is applicable and effective for an optimization problem involving postbuckling behavior. As its performance is highly affected by multi-axis loadcase, the employment of steered-fiber laminates is only viable in a single dominant loadcase scenario, which can be found in certain aerospace applications e.g. fuselage keel and crown panels, launch vehicle, or upper wing skin. Taking its manufacturing specifics into account, it is not worth exploiting steered-fiber laminates in general applications without a thorough study on loads and requirements. Nonetheless, a proper optimization of fiber orientations and stacking sequence, whether in conventional or curvilinear-fiber laminates, has proved to be highly influencing on structural performance, especially on the buckling resistance. A more effective optimization approach that accounts for resulting design response multi-modality will significantly improve the fruition of unconventional fiber orientations in real-world applications.

A

Appendix

A.1. Semi-Analytical Omega-Stiffened Panel Collapse Load Formulation

Design variables:
ply thickness: t_{sk}, t_{str}
ply orientation: α_1, α_2, β_1, β_2, γ_1, γ_2

Constants:
lamina Young's modulus along fibers, E_{11} = 157000 MPa
lamina Young's modulus normal to fibers, E_{22} = 12000 MPa
lamina shear modulus, G_{12} = 5929 MPa
lamina Poisson's ratio, ν_{12} = 0.32
panel length, a = 586.7mm
panel arc length, c = 1139.5 mm
omega stringer's web half length, d = 12.08 mm
omega stringer's feet length, f_1 = 30 mm
omega stringer's flange length, f_2 = 10 mm
one-half of reinforcing omega pitch, p = 30 mm
omega stringer's web angle, θ = 0.972 rad
number of buckle half-waves in longitudinal direction, m = 1
number of buckle half-waves in circumferential direction, n = 2
omega stringer height, h_c = 22 mm
radius of omega stringer corners, R = 0 mm

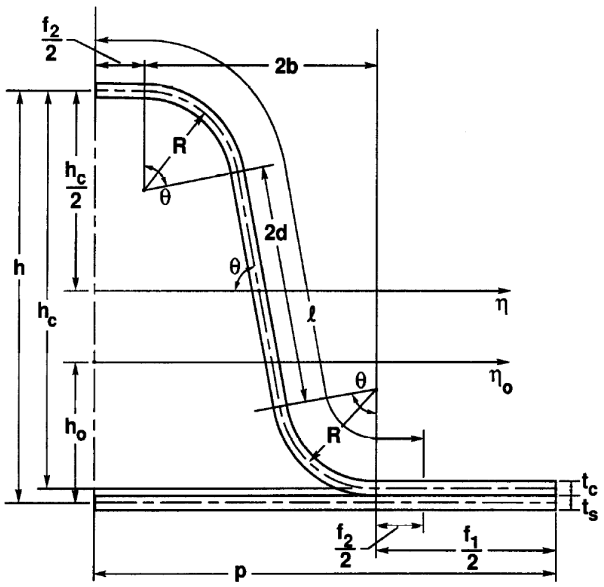

Figure A.1.: Half segment of omega-stiffened panel[26]

From the given design variables and constants, total skin thickness t_s, total stringer thickness t_c, equivalent skin moduli $E_{sk,xx}$, $E_{sk,yy}$, G_{sk}, equivalent stringer moduli $E_{str,xx}$, $E_{str,yy}$, G_{str} can be calculated based on the classical lamination theory. Note that for straight-fiber

laminate formulation, α_1=α_2, β_1=β_2, and γ_1=γ_2 are enforced.

Global panel collapse force, $N_{x,global}$, then can be determined according to Ko and Jackson[26] as follows:

$$N_{x,global} = k_{x,global}\frac{\pi^2}{c}E_{sk,xx}I_{sk} \tag{A.1}$$

where

$$k_{x,global} = \frac{a_{11}(a_{23}a_{32} - a_{22}a_{33}) + a_{21}(a_{12}a_{33} - a_{13}a_{32})}{a_{12}a_{23} - a_{22}a_{13}} \tag{A.2}$$

and

$$\begin{aligned}
a_{11} &= \frac{m}{\beta}\Big[\frac{1}{1-\nu_{sk}^2}\frac{D_x}{E_{sk,xx}I_{sk}}\frac{m^2}{\beta^2} + \Big(\frac{\nu_{sk}}{1-\nu_{sk}^2}\frac{D_x}{E_{sk,xx}I_{sk}} + \frac{D_{xy}}{E_{sk,xx}I_{sk}}\Big)n^2\Big] \\
a_{12} &= -\Big[1 + \frac{\pi^2 E_{sk,xx}I_{sk}}{c^2 D_{Qx}}\Big(\frac{1}{1-\nu_{sk}^2}\frac{D_x}{E_{sk,xx}I_{sk}}\frac{m^2}{\beta^2} + \frac{1}{2}\frac{D_{xy}}{E_{sk,xx}I_{sk}}n^2\Big)\Big] \\
a_{13} &= -\frac{\pi^2 E_{sk,xx}I_{sk}}{c^2 D_{Qy}}\Big(\frac{\nu_{sk}}{1-\nu_{sk}^2}\frac{D_x}{E_{sk,xx}I_{sk}} + \frac{1}{2}\frac{D_{xy}}{E_{sk,xx}I_{sk}}\Big)\frac{mn}{\beta} \\
a_{21} &= n\Big[\frac{1}{1-\nu_{sk}^2}\frac{D_y}{E_{sk,xx}I_{sk}}n^2 + \Big(\frac{\nu_{sk}}{1-\nu_{sk}^2}\frac{D_y}{E_{sk,xx}I_{sk}} + \frac{D_{xy}}{E_{sk,xx}I_{sk}}\Big)\frac{m^2}{\beta^2}\Big] \\
a_{22} &= -\frac{\pi^2 E_{sk,xx}I_{sk}}{c^2 D_{Qx}}\Big(\frac{\nu_{sk}}{1-\nu_{sk}^2}\frac{D_y}{E_{sk,xx}I_{sk}} + \frac{1}{2}\frac{D_{xy}}{E_{sk,xx}I_{sk}}\Big)\frac{mn}{\beta} \\
a_{23} &= -\Big[1 + \frac{\pi^2 E_{sk,xx}I_{sk}}{c^2 D_{Qy}}\Big(\frac{1}{1-\nu_{sk}^2}\frac{D_y}{E_{sk,xx}I_{sk}}n^2 + \frac{1}{2}\frac{D_{xy}}{E_{sk,xx}I_{sk}}\frac{m^2}{\beta^2}\Big)\Big] \\
a_{32} &= -\frac{\beta}{m} \\
a_{33} &= -\frac{\beta^2}{m^2}n
\end{aligned} \tag{A.3}$$

and

$$D_x = E_{str,xx}\overline{I_c} + E_{sk,xx}I_{sk} \tag{A.4}$$

$$D_y = E_{sk,yy}I_{sk}\frac{1 + \frac{E_{str,yy}\overline{I_c}}{E_{sk,yy}I_{sk}}}{1 + (1-\nu_{sk}^2)\frac{E_{str,yy}\overline{I_c}}{E_{sk,yy}I_{sk}}} \tag{A.5}$$

$$I_{sk} = t_s h_o^2 + \frac{1}{12}t_s^3 \tag{A.6}$$

while $\bar{I}_c$ is the moment of inertia of the combined stringer foot and skin, taken with respect to neutral axis η_o:

$$\bar{I}_c = \frac{I_c^*}{p} + \frac{A_{str}}{p}\Big[\frac{1}{2}(h_c + t_c + t_s) - h_o\Big]^2 + \frac{1}{24p}(f_1 - f_2)t_c^3 + \frac{f_1 - f_2}{2p}t_c\Big(h_o - \frac{t_c + t_s}{2}\Big)^2 \tag{A.7}$$

where h_o is the distance between the middle skin surface and the centroid of the global stiffened panel:

$$h_o = \frac{1}{2\bar{A}}\Big[A_{str}(h_c + t_c + t_s) + \frac{1}{2}t_c(f_1 - f_2)(t_c + t_s)\Big] \tag{A.8}$$

D_{xy} can be obtained as the following.

$$D_{xy} = 2\overline{GJ} \tag{A.9}$$

where

$$\overline{GJ} = \Big[G_{sk}t_s k_{\overline{GJ}}^2 + \frac{pG_{str}t_c^2}{A_c}(k_{\overline{GJ}} - k_{str})^2\Big]h^2 \tag{A.10}$$

and

$$k_{\overline{GJ}} = \frac{k_{str}}{1 + \frac{A_c G_{sk} t_s}{pG_{str}t_c}} \tag{A.11}$$

$$k_{str} = \frac{1}{2}\Big[1 - \frac{(f_1 - f_2)h_c}{2ph}\Big] \tag{A.12}$$

$$A_c = \Big[l + \frac{1}{2}(f_1 - f_2)\Big]t_c \tag{A.13}$$

and

$$D_{Qx} = \frac{G_{str}t_c h^2}{pl} \tag{A.14}$$

$$D_{Qy} = \bar{S}h\frac{E_{str,yy}}{1 - \nu_{str}^2}\Big(\frac{t_c}{h_c}\Big)^3 \tag{A.15}$$

where

$$\bar{S} = \frac{6\frac{h_c}{p}D_z^F\frac{t_s}{t_c} + \Big(\frac{p}{h_c}\Big)^2}{12\Big\{\frac{h}{h_c}\frac{p}{h_c}D_z^F - 2\Big(\frac{p}{h_c}\Big)^2 D_z^H + \frac{h_c}{h}\Big[6\frac{t_s}{t_c}\Big(D_z^F D_y^H - (D_z^H)^2\Big) + \Big(\frac{p}{h_c}\Big)^3 D_y^H\Big]\Big\}} \tag{A.16}$$

where

$$D_z^F = \frac{2}{3}\Big(\frac{d}{h_c}\Big)^3\cos^2\theta + \frac{2}{3}\frac{I_{str}}{I_f}\Big[\frac{1}{8}\Big(\frac{p}{h_c}\Big)^3 - \Big(\frac{b}{h_c}\Big)^3\Big] + \frac{I_{str}}{h_c^2 t_c}\Big(2\frac{d}{h_c}\sin^2\theta\Big) \tag{A.17}$$

$$D_z^H = \frac{2}{3}\left(\frac{d}{h_c}\right)^3 \sin\theta\cos\theta + \frac{1}{2}\frac{I_{str}}{I_f}\left[\frac{1}{4}\left(\frac{p}{h_c}\right)^2 - \left(\frac{b}{h_c}\right)^2\right] - \frac{I_{str}}{h_c^2 t_c}\left(2\frac{d}{h_c}\sin\theta\cos\theta\right) \tag{A.18}$$

$$D_y^H = \frac{2}{3}\left(\frac{d}{h_c}\right)^3 \sin^2\theta + \frac{1}{2}\left(\frac{1}{2}\frac{f}{h_c}\frac{I_{str}}{I_f}\right) + \frac{I_{str}}{h_c^2 t_c}\left(\frac{f}{h_c}\frac{t_c}{t_f} + 2\frac{d}{h_c}\cos^2\theta\right) \tag{A.19}$$

where

$$f = \frac{1}{2}(f_1 + f_2) \tag{A.20}$$

$$I_{str} = \frac{1}{12}t_c^3 \tag{A.21}$$

$$I_f = \frac{1}{12}t_s^3 \tag{A.22}$$

$$b = \frac{1}{2}\left[p - \frac{1}{2}(f_1 + f_2)\right] \tag{A.23}$$

Complementary equations:

$$\beta = \frac{a}{c} \tag{A.24}$$

$$l = f_2 + 2d + 2R\theta \tag{A.25}$$

$$A_{str} = lt_c \tag{A.26}$$

$$\bar{A} = A_{str} + pt_s + \frac{1}{2}(f_1 - f_2) \tag{A.27}$$

$$I_c^* = h_c^3 t_c\left\{\frac{1}{4}\frac{f_2}{h_c}\left(1 + \frac{1}{3}\frac{t_c^2}{h_c^2}\right) + \frac{2}{3}\frac{d^3}{h_c^3}\left(\sin^2\theta + \frac{1}{4}\frac{t_c^2}{d^2}\cos^2\theta\right)\right\} \tag{A.28}$$

A.2. Semi-Empirical Omega Stiffener Crippling Load Formulation

Design variables:
ply thickness: t_{sk}, t_{str}
ply orientation: α_1, α_2, β_1, β_2, γ_1, γ_2

Constants:
lamina Young's modulus along fibers, E_{11} = 157000 MPa
lamina Young's modulus normal to fibers, E_{22} = 12000 MPa
lamina shear modulus, G_{12} = 5929 MPa
lamina Poisson's ratio, ν_{12} = 0.32
omega stringer's feet length, f_1 = 30 mm
omega stringer's flange length, f_2 = 10 mm
one-half of reinforcing omega pitch, p = 30 mm
radius of omega stringer corners, R = 0 mm
omega stringer section 1 width, b_1 = 15.00 mm
omega stringer section 2 width, b_2 = 24.16 mm
omega stringer section 3 width, b_3 = 10.00 mm
omega stringer section 4 width, b_4 = 30.00 mm
lamina compressive failure strain in fiber direction, $s_{11,c}$ = 0.0108

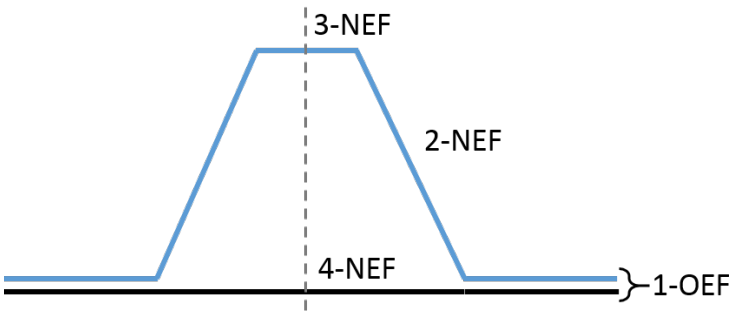

Figure A.2.: Omega stringer segmentation for crippling calculation

From the given design variables and constants, total section thickness t_i, section ABD matrix coefficients in longitudinal direction $A_{11,i}$ and $D_{11,i}$ can be calculated based on the classical lamination theory. Note that for straight-fiber laminate formulation, α_1=α_2, β_1=β_2, and γ_1=γ_2 are enforced.

Total panel crippling force, $N_{x,cripp}$, then can be determined according to MIL-HDBK-17-3F[8] as follows.
Section's compressive failure stress based on compressive failure strain:

$$\sigma_{comp,i} = \frac{A_{11,i} s_{11,c}}{t_i}; i = 1, .., 4 \tag{A.29}$$

Section's effective bending stiffness modulus:

$$\bar{E}_i = \frac{12D_{11,i}}{t_i^3}(1 - \nu_{12}\nu_{21}); i = 1, .., 4 \tag{A.30}$$

Section's crippling stress based on empirical normalized crippling data[8]:

Section 1 - One-edge free:

$$\sigma_{cripp,1} = 2.151\sigma_{comp,1}\left(\frac{b_1}{t_1}\right)^{-0.717} \tag{A.31}$$

Section 2 - No-edge free:

$$\sigma_{cripp,2} = 14.92\sigma_{comp,2}\left(\frac{b_2}{t_2}\right)^{-1.124} \tag{A.32}$$

Section 3 - No-edge free:

$$\sigma_{cripp,3} = 14.92\sigma_{comp,3}\left(\frac{b_3}{t_3}\right)^{-1.124} \tag{A.33}$$

Section 4 - No-edge free:

$$\sigma_{cripp,4} = 14.92\sigma_{comp,4}\left(\frac{b_4}{t_4}\right)^{-1.124} \tag{A.34}$$

Stringer's crippling stress:

$$\sigma_{cripp,str} = \frac{2(\sigma_{cripp,1}b_1t_1) + 2(\sigma_{cripp,2}b_2t_2) + (\sigma_{cripp,3}b_3t_3) + (\sigma_{cripp,4}b_4t_4)}{2b_1t_1 + 2b_2t_2 + b_3t_3 + b_4t_4} \tag{A.35}$$

Total panel crippling force:

$$N_{x,cripp} = 7\sigma_{cripp,str}(2\bar{A}) \tag{A.36}$$

where

$$\bar{A} = A_{str} + pt_s + \frac{1}{2}(f_1 - f_2) \tag{A.37}$$

$$A_{str} = lt_c \tag{A.38}$$

$$l = f_2 + 2d + 2R\theta \tag{A.39}$$

Total panel crippling force with FEM correction factor, $R_{cripp,FEM}$ =1.05:

$$\begin{aligned} N_{x,cripp} &= R_{cripp,FEM} \times \left[7\sigma_{cripp,str}(2\bar{A})\right] \\ N_{x,cripp} &= 1.05 \times \left[7\sigma_{cripp,str}(2\bar{A})\right] \end{aligned} \tag{A.40}$$

A.3. MSC Nastran DMAP for Equivalent Static Load Generation

There are three necessary steps for equivalent static load deployment in an optimization routine. Firstly, displacement field must be extracted from the original nonlinear analysis. Secondly, equivalent static load is generated based on the nonlinear analysis displacement previously extracted. Lastly, the generated equivalent static load representing nonlinear analysis displacement at a certain time step is supplied to the chosen optimization procedure. MSC Nastran executive control section in .bdf input file was modified according to DMAP grammar as shown in the following in order to implement aforementioned steps.

A.3.1. Nonlinear Analysis Displacement Extraction

Input file: SOL106_SPCD_RIKS.bdf

```
ASSIGN OUTPUT4='D:\UG106.op4',UNIT=60,FORM=formatted
SOL 106
MALTER ', ETC. DATA RECOVERY, SORT1'(,-1)
OUTPUT4 UG,,,,//-1/60/1/FALSE/9
COMPILE NLSTATIC
ALTER 1177
DRMS1 OEFIT,,,/TFI,MFI,,,,,,/0
OUTPUT4 MFI,,,,//-1/61/1/FALSE/6
CEND
```

Output file: UG106.op4

A.3.2. Equivalent Static Load Extraction

Input files: UG106.op4 and SOL101_ESL.bdf

```
ASSIGN INPUTT4='D:\106.op4',UNIT=60,FORM=formatted
SOL 101
COMPILE semg
ALTER 'mjjx,.*mass'
INPUTT4 /ug2,,,,/1/60//0
mpyad kjjz,ug2,/esl
MATMOD ESL,EQEXINS,,,,/MATPOOLF,/16/1/1/////////'ESLDMIG'/
OUTPUT4 ESL,,,,//-1/43/1/FALSE/9
CEND
```

Output file: SOL101_ESL.pch

A.3.3. Equivalent Static Load Utilization in Optimization Routine

Input files: SOL101_ESL.pch and SOL200_VS.bdf

```
SOL 200
CEND
P2G = ESLDMIG
SUBCASE 1
ANALYSIS=STATICS
...
BEGIN BULK
include 'SOL101_ESL.pch'
...
```

A.4. Complete Optimization Results

A.4.1. Fuselage Keel Panels, $\lambda_{comp} \geq 0.5$

Straight-Fiber

Table A.1.: Straight-Fiber Keel Panel Optimization History, $\lambda_{comp} \geq 0.5$: 1/5

Iteration	Linear-loop iterations	Mass [kg]	t_{sk} [mm]	t_{str} [mm]	D [°]	E [°]	F [°]
0		2.202	0.0213	0.0756	81	81	87
1	26	2.572	0.0299	0.0607	69	29	29
2	5	2.356	0.0295	0.0435	89	23	19
3	2	2.460	0.0312	0.0432	89	24	21
4	2	2.461	0.0313	0.0431	90	24	21

Active constraints at the best feasible iteration: n/a (violated FI constraints)

Table A.2.: Straight-Fiber Keel Panel Optimization History, $\lambda_{comp} \geq 0.5$: 2/5

Iteration	Linear-loop iterations	Mass [kg]	t_{sk} [mm]	t_{str} [mm]	D [°]	E [°]	F [°]
0		2.411	0.0248	0.0748	74	86	43
1	18	2.351	0.0255	0.0652	61	67	22
2	4	2.358	0.0282	0.0509	27	89	21

Active constraints at the best feasible iteration: n/a (violated FI constraints)

Table A.3.: Straight-Fiber Keel Panel Optimization History, $\lambda_{comp} \geq 0.5$: 3/5

Iteration	Linear-loop iterations	Mass [kg]	t_{sk} [mm]	t_{str} [mm]	D [°]	E [°]	F [°]
0		2.427	0.0288	0.0977	75	76	56
1	14	2.319	0.0244	0.0686	34	90	49
2	6	2.351	0.0286	0.0480	26	89	20
3	3	2.465	0.0313	0.0434	26	89	22
4	**2**	**2.489**	**0.0316**	**0.0438**	**28**	**89**	**23**

Active constraints at the best feasible iteration: FI, collapse, crippling

Table A.4.: Straight-Fiber Keel Panel Optimization History, $\lambda_{comp} \geq 0.5$: 4/5

Iteration	Linear-loop iterations	Mass [kg]	t_{sk} [mm]	t_{str} [mm]	D [°]	E [°]	F [°]
0		2.486	0.0243	0.0838	29	61	77
1	5	2.348	0.0295	0.0432	17	23	90
2	4	2.456	0.0308	0.0453	27	25	90
3	2	2.488	0.0313	0.0455	28	26	90
4	2	2.518	0.0320	0.0441	28	26	90
5	**2**	**2.528**	**0.0321**	**0.0446**	**28**	**26**	**90**

Active constraints at the best feasible iteration: FI, collapse, crippling

Table A.5.: Straight-Fiber Keel Panel Optimization History, $\lambda_{comp} \geq 0.5$: 5/5

Iteration	Linear-loop iterations	Mass [kg]	t_{sk} [mm]	t_{str} [mm]	D [°]	E [°]	F [°]
0		2.509	0.0289	0.0603	78	11	45
1	8	2.362	0.0297	0.0433	83	22	18
2	3	2.486	0.0318	0.0426	90	22	19
3	**2**	**2.469**	**0.0314**	**0.0432**	**90**	**25**	**22**

Active constraints at the best feasible iteration: FI, collapse

Steered-Fiber

Table A.6.: Steered-Fiber Keel Panel Optimization History, $\lambda_{comp} \geq 0.5$: 1/5

Iteration	Linear-loop iterations	Mass [kg]	t_{sk} [mm]	t_{str} [mm]	α_1 [°]	β_1 [°]	γ_1 [°]	α_2 [°]	β_2 [°]	γ_2 [°]
0		2.218	0.0212	0.0775	46	84	50	59	7	64
1	16	2.256	0.0232	0.0700	38	45	90	78	23	90
2	5	2.319	0.0282	0.0476	25	31	88	22	18	90
3	4	2.377	0.0286	0.0504	17	25	89	28	25	90
4	5	2.481	0.0309	0.0470	11	11	89	32	30	90
5	30	2.608	0.0328	0.0477	10	11	90	36	34	90
6	**38**	**2.600**	**0.0336**	**0.0426**	**17**	**17**	**90**	**33**	**29**	**90**

Active constraints at the best feasible iteration: FI, stringer buckling, collapse, crippling

Table A.7.: Steered-Fiber Keel Panel Optimization History, $\lambda_{comp} \geq 0.5$: 2/5

Iteration	Linear-loop iterations	Mass [kg]	t_{sk} [mm]	t_{str} [mm]	α_1 [°]	β_1 [°]	γ_1 [°]	α_2 [°]	β_2 [°]	γ_2 [°]
0		2.327	0.0238	0.0730	86	69	37	5	63	12
1	18	2.236	0.0273	0.0456	29	42	40	11	73	10
2	40	2.354	0.0296	0.0432	3	15	90	19	90	0
3	21	2.702	0.0332	0.0534	0	14	82	43	89	0
4	40	3.191	0.0417	0.0496	0	7	69	90	52	0
5	40	3.362	0.0446	0.0486	1	6	58	90	55	0
6	40	3.437	0.0455	0.0500	6	9	90	90	42	1
7	11	2.474	0.0295	0.0542	10	11	85	33	80	2
8	29	3.373	0.0440	0.0529	11	16	89	49	90	0
9	24	2.466	0.0293	0.0543	10	23	84	39	90	1
10	37	3.246	0.0422	0.0518	7	14	63	50	90	4

Active constraints at the best feasible iteration: n/a (non-converged optimization)

Table A.8.: Steered-Fiber Keel Panel Optimization History, $\lambda_{comp} \geq 0.5$: 3/5

Iteration	Linear-loop iterations	Mass [kg]	t_{sk} [mm]	t_{str} [mm]	α_1 [°]	β_1 [°]	γ_1 [°]	α_2 [°]	β_2 [°]	γ_2 [°]
0		2.348	0.0204	0.0932	71	73	62	30	51	42
1	21	2.171	0.0233	0.0615	52	90	38	26	90	19
2	19	2.416	0.0281	0.0568	57	89	34	34	90	23
3	14	2.605	0.0302	0.0615	61	67	33	84	90	23
4	5	2.435	0.0299	0.0484	17	80	13	40	90	17
5	**3**	**2.444**	**0.0306**	**0.0454**	**10**	**89**	**10**	**31**	**90**	**25**

Active constraints at the best feasible iteration: FI, panel compression buckling, crippling

Table A.9.: Steered-Fiber Keel Panel Optimization History, $\lambda_{comp} \geq 0.5$: 4/5

Iteration	Linear-loop iterations	Mass [kg]	t_{sk} [mm]	t_{str} [mm]	α_1 [°]	β_1 [°]	γ_1 [°]	α_2 [°]	β_2 [°]	γ_2 [°]
0		2.380	0.0222	0.0861	27	80	73	3	58	63
1	29	2.269	0.0282	0.0434	4	68	31	2	5	87
2	9	2.598	0.0336	0.0425	2	90	42	3	6	90
3	**40**	**2.809**	**0.0373**	**0.0403**	**0**	**90**	**3**	**14**	**1**	**90**
4	11	2.661	0.0317	0.0584	0	89	0	39	0	90
5	1	2.661	0.0317	0.0584	0	89	0	39	0	90

Active constraints at the best feasible iteration: FI, collapse

Table A.10.: Steered-Fiber Keel Panel Optimization History, $\lambda_{comp} \geq 0.5$: 5/5

Iteration	Linear-loop iterations	Mass [kg]	t_{sk} [mm]	t_{str} [mm]	α_1 [°]	β_1 [°]	γ_1 [°]	α_2 [°]	β_2 [°]	γ_2 [°]
0		2.150	0.0209	0.0735	73	37	51	72	81	4
1	**5**	**2.171**	**0.0240**	**0.0578**	**90**	**38**	**49**	**90**	**27**	**7**

Active constraints at the best feasible iteration: n/a (violated FI constraints)

A.4.2. Fuselage Keel Panels, $\lambda_{comp} \geq 1.0$

Straight-Fiber

Table A.11.: Straight-Fiber Keel Panel Optimization History, $\lambda_{comp} \geq 1.0$: 1/3

Iteration	Linear-loop iterations	Mass [kg]	t_{sk} [mm]	t_{str} [mm]	D [°]	E [°]	F [°]
0		2.679	0.0300	0.0696	66	79	76
1	16	3.256	0.0404	0.0626	9	39	50
2	5	2.932	0.0389	0.0422	5	50	90
3	**1**	**2.932**	**0.0389**	**0.0422**	**5**	**50**	**90**

Active constraints at the best feasible iteration: n/a (violated FI constraints)

Table A.12.: Straight-Fiber Keel Panel Optimization History, $\lambda_{comp} \geq 1.0$: 2/3

Iteration	Linear-loop iterations	Mass [kg]	t_{sk} [mm]	t_{str} [mm]	D [°]	E [°]	F [°]
0		2.782	0.0261	0.0999	82	78	58
1	35	4.129	0.0549	0.0587	65	65	33
2	5	3.092	0.0412	0.0436	90	90	10
3	**1**	**3.092**	**0.0412**	**0.0436**	**90**	**90**	**10**

Active constraints at the best feasible iteration: panel compression buckling, collapse

Table A.13.: Straight-Fiber Keel Panel Optimization History, $\lambda_{comp} \geq 1.0$: 3/3

Iteration	Linear-loop iterations	Mass [kg]	t_{sk} [mm]	t_{str} [mm]	D [°]	E [°]	F [°]
0		2.675	0.0278	0.0814	72	71	60
1	35	3.920	0.0519	0.0575	60	69	31
2	5	3.094	0.0412	0.0438	90	90	8
3	**1**	**3.094**	**0.0412**	**0.0438**	**90**	**90**	**8**

Active constraints at the best feasible iteration: panel compression buckling, collapse

Steered-Fiber

Table A.14.: Steered-Fiber Keel Panel Optimization History, $\lambda_{comp} \geq 1.0$: 1/3

Iteration	Linear-loop iterations	Mass [kg]	t_{sk} [mm]	t_{str} [mm]	α_1 [°]	β_1 [°]	γ_1 [°]	α_2 [°]	β_2 [°]	γ_2 [°]
0		2.600	0.0272	0.0779	64	87	64	29	13	67
1	20	2.996	0.0352	0.0685	37	45	90	48	53	90
2	31	3.104	0.0373	0.0661	19	46	90	66	47	90
3	17	2.960	0.0357	0.0623	40	43	90	67	41	90
4	35	3.301	0.0410	0.0633	40	52	90	40	42	90
5	17	3.090	0.0385	0.0587	24	28	64	40	83	87
6	12	2.980	0.0364	0.0606	37	37	90	37	90	90
7	22	2.893	0.0340	0.0659	43	57	89	36	45	89
8	40	2.961	0.0349	0.0668	39	52	87	44	45	87
9	18	3.118	0.0371	0.0689	29	39	89	62	78	89
10	18	3.185	0.0387	0.0656	35	16	89	59	59	90

Active constraints at the best feasible iteration: n/a (non-converged optimization)

Table A.15.: Steered-Fiber Keel Panel Optimization History, $\lambda_{comp} \geq 1.0$: 2/3

Iteration	Linear-loop iterations	Mass [kg]	t_{sk} [mm]	t_{str} [mm]	α_1 [°]	β_1 [°]	γ_1 [°]	α_2 [°]	β_2 [°]	γ_2 [°]
0		2.767	0.0286	0.0847	53	82	73	2	45	82
1	18	3.081	0.0408	0.0449	15	45	23	2	47	75
2	22	3.029	0.0407	0.0410	15	49	18	1	75	87
3	11	2.924	0.0388	0.0424	50	58	16	1	55	71
4	**29**	**2.751**	**0.0354**	**0.0458**	**47**	**90**	**38**	**0**	**90**	**75**
5	8	3.029	0.0407	0.0410	22	90	13	1	90	69
6	1	3.022	0.0404	0.0419	26	90	13	1	90	90

Active constraints at the best feasible iteration: panel compression buckling, collapse, crippling

Table A.16.: Steered-Fiber Keel Panel Optimization History, $\lambda_{comp} \geq 1.0$: 3/3

Iteration	Linear-loop iterations	Mass [kg]	t_{sk} [mm]	t_{str} [mm]	α_1 [°]	β_1 [°]	γ_1 [°]	α_2 [°]	β_2 [°]	γ_2 [°]
0		2.619	0.0276	0.0775	58	55	70	87	20	69
1	**18**	**2.939**	**0.0388**	**0.0432**	**27**	**23**	**49**	**88**	**19**	**90**
2	17	3.149	0.0420	0.0440	20	22	78	70	27	84
3	24	3.075	0.0388	0.0554	22	29	90	73	36	90
4	16	2.980	0.0361	0.0619	39	37	90	87	39	90
5	40	3.167	0.0381	0.0673	48	68	90	46	38	90
6	17	3.182	0.0376	0.0717	26	33	82	87	90	90

Active constraints at the best feasible iteration: panel compression buckling, collapse, crippling

A.4.3. Fuselage Window Panels, $\lambda_{shear} \geq 1.0$

Straight-Fiber

Table A.17.: Straight-Fiber Window Panel Optimization History, $\lambda_{shear} \geq 1.0$: 1/3

Iteration	Linear-loop iterations	Mass [kg]	t_{sk} [mm]	$t_{sk,win}$ [mm]	D [°]	E [°]	F [°]
0		4.420	0.0458	0.0458	18	68	74
1	**24**	**3.678**	**0.0324**	**0.0368**	**12**	**73**	**40**
2	20	3.807	0.0331	0.0403	12	45	47
3	21	3.775	0.0336	0.0387	9	53	47

Active constraints at the best feasible iteration: FI, combined compression-shear buckling

Table A.18.: Straight-Fiber Window Panel Optimization History, $\lambda_{shear} \geq 1.0$: 2/3

Iteration	Linear-loop iterations	Mass [kg]	t_{sk} [mm]	$t_{sk,win}$ [mm]	D [°]	E [°]	F [°]
0		4.420	0.0458	0.0458	15	88	51
1	23	3.976	0.0346	0.0443	36	28	28
2	40	3.748	0.0320	0.0397	63	35	30
3	**20**	**3.723**	**0.0334**	**0.0371**	**81**	**21**	**23**

Active constraints at the best feasible iteration: combined compression-shear buckling

Table A.19.: Straight-Fiber Window Panel Optimization History, $\lambda_{shear} \geq 1.0$: 3/3

Iteration	Linear-loop iterations	Mass [kg]	t_{sk} [mm]	$t_{sk,win}$ [mm]	D [°]	E [°]	F [°]
0		4.420	0.0458	0.0458	5	51	88
1	34	3.976	0.0332	0.0398	8	50	42
2	**28**	**3.723**	**0.0331**	**0.0396**	**4**	**49**	**45**

Active constraints at the best feasible iteration: combined compression-shear buckling

Steered-Fiber

Table A.20.: Steered-Fiber Window Panel Optimization History, $\lambda_{shear} \geq 1.0$: 1/3

Iteration	Linear-loop iterations	Mass [kg]	t_{sk} [mm]	$t_{sk,win}$ [mm]	α_1 [°]	β_1 [°]	γ_1 [°]	α_2 [°]	β_2 [°]	γ_2 [°]	α_3 [°]	β_3 [°]	γ_3 [°]
0		4.420	0.0458	0.0458	70	27	23	80	9	53	85	86	64
1	21	3.761	0.0357	0.0356	23	41	22	82	4	30	52	77	29
2	**33**	**3.698**	**0.0341**	**0.0356**	**15**	**48**	**15**	**88**	**4**	**32**	**48**	**71**	**29**
3	40	3.697	0.0338	0.0359	16	51	17	84	5	31	59	76	22

Active constraints at the best feasible iteration: shear buckling, combined compression-shear buckling

Table A.21.: Steered-Fiber Window Panel Optimization History, $\lambda_{shear} \geq 1.0$: 2/3

Iteration	Linear-loop iterations	Mass [kg]	t_{sk} [mm]	$t_{sk,win}$ [mm]	α_1 [°]	β_1 [°]	γ_1 [°]	α_2 [°]	β_2 [°]	γ_2 [°]	α_3 [°]	β_3 [°]	γ_3 [°]
0		4.420	0.0458	0.0458	36	49	82	1	57	87	87	67	47
1	**26**	**3.698**	**0.0367**	**0.0339**	**50**	**5**	**13**	**3**	**79**	**58**	**54**	**49**	**58**
2	24	3.761	0.0386	0.0316	42	0	1	3	80	69	41	53	65

Active constraints at the best feasible iteration: shear buckling, combined compression-shear buckling

Table A.22.: Steered-Fiber Window Panel Optimization History, $\lambda_{shear} \geq 1.0$: 3/3

Iteration	Linear-loop iterations	Mass [kg]	t_{sk} [mm]	$t_{sk,win}$ [mm]	α_1 [°]	β_1 [°]	γ_1 [°]	α_2 [°]	β_2 [°]	γ_2 [°]	α_3 [°]	β_3 [°]	γ_3 [°]
0		4.420	0.0458	0.0458	41	26	30	80	21	89	29	13	59
1	**22**	**3.718**	**0.0323**	**0.0383**	**36**	**33**	**32**	**46**	**40**	**90**	**28**	**23**	**90**
2	23	3.775	0.0352	0.0367	30	25	24	46	43	89	24	26	87
3	19	3.791	0.0356	0.0368	33	26	26	46	45	84	25	29	90

Active constraints at the best feasible iteration: shear buckling, combined compression-shear buckling

B

Bibliography

[1] 3M. 3m scotch-weld ec-9323 b/a technical data sheet. Technical report, Aerospace and Commercial Transportation Division, 3M Company, 2013.

[2] European Aviation Safety Agency. *Certification Specifications and Acceptable Means of Compliance for Large Aeroplanes CS-25*. European Aviation Safety Agency, amendment 17 edition, July 2015.

[3] *HyperWorks 13.0 Desktop User Guides - OptiStruct 13.0*. Altair Engineering, Inc., 2014.

[4] Horst Baier. *Multidisciplinary Design Optimization*. Technische Universitaet Muenchen, 2015.

[5] Richard Butler, Neil Baker, and Wenli Liu. Damage tolerance of buckling optimized variable angle tow panels. In *50th AIAA/ASME/ASCE/AHS/ASC Structures, Structural Dynamics, and Materials Conference*, 2009.

[6] E. Clarkson. Hexcel 8552 im7 unidirectional prepreg 190 gsm & 35qualification statistical analysis report. Technical Report NCP-RP-2009-028 Rev N/C, National Institute for Aviation Research, Wichita State University, 2011.

[7] Broderick H. Coburn, Zhangming Wu, and Paul M. Weaver. Buckling analysis of stiffened variable angle tow panels. *Composite Structures*, 111:259–270, May 2014.

[8] USA Department of Defense. *COMPOSITE MATERIALS HANDBOOK: VOLUME 3. POLYMER MATRIX COMPOSITES MATERIALS USAGE, DESIGN, AND ANALYSIS*. Department of Defense, USA, 2002.

[9] Kazem Fayazbakhsh, Mahdi Arian Nik, Damiano Pasini, and Larry Lessard. Defect layer method to capture effect of gaps and overlaps in variable stiffness laminates made by automated fiber placement. *Composite Structures*, 2013.

[10] C. Fleury, M. Bruyneel, B. Colson, and A. Remouchamps. Buckling optimization of composite stiffened panels; some important issues. In *2nd International conference on Engineering Optimization*, September 2010.

[11] J. L. Grenestedt and P. Gudmundson. Lay-up optimisation of composite material structures. In *IUTAM Symposium on Optimal Design with Advanced Materials*, 1993.

[12] Z. Gürdal and R. Olmedo. In-plane response of laminates with spatially varying fiber orientations - variable stiffness concept. *AIAA Journal*, 1993.

[13] Z. Gürdal and B. Tatting. Tow-placement technology and fabrication issues for laminated composite structures. In *46th AIAA/ASME/ASCE/AHS/ASC Structures, Structural Dynamics, and Materials Conference*, 2005.

[14] *Prepreg Properties - HexPly 8552 UD Carbon Prepregs - IM7*. Hexcel Composites, February 2013.

[15] Nicolas Hofheinz. Untersuchung von tragenden transparenten strukturen in rumpfsegmenten. Master's thesis, Institute of Lightweight Structures, Department of Mechanical Engineering, Technische Universitt Mnchen, 2011.

[16] Shinya Honda, Teruki Igarashi, and Yoshihiro Narita. Multi-objective optimization of curvilinear fiber shapes for laminated composite plates by using nsga-ii. *Composites: Part B*, 2013.

[17] M. Hyer and R. Charette. Innovative design of composite structures: The use of curvilinear fiber format in composite structure design. Technical report, Virginia Polytechnic Institute and State University, NASA Langley Research Center, March 1990.

[18] M.W. Hyer and H.H. Lee. The use of curvilinear fiber format to improve buckling resistance of composite plates with central circular holes. *Composite Structures*, 1991.

[19] Samuel T. Ijsselmuiden, Mostafa M. Abdalla, and Zafer Gürdal. Optimization of variable-stiffness panels for maximum buckling load using lamination parameters. *AIAA Journal*, 2010.

[20] Momchil Jeliazkov, Peyman Mouri Sardar Abadi, Claudio S. Lopes, Mostafa Abdalla, and Daniel Peeters. Buckling and first-ply failure optimization of stiffened variable aangle tow panels. In *20th International Conference on Composite Materials*, 2015.

[21] Robert M. Jones. *Mechanics of Composite Materials*. Scripta Book Company, 1975.

[22] Sachin Rajkumar Kamath. Optimization of steered fiber sagitta ucav panel with pre and postbuckling constraints. Master's thesis, Institute of Lightweight Structures, Department of Mechanical Engineering, Technische Universitaet Muenchen, 2015.

[23] C. Kassapoglou. Ae4509 advanced design and optimization of composite structures i: Crippling of stiffeners. Course material, 2016. URL `https://ocw.tudelft.nl/course-lectures/crippling-of-stiffeners/`.

[24] Byung Chul Kim, Kevin Potter, and Paul M. Weaver. Continuous tow shearing for manufacturing variable angle tow composites. *Composites: Part A*, 2012.

[25] Yong Il Kim and Gyung-Jin Park. Nonlinear dynmaic response structural optimization using equivalent static loads. *Computer Methods in Applied Mechanics and Engineering*, 2010.

[26] William L. Ko and Raymond H. Jackson. Compressive buckling analysis of hat-stiffened panel. Technical memorandum 4310, NASA, August 1991.

[27] Andreas Kollmannsberger. Automated fiber placement. Website, 2015. URL `http://www.lcc.mw.tum.de/en/research-groups/process-technology-for-fibers-and-textiles/automated-fiber-placement/`.

[28] Hyun-Ah Lee and Gyung-Jin Park. A software development framework for structural optimization considering non linear static responses. *Structural and Multidisciplinary Optimization*, 2015.

[29] Wenli Liu and Richard Butler. Buckling optimization of variable-angle-tow panels using the infinite-strip method. *AIAA Journal*, 2013.

[30] LLB. Werkstoffdatenblatt llb. Material Database, 2016.

[31] Tao Luo. Optimization of variable-stiffness hybrid laminated plates with central cutout subjected to multiple loads. Master's thesis, Institute of Lightweight Structures, Department of Mechanical Engineering, Technische Universitaet Muenchen, 2012.

[32] Zhifan Luo. Benchmark of hyperstudy optimization algorithms. Technical report, Altair Engineering Inc., 2014.

[33] Scott Malaznik. Crippling of thin-walled composite sections using progressive failure analysis. In *MSC Software 2013 Users Conference*. Lockheed Martin Corporation, 2013.

[34] O. Meyer. *Kurzfaser-Preform-Technologie zur kraftflussgerechten Herstellung von Faserverbundbauteilen*. PhD thesis, Institute of Aircraft Design, University of Stuttgart, 2008.

[35] *MSC Nastran 2014: Quick Reference Guide*. MSC Software Corporation, 2014.

[36] *MSC Nastran 2014: Design Sensitivity and Optimization Users Guide*. MSC Software Corporation, 2014.

[37] S. Nagendra, S. Kodiyalam, J. Davis, and V. Parthasarathy. Optimization of tow fiber paths for composite design. In *36th AIAA/ASME/ASCE/AHS/ASC Structures, Structural Dynamics, and Materials Conference*, 1995.

[38] Michael C. Y. Niu. *Composite Airframe Structures*. Conmilit Press Ltd., 1992.

[39] Oxeon. Kolfiberarmering fr avancerade tillmpningar. Presentation, October 2012. URL `http://www.svenskkompositforening.se/uploads/Oxeon%20-%20Svensk%20Kompositf%C3%B6rening%20121010_pub.pdf`.

[40] Joseph Pajot. Optimal design exploration using global response surface method: Rail crush. Technical report, Altair Engineering Inc., 2013.

[41] G.J. Park and B.S. Kang. Validation of a structural optimization algorithm transforming dynamic loads into equivalent static loads. *Journal of Optimization Theory and Applications*, 118 (1):191–200, 2003.

[42] Gyung-Jin Park. Technical overview of the equivalent static loads method for non-linear static response structural optimization. *Structural and Multidisciplinary Optimization*, 43 (3):319–337, 2011.

[43] T. Rahman, S. T. Ijsselmuiden, M. M. Abdalla, and E. L. Jansen. Postbuckling analysis of variable stiffness composite plates using a finite element-based pertubation method. *International Journal of Structural Stability and Dynamics*, 2011.

[44] G. Raju, Zhangming Wu, and Paul M Weaver. Postbuckling analysis of variable angle tow plates using differential quadrature method. *Composite Structures*, 2013.

[45] Gangadharan Raju, Zhangming Wu, and Paul M. Weaver. Buckling and postbuckling of variable angle tow composite plates under in-plane shear loading. *International Journal of Solids and Structures*, 2015.

[46] Aravind Sasikumar. Investigation of the multi-modality and computational effort in the optimization of steered fiber laminates. Master's thesis, ISAE- SUPAERO, 2015.

[47] Moon-Kyun Shin, Ki-Jong Park, and Gyung-Jin Park. Optimization of structures with nonlinear behavior using equivalent loads. *Computer Methods in Applied Mechanics and Engineering*, 196 (4-6):1154–1167, 2007.

[48] Mathias Stolpe. On the equivalent static loads approach for dynamic response structural optimization. *Structural and Multidisciplinary Optimization*, 2014.

[49] B.F. Tatting and Z. Gürdal. Design and manufacture of elastically tailored tow-placed plates. Technical report, NASA, 2002.

[50] Tanut Ungwattanapanit. Structural optimization of carbon composite fuselage panel including buckling and manufacturing constraints. Master's thesis, Institute of Lightweight Structures, Department of Mechanical Engineering, Technische Universitaet Muenchen, 2011.

[51] Tanut Ungwattanapanit and Horst Baier. Postbuckling optimization of composite stiffened fuselage panels using steered fibers. In *4th Aircraft Structural Design Conference - Royal Aeronautical Society*, 2014.

[52] Tanut Ungwattanapanit and Horst Baier. Gradient-based optimization of steered-fibre aircraft panels with postbuckling consideration using equivalent static loads. In *57th AIAA/ASCE/AHS/ASC Structures, Structural Dynamics, and Materials Conference*, 2016.

[53] Tanut Ungwattanapanit and Horst. Weight optimizaiton of stiffened steered-fiber panels using equivalent static loads for postbuckling responses. In *3rd International Conference on Buckling and Postbuckling Behaviour of Composite Laminated Shell Structures*, 2015.

[54] Julien van Campen, Christos Kassapogglou, and Zafer Gürdal. Generating realistic laminate fiber angle distributions for optimal variable stiffness laminates. *Composites: Part B*, 2012.

[55] W. van den Brink, W. Vankan, and R. Maas. Buckling-optimized variable stiffness laminates for a composite fuselage window section. In *28th International Congress of The Aeronautical Sciences (ICAS 2012)*, 2012.

[56] S.C. White, G.Raju, and P.M.Weaver. Initial post-buckling of variable-stiffnesscurved panels. *Journal of the Mechanics and Physics of Solids*, 2014.

[57] K. Chauncey Wu, Brian F. Tatting, Brett H. Smith, Randy S. Stevens, Gina P. Occhipinti, Jonathan B. Swift, David C. Achary, and Robert P. Thornburgh. Design and manufacturing of tow-steered composite shells using fiber placement. In *50th AIAA/ASME/ASCE/AHS/ASC Structures, Structural Dynamics, and Materials Conference*, 2009.

[58] Zhangming Wu and Gangadharan Raju. Feasible region of lamination parameters for optimization of variable angle tow (vat) composite plates. In *54th AIAA/ASME/ASCE/AHS/ASC Structures, Structural Dynamics, and Materials Conference*, 2013.

[59] Zhangming Wu, Paul M. Weaver, Gangadharan Raju, and Byung Chul Kim. Buckling analysis and optimisation of variable angle tow composite plates. *Thin-Walled Structures*, 2012.

[60] Zhangming Wu, Gangadharan Raju, and Paul M. Weaver. Postbuckling analysis of variable angle tow composite plates. *International Journal of Solids and Structures*, 50 (10): 1770–1780, May 2013.